FINAL REPORT

PURIFICATION OF CRUDE GLYCEROL AND ITS CONVERSION TO BIO-CHEMICALS

(ADF Project: ADF 20130289)

Principal Investigator

Dr. Ajay. K. Dalai

Catalysis and Chemical Reaction Engineering Laboratories, Department of Chemical and Biological Engineering, University of Saskatchewan, Saskatoon, SK, S7N 5A9, Canada.
Tel.: +1 306 966 4771; Fax: +1 306 966 4777.
E-mail address: ajay.dalai@usask.ca (A.K. Dalai).

Submitted to

SASKATCHEWAN MINISTRY OF AGRICULTURE (CANADA)

September 30, 2017

ACKNOWLEDGMENT

Author acknowledges the financial support of Agriculture Development fund (ADF) from Saskatchewan Ministry of Agriculture (Canada) for this research.

Executive summary

The presence of impurities decreases the calorific and economic value of glycerol. Thus, glycerol impurities must be greatly reduced if it is to be used as a fuel or feedstock for chemicals. A sequential procedure for crude glycerol refining that includes saponification, acidification, neutralization, membrane filtration, solvent extraction, and activated charcoal adsorption was investigated in the present work. In the first phase, dead-end membrane filtration in batch process was studies while in the next phase, tubular membrane filtration in semi-continuous mode was studies. Membrane filtration was studied at temperature and pressure ranges of 25-60°C and 50-350 kPa, respectively. A range of ultra-filtration (UF) and fine ultra-filtration (UFF) (1, 3, 5, 8, and 15 kDa) were utilized to obtain highly enriched glycerol. Membrane filtration at 60°C and 350 kPa using 1 kDa membrane, solvent and water evaporation and activated charcoal treatment produced the maximum concentration of glycerol (97.5%) observed. Acid value and free fatty acid (FFA) content of all treated samples were found to be <1%. Crude, enriched crude (purified) and ACS grade glycerol were characterized using FTIR and bomb calorimeter further confirmed the purity of obtained glycerol.

In the next phase, crude glycerol was purified by a combination of physico-chemical purification processes and semi-continuous membrane filtration using a 5kDa ultrafiltration membrane. To study membrane filtration of treated glycerol feed, temperature, pressure, and flow rate were studied. A maximum glycerol purity of >85% was obtained from crude glycerol of 40% purity after the physico-chemical treatment and membrane filtration at a temperature range of 42.5-50^{o}C, low to moderate flow rate of 50-100 mL/min and low to moderate pressure of 50-150 psi. The present study shows a potential for purification of crude glycerol.

The catalytic conversion of glycerol to value added chemicals and application of glycerol as biofuel was also studied in the present project. A solid acid (heterogeneous) catalysts for etherification of glycerol was developed. These zeolite based acid catalysts are highly active and the catalytic activity of these catalysts is tested in bench scale batch reactors. A 55% TPA (12-Tungstophosphoric acid)/H-β catalyst yielded 100% conversion, when 2.5 (w/v) % catalyst and 1:5 glycerol to tert-butanol (TBA) molar ratio were used at 120°C, reaction pressure of 1 MPa and reaction time of 5 h. Later the same catalyst was used for co-production of biodiesel and glycerol-ether, and the mixture of biodiesel and glycerol-ether is called biofuel. The fuel properties analysis indicates that biofuel has better fuel properties as compared to those for biodiesel. The techno-economic analysis indicated that co-production of biodiesel and glycerol-ether is environment friendly.

This project work also focused on the development of a green process for the production of glycerol carbonate from glycerol and dimethyl carbonate using a Ti-SBA-15 catalyst. Ti-SBA-15 catalysts with varying Si/Ti ratio were synthesized in situ using sol gel method and characterized using various chemical and spectroscopic techniques to study the effect of Ti incorporation on surface and catalytic properties of Ti-SBA-15 catalysts. The process parameters were optimized

to obtain high glycerol conversion and glycerol carbonate selectivity. Ti-SBA-15 catalysts with lower Si/Ti ratio demonstrated higher glycerol conversion and GYC selectivity as compared to the catalysts with higher Si/Ti ratio. A regression model was developed to analyze the correlation between reaction parameters and reaction outcomes which suggest that the reaction temperature has the most significant effect on the glycerol conversion and GYC selectivity. A reaction mechanism portraying the role of Ti-SBA-15 in facilitating the formation of GYC was presented. GYC was formed via the formation of O-methoxy carbonyl intermediate and the reaction was catalyzed by the Lewis acidic nature of Ti-SBA-15 catalyst. A kinetic model was proposed based on the results obtained from this study. In addition, an economic feasibility study of the production of glycerol carbonate from glycerol using Ti-SBA-15 suggests that the process has the commercialization potential.

A techno-economic analysis based on a scenario where all the purified glycerol is converted to value added chemicals – solketal and glycerol carbonate was carried out and it showed that it is economically feasible to purify glycerol. In this scenario (Scenario 3), the required capital investment is $0.72 M and the net present value of the project is $26 M over 10 years of operation after start-up with capital investment in the initial three year period with no returns. The unit cost of purifying a kg of crude glycerol is $13.62 in this scenario and the unit revenue is $116.62, making it a promising undertaking. While this project will be an addition to a billion dollar biodiesel production plant meaning the $26 M in net present value is not substantial, it is still significant in offsetting the larger biodiesel plant costs and improving the overall company bottom-line.

TABLE OF CONTENTS

LIST OF ABBREVIATION

BET	Brunauer–Emmett–Teller
CCD	Central composite design
FAME	Fatty acid methyl ester
FFA	Free fatty acid
FTIR	Fourier transform infrared
GYC	Glycerol carbonate
MONG	Matter organic non glycerol
MWCO	Molecular weight cut off
NPV	Net present value
RSM	Response surface methodology
SFA	Saponified fatty acid
TPA	Tungstophosphoric acid
UF	Ultra filtration
UFF	Fine ultra filtration
VOC	Volatile organic carbon
XPS	X-ray photoelectron spectroscopy

List of Tables

LIST OF FIGURES

1. Introduction and literature review

Glycerol is the main by-product or co-product of the biodiesel industry and it is produced in significant quantities up to 10 wt% in biodiesel (Vlysidis et al., 2011; Almena et al., 2015; Posada et al., 2012; Apostolakou et al., 2009; Xiao et al., 2013). Glycerol, also known as crude glycerine, 1,2,3-propanetriol, glyceritol, glycyl alcohol or 1,2,3-trihydroxypropane, has a purity of 30-80% w/w and a chemical formula of $C_3H_8O_3$ (Ardi et al., 2015; Dhabhai et al., 2016). It is a liquid at room temperature and is colorless and odorless and also viscous, biodegradable and hygroscopic (Dhabhai et al., 2016).

The composition of crude glycerol varies widely according to the method of biodiesel production (Xiao et al., 2013). Generally, there are four processes for producing biodiesel and hence glycerol. These processes are: Transesterification (biodiesel production), saponification (manufacturing of soap), hydrolysis (fatty acid production) and microbial fermentation. Table 1 shows the compositions of different crude glycerol produced by transesterification, saponification and hydrolysis (Gerpen et al., 2004; Tan et al., 2013).

Table 1 Different compositions of crude glycerol produced by different processes

Component	Transesterification (%)	Saponification (%)	Hydrolysis (%)
Glycerol	30-60	83-84	88-90
Ash	10-19	8.5-9.5	0.7-1.0
Water	<=10	6-7	8-9
MONG (Matter Organic Non-Glycerol)	<=40	3-4	0.7-1.0
Trimethylene glycol	1	0.1	0.2

Transesterification of triglycerides for biodiesel production is the main source of most crude glycerol production (Dhabhai et al., 2016). The chemical composition of crude glycerol varies with the type of catalyst used to produce biodiesel, the efficiency of the transesterification process, the recovery efficiency of biodiesel, the other impurities in the feedstock, and methanol and catalysts recovery (Yang et al., 2012). Glycerol content of crude glycerol ranges from 38-96% with some samples having more than 14% methanol and 29% ash (Yang et al., 2012). Homogeneous catalytic transesterification reactions are the major sources of glycerol, which is often termed as crude glycerol (Dhabhai et al., 2016).

Most biodiesel production involves the use of methanol and a homogeneous alkaline catalyst (sodium methoxide, potassium hydroxide or sodium hydroxides). Accordingly, soap, catalysts, inorganic salts, methanol, other matter organic non-glycerol (MONG) and water impurities are usually contained in crude glycerol (Yang et al., 2012). Matter organic non-glycerol (MONG) consists of fatty acid methyl esters (FAME), tri-, di- and mono-glycerides, several types of free

fatty acids (FFAs) and methanol or ethanol (Dhabhai et al., 2016). Crude glycerol from sunflower oil biodiesel production has the following composition: Glycerol (30%), methanol (50%), soap (13%), moisture (2-3%), salts of potassium and sodium (2-3%) and other impurities, mostly fatty acids (2-3%) (Yang et al., 2012). The homogeneous catalytic transesterification reaction commonly used to produce crude glycerol is as shown in Fig. 1 (Hu et al., 2014; Tan et al., 2014). In the transesterification of vegetable oils, the catalyst used are either acidic or basic in the form of sulphuric, hydrochloric acid or hydroxides of sodium and potassium or enzymes or heterogeneous catalysts (Shibasaki-Kitakawa et al. 2007; Tesser et al. 2005). Industrially the use of sodium methylate is most common in biodiesel production.

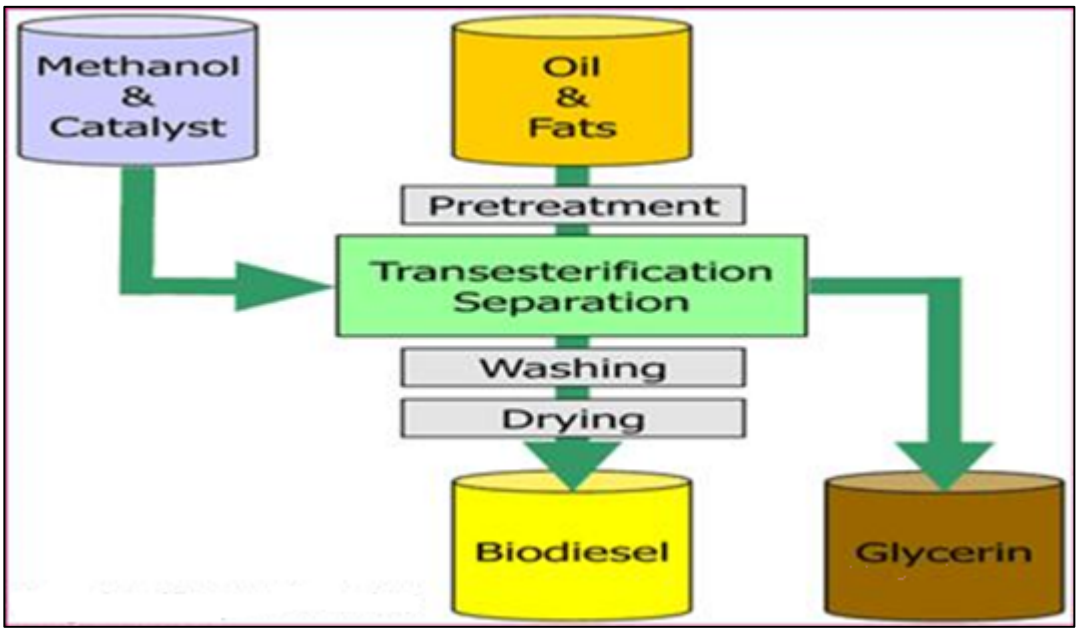

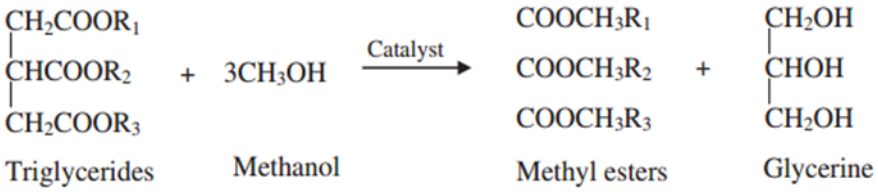

Fig. 1 Transesterification reaction

Crude glycerol is produced in surplus and it is of little economic value. Glycerol purification is therefore important to enhance its economic value (Vlysidis et al., 2011). Crude glycerol is limited in applications due to the presence of inorganic salts and other impurities and has a much lower selling price compared to pure glycerol, which can be considered as a renewable building block or feedstock for biorefineries (food, chemical and pharmaceutical industries) or used in the production of fuels or fuel additives (Ardi et al., 2015; Dhabhai et al., 2016). Purification of glycerol increases its economic and applicable value and makes biodiesel production more viable

(Dhabhai et al., 2016). In the last decade, crude glycerol prices have declined to ~$0.1/kg while the market price of pure glycerol has steadied at about $1/kg (Dhabhai et al., 2016). Glycerol quality is defined by its grade (wt%) with 95% purity glycerol being classed as technical grade, 96-99% purity glycerol as USP grade glycerol and 99.7% purity glycerol as Kosher glycerol (Dhabhai et al., 2016). Technical grade is an industrial term used to refer to chemical products that are not used in food production. USP (United States Pharmacopeia) grade glycerol is employable in foods and pharmaceuticals, while Kosher glycerol is used in Kosher foods production (Dhabhai et al., 2016).

Crude glycerol is purified by different methods such as –distillation, ion exchange and sequential physico-chemical treatments, which include saponification, acidification, phase separation, solvent extraction, neutralization and activated carbon or yeast adsorption. Chemical treatment by acidification at low pH can increase glycerol content and reduce the amount of ash in recovered glycerol. It might however lead to higher material organic non-glycerol (MONG) content in the resultant enriched glycerol due to formation of free fatty acids (FFAs) from acidification of saponified fatty acids (SFA) by mineral acid (H^+) (Dhabhai et al., 2016).

The salt content in the crude glycerol often remains in the range from 5 to 7%. It stems from transesterification of vegetable oils by using homogeneous catalyst. Impurities in the form of methanol, water, catalyst and soap get accumulated in the crude glycerol (Xavier Lancrenon and Jon Fedders 2008).

An important glycerol purification step includes acidification/neutralization to adjust pH and evaporation/distillation to separate water and excess methanol for reuse. Generally, excess methanol is recovered. However, because recovery of methanol is less cost effective than using new methanol, this is not always the case (Quispe et al., 2013). Different methods have been used to purify crude glycerol such as distillation, filtration, chemical treatment, adsorption (using activated carbon), ion-exchange (using resin), extraction, decantation and crystallization whereby each of the purification techniques uses different properties of crude glycerol (Aziz and Aroua, 2013).

Vacuum filtration, ion exchange, membrane separation and activated carbon adsorption are regarded as deep refining technologies. Simple distillation is not appropriate for glycerol purification as glycerol is prone to thermal degradation or oxidation at various high temperature conditions. Glycerol thermally degrades by polymerization or dehydration. Vacuum distillation is an energy-intensive process for purifying glycerol that results in high energy input requirement to elevate and vaporize glycerol because glycerol has a high specific heat as well as a high heat of vaporization (Dhabhai et al., 2016).

Among deep refining technologies, ion exchange is the most common industrial method of glycerol purification and is advantageous in that it is suitable for small- to large-scale continuous operations; has low chemical costs; is adaptable process-wise and yields acceptable levels of glycerol purity (>95.5 wt% purity). It is however disadvantageous because it is energy-intensive,

which translates to a higher overall process cost (Dhabhai et al., 2016; Luo et al., 2016). The high inorganic salt content of glycerol from biodiesel production makes ion-exchange uneconomical (Dhabhai et al., 2016; Luo et al., 2016).

Membrane exchange is an emerging technology in glycerol purification and is highly appealing because of its simple operability, low energy requirement and therefore low cost and superior purification performance (~99 wt% glycerol output), and environmental friendliness. Despite many great promises, membrane separation technology presents the challenges of easy fouling, lack of durability and operational specificity (Dhabhai et al., 2016; Luo et al., 2016). Ceramic membranes are however emerging as good alternatives to conventional membranes because of their great thermal, chemical and mechanical stability properties.

Activated carbon adsorption technique removes color in crude glycerol and eliminates fatty acids (lauric and myristic acids) by adsorbing them along with other molecular compounds. Activated carbon adsorption is carried out as the final step in the purification of crude glycerol (Dhabhai et al., 2016; Luo et al., 2016). In research and industrial applications, vacuum distillation at high temperatures (150-200˚C) is employed as the finishing step to obtain a refined grade of glycerol (>99.5wt% purity). This step however adds large capital and operating costs to the purification process making it less economical overall. Fig. 2 presents the most commonly employed methods for purification of glycerol.

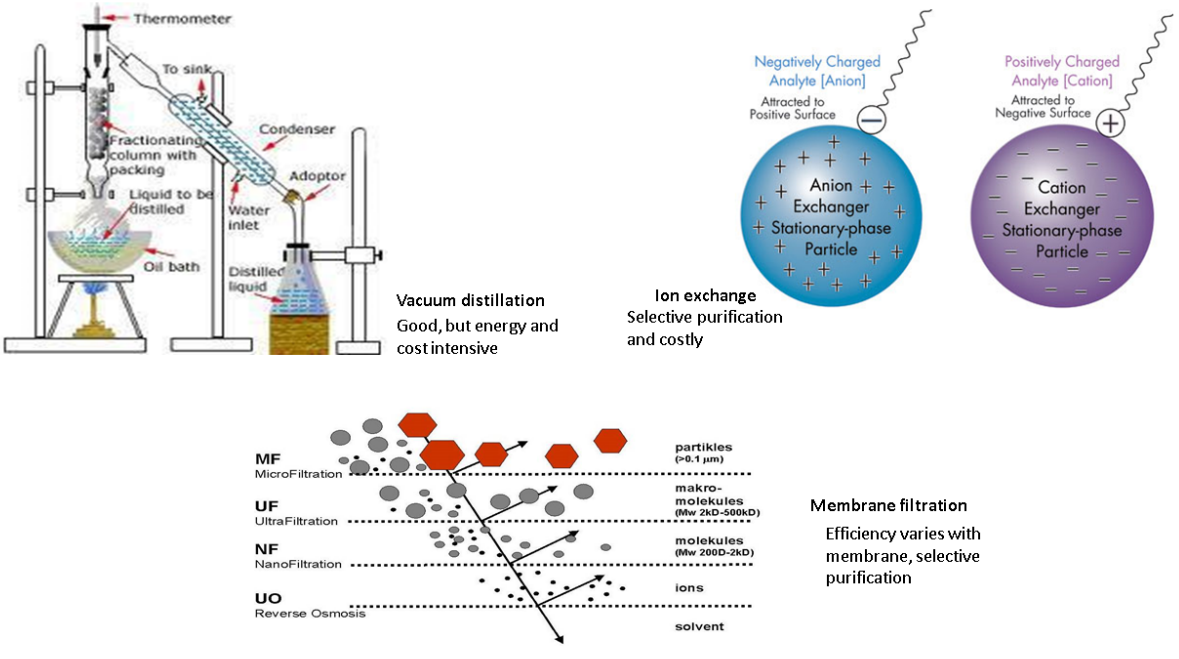

Fig. 2 Different methods for the purification of crude glycerol

The overall procedure employed in this work for glycerol purification is summarized in Fig. 3 which consists of saponification, acidification, overnight phase separation to get rid of free fatty acids (FFA) from glycerol phase, additional solvent extraction phases for residual FFA removal, followed by membrane filtration under temperature, pressure and flow rate conditions and the final finishing steps are solvent and water removal and activated charcoal treatment.

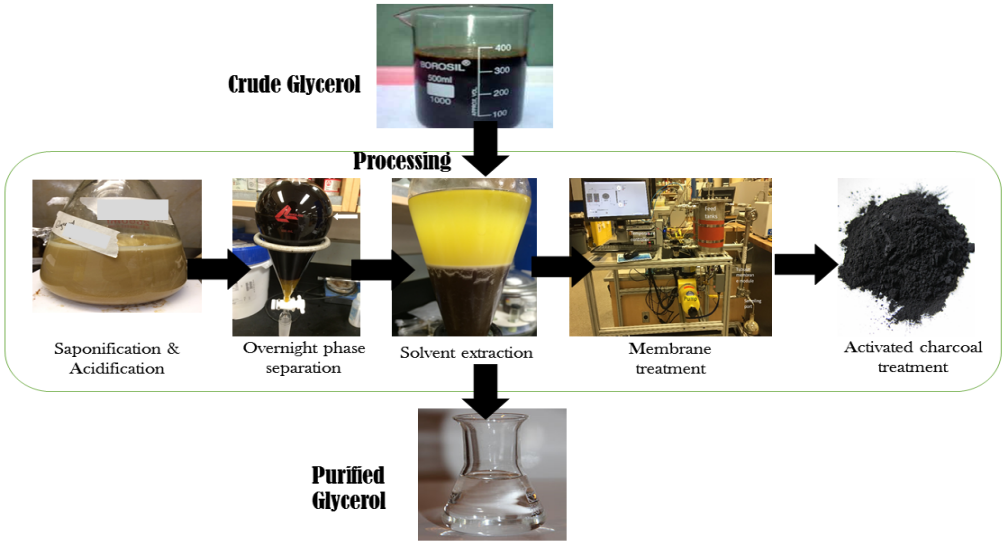

Fig. 3 Different stages in the purification of crude glycerol purification

Glycerol has been used as a resource for synthesis of various chemicals using different processes like esterification, transesterification, acetalization, dehydrogenation and polymerization etc. (Bagheri et al., 2014; Bai et al., 2014; Chang and Chen, 2011; Gholami et al., 2014). This work focuses on the development of a green processes for the conversion of glycerol to glycerol ethers and glycerol carbonate.

One of the most celebrated products in the past five years is glycerol carbonate (GYC). It is a very high value added product with the market price greater than 8141 US $/ton, whereas glycerol has market price of 240 US $/ton (Teng, 2014). On the other hand, GYC has great potential to replace petro-derivative compounds. This has gained much interest over the last twenty years for two main reasons, one among them being its wide reactivity, implying numerous applications, and the other being a way to valorize glycerol, which is becoming widely available as a major bio based by-product from the biodiesel and other chemicals (Sonnati, 2013).

Glycerol carbonate (GYC) has gained interest over last 20 years because of many reasons. Increasing industrial attention for GYC is based on its reactivity as well as its physical properties. GYC has a high renewable content (the mass percentage of molecule coming from renewable energy sources). GYC is not flammable because the fire point of GYC is greater than 204^{o}C. It is water-soluble, non-toxic, and viscous (84.5 mPa.s at 25^{o}C) liquid with very low evaporation rate

with boiling point of 110-115^{o}C at 0.1mm Hg (Ochoa-Gomez, 2012). Moreover, GYC is a bio-sustainable, and biodegradable compound.

Main advantage of GYC is its wide reactivity due to the presence of both hydroxyl group and a 2-oxo-1,3-dioxolane group. GYC can be converted to epichlorohydrin, a product that has a large industrial application, under very mild conditions. Glycerol carbonate and its esters are potential low volatile organic compound (VOC) solvents for many applications for a bio-based alternative to organic solvents (Sonnati, 2013). GYC has interesting properties that lie between the cyclic alkylene carbonates and glycerol, making it useful as a carbon dioxide absorption solvent, curing agent in cement, plasticizer, and nail lacquer gel remover in the cosmetics industry, a liquid membrane in gas separation and an electrolyte in lithium-ion batteries. It also finds indirect applications in the synthesis of surfactants, polymers and chemical intermediates in organic synthesis.(Teng, 2014), (Sonnati, 2013)

In literature, various base catalysts have been tested for synthesis of glycerol carbonate from glycerol and urea. Heterogeneous catalysts may be more useful for post-reaction procedures like easy recovery and reuse of catalysts, compared to these homogeneous ones. Many catalysts have been studied by previous authors and they are listed in Table 2.

Table 2 Literature review on glycerol carbonate production process

Catalyst	Results					References
	Temp. (^{o}C)	Pressure	Time (h)	Conversion (%)	Selectivity (%)	
ZnO (Hetero)				61	69	Fujita,2013
Smectitie (Zn) (Hetero)				65	75	Fujita,2013
Hydrotalcite(Zn) (Hetero				82	80	Fujita,2013
$ZnCl_2$ (Homo)	130	3 kPa	3	84	97	Fujita,2013
$ZnBr_2$(Homo)				82	96	Fujita,2013
$ZnSO_4$(Homo)				81	92	Fujita,2013
$(CH_3COO)_2Zn.2H_2O$(Homo)				65	80	Fujita,2013
Alloy Al-Ce-Ga				30		Aresta, 2009
TiO_2				32		Aresta, 2009
CeO_2				32		Aresta, 2009
Rh(diphos)BPh4				35		Aresta, 2009
Bu_2SnO				36		Aresta, 2009

Titanosilicalite	140	20 Pa	3	36	Aresta, 2009
Titanosilicalite				58	Aresta, 2009
Bi_2O_3				42	Aresta, 2009
ZnO				48	Aresta, 2009
Ɣ- ZrP Zn				62	Aresta, 2009
Ɣ – ZrP not Calcined				60	Aresta, 2009
Ɣ- ZrP not Calcined				68	Aresta, 2009
Ɣ-ZrP Calcined				76	Aresta, 2009

Since a Ɣ-ZrP catalyst showed promising activity in the glycerol carbonate production process, a comparative techno-ecnomic study is conducted as a part of the research between the previously developed glycerol etherification process and glycerol carbonate process.

GYC is a high value product associated with positive physicochemical properties such as low toxicity, low flammability and low vapour pressure. GYC has wider applications in paint and pharmaceutical industries. It is used as a monomer for polyurethane formation, a component of detergents and coatings and a novel component of gas-separation membranes (Álvarez et al., 2013; Jiao et al., 2015; Simanjuntak et al., 2015). GYC has been synthesized from glycerol by transesterification alkyl carbonates (Esteban et al., 2015), carbonylation with urea (Aresta et al., 2009) and carbonation of glycerol with carbon dioxide (CO_2) (Liu et al., 2016). The carbonation of glycerol with CO_2 provides a low GYC yield and the use of elevated temperature and pressure conditions in the presence of a catalyst limits wider application of this process (Aresta et al., 2007). The reaction of glycerol with urea is another method but it gives side products such as isocyanic acid and biuret and also the reaction requires the use of vaccum to remove ammonia from the reaction mixture to initiate the reaction (Aresta et al., 2009). Alkyl carbonates have been used as alternative transesterification agents to produce GYC at much milder conditions (Simanjuntak et al., 2011).

Basic oxide catalysts have been extensively studied for these reactions due to their high stability in liquid-phase reactions and presence of relatively strong basic sites. However, these basic catalysts exhibit low activity during recycling (Jagadeeswaraiah et al., 2014). Titanium-silica based catalysts have attracted considerable attention due to their excellent properties as mildly acidic catalysts for selective catalytic reactions (Bérubé et al., 2008). A study from our research group demonstrates that solid acid catalysts can effectively catalyze both esterification and transesterification reactions to produce biodiesel from canola oil (Sharma et al., 2014). The present

work is designed to examine titanium-SBA-15 (Ti-SBA-15) based solid acidic catalysts for the transesterification reaction of dimethyl carbonate (DMC) and glycerol to produce GYC. The incorporation of Ti into the silica matrix can be performed using two methods (i) post-grafting of Ti on pre-synthesized silicate material (SBA-15) and (ii) *in-situ* synthesis by incorporation Ti and Si precursors mixture into acidic solution [18]. Generally, *in-situ* method is preferred compared to post-grafting method as it allows the uniform distribution of Ti and prevent the formation of TiO_2 clusters on SBA-15 surface. However, it is very difficult to control the retention and dispersion behavior of titanium as Ti species are very sensitive to change in synthesis conditions and thermal profile (Aresta et al., 2009; Bérubé et al., 2010; Araújo et al., 2016). Therefore, it is important to study the effects of Ti loading on chemical nature of Ti species in Ti-SBA-15. The aim of the present study is to investigate the effects of Ti loading on surface properties and chemical nature of Ti-SBA-15 catalyst and evaluate the catalytic activity of Ti-SBA-15 on the conversion of glycerol to GYC.

Glycerol ethers, a derivative of glycerol, can be used as fuel additives which enhance fuel combustion properties and help in decreasing the cloud point of biodiesel (Klepacova et al., 2003). Glycerol ethers can be produced from etherification of glycerol in the presence of another alcohol and acid catalysts. The acid catalysts initiate the etherification reaction between the two alcohols (Gu et al., 2008). The nature of the reaction is a condensation reaction mainly producing mono glycerol-ether. This mono ether undergoes further etherification to form di and tri glycerol ethers if molar excess of alcohol is present (Fig. 11) (Zhao et al., 2013; Da Silva et al., 2009). A *tert*-butyl glycerol ether (TTBG) produced from *tert*-butanol (TBA) and glycerol has a potential for blending with petro-diesel (Wessendorf and Erdol, 1995). Especially, di-*tert*-butyl glycerol ethers (DTBG) and tri-*tert*-butyl glycerol-ether (TTBG) are preferred as additives over mono-*tert*- butyl glycerol-ether (MTBG) because of their higher solubility in diesel/biodiesel compared to that of MTBG (Xiao et al., 2009).

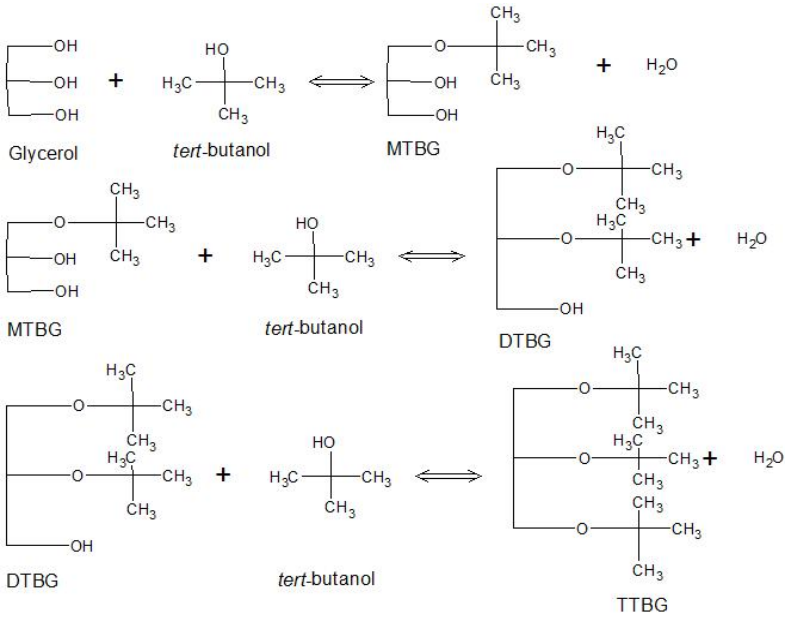

Fig. 4 Reaction scheme for the glycerol etherification

Heteropoly acids (HPA) made up of heteropoly anions show strong Brønsted acidity (Devassy and Halligudi, 2005; Busca, 2007; Okuhara et al., 2000). 12-Tungstophosphoric acid (TPA) with Keggin structure is thermally stable and depicts super acidity compared to other HPA compounds Kozhevnikov, 2007). Heteropoly acids have lower surface area (1 – 10 m^2/g) and are soluble in polar solvents (Kulkarni et al., 2006). These problems can be avoided by supporting TPA on various carriers. Zeolite is a crystalline poroussolid typically made up of Si, Al, and O atoms and a catalytic material with wide industrial applications. Among these, β zeolite is one of the most typical and commercially available zeolites.

This work was designed with the following objectives: (i) purification of crude glycerol obtained from transesterification process using physico-chemical treatment; (ii) study the effects of operating parameters on dead-end membrane filtration (batch mode) of treated feed; (iii) study the effects of operating parameters on semi-continuous membrane filtration; (iv) characterization of purified glycerol; (v) catalytic etherifiction of glycerol to produce value added chemicals; (vi) production of glycerol carbonate by catalytic conversion of glycerol; and (vii) detailed techno-economic analysis of the process.

1.1 Economics of glycerol and market analysis

Glycerol is generally divided into three main classes which is based on its usage: 1) technical grade (95.5% purity) which is used as a raw material for synthesis of variety of chemicals, but not used for food or drug formulation; 2) United States Pharmacopeia (USP) glycerol (>95.5-99.5% purity) from animal fat or plant oil sources which is suitable for food product and in pharmaceuticals; 3) kosher glycerol (99.5-99.7% purity) from plant oil sources which is suitable for use in kosher foods. Other purity grades not governed by USP/FCC (Food Chemical Codex) are also available in the market in cheaper price. However, crude glycerol, even at 80% purity, cannot be used by traditional oleo-chemical refiners because it would damage expensive pipe and storage equipment because of the impurities present (Ciriminna et al., 2014).

The global glycerol production in 2003 was 200,000 metric tons, which increased ten times in a decade, and reached about 2 million metric tons in 2013 and is expected to reach 6 million metric tons by 2024 (Ciriminna et al., 2014). During the last 10-15 years, with the increased glycerol production, the price of crude glycerol has declined significantly (~$0.1/kg), while that of pure glycerol is almost stable (~$1/kg) (Quispe et al., 2013). The biodiesel industry alone produced 66.2% of the total glycerol in 2011(Hazimah, Ooi and Salmiah 2003). The increase in glycerol production was not realized until 2005-06. At this time, several countries such as USA, Malaysia, Indonesia, India, China, and others started producing biodiesel which led to sharp increase in crude glycerol production. After 2007, the production of crude glycerol rapidly increased due to huge production of biodiesel by all these countries (Ayoub and Abdullah, 2012). The major global players in the glycerol market are European Union, United States of America and Southeast Asia. As there is growth of the biodiesel production in the countries like India, Canada, and South

America, it is likely that will impact the glycerol production in the coming future (Abdullah et al. 2009b).

Fig. 2 presents the fluctuations in the production and price of crude and pure glycerol. The increase in biodiesel production results in a subsequent increase in glycerol production from 0.7 million tons in 2002 to more than double (1.5 million tons) in 2011 (Quispe et al., 2013). The price of the purified glycerol was $1800/ton in 2006 which had fallen down to $800/ton in 2011 due to the recent oversupply of crude glycerol and the impurities present in crude glycerol (Quispe et al., 2013). To overcome this paradigm shift in the price of glycerol and make it a sustainable product, it has become essential to develop new markets and technologies for purification and convertion of glycerol to value added products (Zhou et al. 2008).

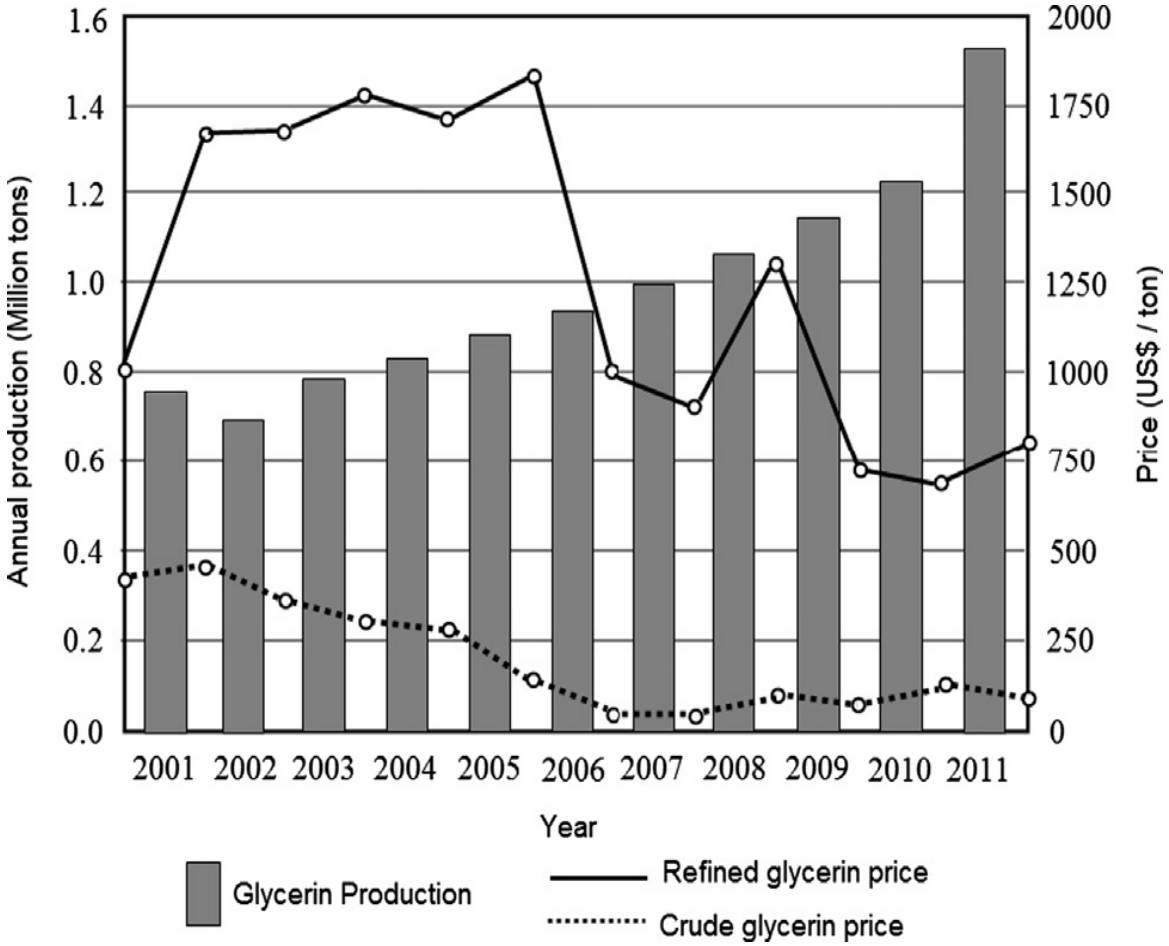

Fig. 5 Glycerol production and fluctuations in the pricing of refined and crude glycerol (Quispe et al., 2013)

The synthetic glycerol market has been hit very hard due to overproduction of glycerol by biodiesel industry. Dow chemical company, the sole producer of synthetic glycerol in United States in the tune of 140 million pounds has to close down the facility due to oversupply of glycerol in the

market. The position of the manufacturer of synthetic glycerol in Europe and south East Asia is also of similar kind (U.S. Soybean Export Council Inc., 2012).

Due to the high cost of purification and saturation of glycerol market, the price of crude glycerol is declining at a rapid pace which affects the cost of biodiesel production as well. This situation will continue as more biodiesel production facilities are starting. Today, the cost of biodiesel production is in the range of $0.17 to $0.42 per liter. Presently, glycerol stock in the market is increasing coupled with its decreasing price. As the glycerol market is oversaturated, the price of glycerol will continue to fall. There can be a possibility if glycerol prices may drop to a level that will not justify its use even as a burner fuel (Ayoub and Abdullah, 2012). Therefore, responsible authorities in biodiesel producing countries should take necessary proactive actions to stop subsidies for its production in order to reduce the overproduction of crude glycerol (Ayoub and Abdullah, 2012).

2. Purification of crude glycerol by physico-chemical treatment and dead-end membrane filtration in batch mode

(**Publication details:** R Dhabhai, E Ahmadifeijani, AK Dalai, M Reaney (2016) Separation and Purification Technology, 168, 101-106)

Objective: Optimization of glycerol purification proecss in batch system

Abstract

The presence of impurities decreases the calorific and economic value of glycerol. Thus, glycerol impurities must be greatly reduced if it is to be used as a fuel or feedstock for chemicals. A sequential procedure for crude glycerol refining that includes saponification, acidification, neutralization, membrane filtration, solvent extraction, and activated charcoal adsorption was investigated in the present work. Membrane filtration was studied at temperature and pressure ranges of 25-60°C and 50-350 kPa, respectively. A range of ultra-filtration (UF) and fine ultra-filtration (UFF) (1, 3, 5, 8, and 15 kDa) were utilized to obtain highly enriched glycerol. Membrane filtration at 60°C and 350 kPa using 1 kDa membrane, solvent and water evaporation and activated charcoal treatment produced the maximum concentration of glycerol (97.5%) observed. Acid value and free fatty acid (FFA) content of all treated samples were found to be <1%. Crude, enriched crude (purified) and ACS grade glycerol were characterized using FTIR and bomb calorimeter further confirmed the purity of obtained glycerol. The present study shows the potential of this treatment for purification of crude glycerol.

2.1 Materials and methods

2.1.1 Materials

Crude glycerol sample was obtained from Milligan Biofuels, Foam Lake, SK, Canada, while ACS grade glycerol (99.5% wt% purity) was purchased from Fisher scientific, Canada. Ceramic membrane discs DISRAM™ (diameter 47 mm; area 13.1 cm^2) composed of ZrO_2-TiO_2 with TiO_2 support and membrane disc holder were purchased from Tami industries, QC, Canada. All other chemicals were analytical grade unless otherwise stated.

2.1.2 Physico-chemical treatment of crude glycerol (step 1)

Crude glycerol physico-chemical treatments included sequential saponification, acidification, phase separation, and extraction. Crude glycerol was first diluted to about 10 wt% glycerol using methanol to reduce viscosity and improve the ease of operation. Then, KOH (12.5 M) was added to convert FFA to soaps (saponification) at 60ºC for 30 min with constant stirring till pH 12.0. Subsequently the alkaline mixture was acidified to pH 1.0 by addition of concentrated HCl. After acidification samples were stirred for 30 min at room temperature (25ºC) then left overnight in a separatory funnel to allow time for phase separation. Separation produced two phases with the upper layer being primarily FFA. The upper layer was decanted and bottom glycerol rich layer

was extracted by equal volumes of petroleum ether to remove residual FFAs. This was followed by neutralization of the glycerol rich layer with 12.5 M KOH. This treated feed was used for all membrane filtration experiments.

2.1.3 Membrane filtration of treated feed (step 2)

For membrane filtration of treated crude glycerol, a membrane filtration assembly was employed. The schematic of the setup is presented in Fig. 6.

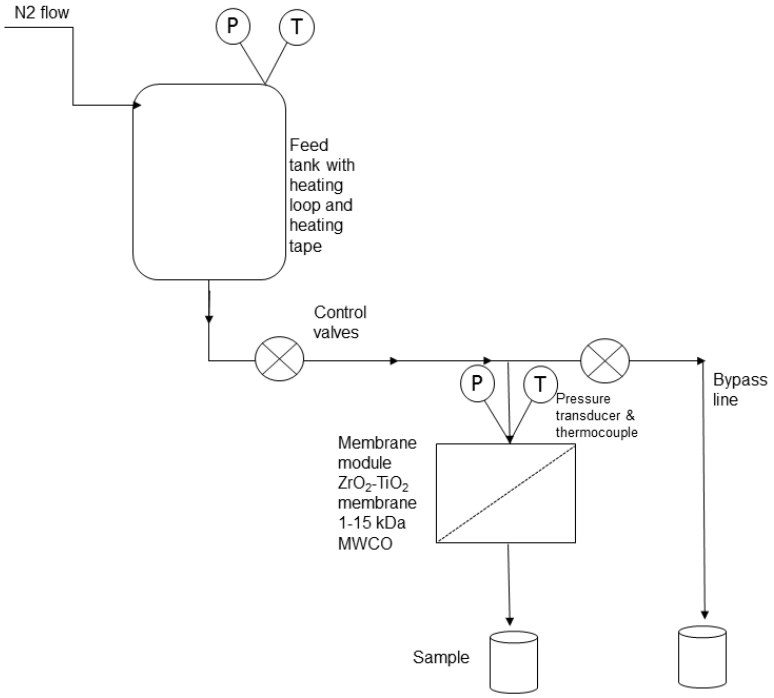

Fig. 6 Schematic of the membrane filtration setup

The apparatus consisted of a feed tank connected with the membrane module and a by-pass. Flow of treated feed in the stainless steel tubing was controlled by ball valves. Temperature control was achieved using a type K thermocouple (Omega) placed between the tubing and heating tape wrapped around the tubing. Temperature and pressure inside the feed tank and membrane module were monitored constantly and controlled by thermocouples (K type, Omega) and pressure transducers (Honeywell) connected to temperature and pressure monitors which were connected to PC using interface LabVIEW software via USB. The feed tank was connected to the nitrogen tank to maintain positive flow of feed in the line and to maintain the desired trans-membrane pressure to pass the filtered product. In order to ensure constant temperature in feed tank, a circulatory bath was also connected to the feed tank *via* a flow through a U tube. To study membrane filtration of treated feed, transmembrane temperature and pressure were varied in the range of 25-60ºC and 50-350 kPa, respectively (as the maximum pressure holding capacity of membrane module was 400 kPa). The details of membrane filtration experiments are presented in Table 3.

Table 3 Experiments carried out for membrane filtration study

Experiments	Pressure (kPa)	Temperature (°C)
1	100	25.0
2	225	42.5
3	225	42.5
4	350	42.5
5	100	60.0
6	225	42.5
7	225	60.0
8	225	25.0
9	50	42.5
10	350	60.0
11	225	42.5
12	225	42.5
13	350	25.0

Treated feed (obtained after step 1) was filled in the feed tank to about two-thirds of tank capacity (about 300-350 ml) and nitrogen was passed in the feed tank at the desire pressure and the tank was heated to the desired temperature. As the solution reached the temperature, valves were opened and feed was allowed to reach through the tubing to the membrane module. When the desired temperature and pressure were reached, the main valve was opened to allow flow through membrane module and a fixed volume of filtrate (15 mL) was collected.

2.1.4 Solvent and water evaporation and activated charcoal treatment (step 3 and 4)

Methanol and water were removed from all the treated and filtered samples using vacuum evaporator (Rotavapor®) for a fixed time to obtain about 3 mL of final purified sample. Samples were clear, did not scatter light, and light brown in color. Color and other impurities were removed by activated charcoal treatment was by mixing commercial granulated activated carbon in the ratio of 1: 10 (100 g/L) with constant stirring for 30 min at room temperature.

2.1.5 Analytical methods

Glycerol and methanol content was determined by gas chromatography (Agilent 7890A series) on a Stabil Wax column (30m× 250 µm× 0.5 µm; Restek Corp., USA) at 250°C, an FID detector at 300°C, nitrogen at 23 psi, and helium as carrier. Water content was determined by an automated Karl-Fischer coulometric titrator (Mettler Toledo DL32) using methanol for dilution as the titrator is sensitive to water content of maximum 5 wt%. Ash content was determined by burning 1 g of sample in muffle furnace at 750°C for 3-4 h. FFA (wt. %) and acid value (wt. %) were determined by acid base titration according to Lubrizol test procedure (TP-TM-001C). Fourier transform

infrared (FTIR) spectra were generated using a FTIR spectrometer (Bruker Vertex 70, MA, USA) with an ATR module. Each spectrum was the average of 16 co-addition of scans with a total scan time of 15 s in the IR range of 400–4000 cm^{-1} at 4 cm^{-1} resolution. Gross calorific (heating) value was determined by an oxygen bomb calorimeter (Parr bomb calorimeter 6400) by burning 1 g sample in a high pressure oxygen atmosphere within a stainless steel pressure vessel or bomb.

2.2 Results and Discussion

2.2.1 Composition of crude glycerol and treated feed

Crude glycerol obtained from the supplier was a dark brown liquid with a high pH (10-11) that was less viscous than pure glycerol. Its composition (as obtained from the supplier) was as follows (on wt% basis): glycerol 40; matter organic not glycerol (MONG) 55; moisture 5.5; and ash 4.9. MONG consisted of free fatty acid (FFA) as saponified fatty acids (SFA) 15%; fatty acid methyl ester (FAME) 10%; and methanol 30%. The ash content of crude glycerol is due to the salts from the unspent catalyst (KOH) which is also a part of SFA, while the water content may be due to the adsorption of moisture from the atmosphere during production processes (Kongjao et al., 2010). The MONG content was more than the glycerol content and the highest concentration of impurity., Crude glycerol samples were diluted with methanol to give a final glycerol concentration of about 10 wt% (confirmed by GC) for ease of operation.

2.2.2 Purification of glycerol by physico-chemical treatment

Saponification of free fatty acids with excess of stong alkali (KOH) resulted in the formation of saponified fatty acids (SFA) (Házek et al., 2010) according to the following equation (1)

$$R - COOCH_3 + KOH \rightarrow R - COOK + CH_3OH \ldots\ldots\ldots\ldots (1)$$

When HCl was added to saponified crude glycerol, it formed two distinct layers or phases – the FFA layer and the glycerol rich layer. As the FFA phase has lower density than glycerol phase (Pott et al., 2014), it forms the upper layer and there is clear distinction between the two layers. H^+ ions from the mineral acid converted soaps (SFA) to insoluble FFA and excess acid was neutralized with base in the crude glycerol to form salts (Manosak et al., 2011). In the present case, H^+ ions from HCl reacted with the basic soap to produce FFA. The Cl^- originating from ionized HCl combined with the K^+ arising from KOH and soaps, forming water soluble KCl. The reaction is presented in equation (2):

$$R - COOK + H^+ \rightarrow R - COOH + K^+ \ldots\ldots\ldots\ldots\ldots\ldots\ldots\ldots (2)$$

Generally, a third layer may be obtained in acidification phase depending on the acid used, which is the inorganic salt layer (at the bottom) (Kongjao et al., 2010), if the salt is insoluble or sparingly soluble in water. However, in the present case, as KCl is soluble in water (342 g/L at 20°C), the third layer was not found.

As the separation of FFA and glycerol rich phases is carried out by gravity sedimentation in a separatory funnel, mixing of the two phases may occur, when glycerol rich phase is neutralized with KOH after acidification any residual FFA and FAME in (that may come from FFA phase) be converted to soaps by reacting with KOH. This residual soap or SFA may increase the MONG or ash content of final enriched (purified) glycerol. This phenomenon has also been observed in previous studies (Kongjao et al., 2010; Manosak et al., 2011). This may be the reason, that physico-chemical treatment alone may not be sufficient to enrich glycerol to technical grade. The composition of the glycerol-rich layer and MONG content is highly dependent on the acid used and the pH of acidification (Manosak et al., 2011). Kongjao et al., (2010) reported that pH 1 favors glycerol yield and eliminates most contaminants. They further reported that increasing pH during acidification step leads to increased yield of the glycerol-rich layer and decreased inorganic salts and the free fatty acid phase (Kongjao et al., 2010). After physico-chemical treatments, glycerol yield of treated feed was found to be 88.6% wt., the water content was 2.9%, the acid value and FFA (%) was 1.1 and 0.6, respectively (shown in Table 2 in section 3.5). In a similar study, after the physico-chemical treatment of crude glycerol, Manosak et al., (2011) obtained a glycerol yield of 82.9%, ash 7%, water 8.5%, and 1.6% MONG (all wt%). The results obtained in the present study are better than that reported by Manosak et al., (2011).

2.2.3 Effect of membrane filtration of treated feed (obtained from step 1)

Ceramic membranes offer many advantages over polymeric membranes such as high chemical, mechanical and thermal resistance to degradation and show higher permeability rates and easier cleaning. Membrane performance is mostly affected by parameters including; membrane composition, temperature, pressure, velocity of flow, and interactions between feedstock components and the membrane surface (Atadashi et al., 2011). The parameters studied in the present work were membrane module temperature and pressure and membrane pore size (MWCO).

Temperature effects were studied in the range of 25-60°C at a fixed pressure of 350 kPa. Temperatures of <25°C were not chosen in the present work due to the significant increase in viscosity at lower temperature, Temperatures higher than 60°C may lead to methanol evaporation which is undesirable. It was assumed that even with the smallest pore size membrane (1 kDa), glycerol would not be retained due to its molecular size (~0.3 nm). Only impurities bigger than the particle size range of roughly 2-5 nm (such as fatty acids (Oleic acid >2 nm); oil droplet 40-80 μm; colloidal particles 1-1000 nm) will be retained by the membrane. Fig. 7 shows the data related to the effect of temperature on membrane filtration of treated feed. At 25°C, least glycerol yield was obtained after membrane filtration.

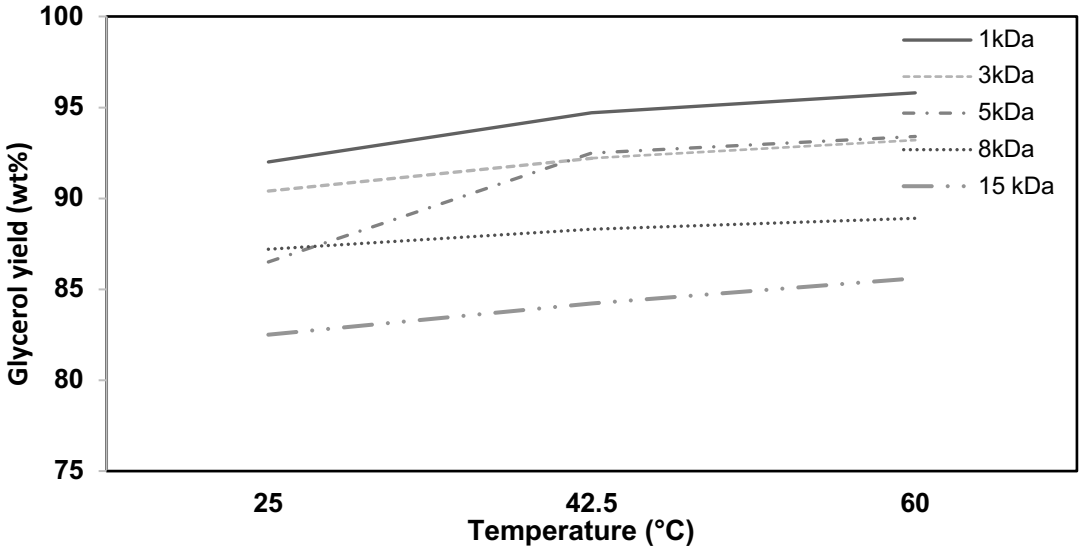

Fig. 7 Effect of temperature of membrane filtration on percent glycerol yield at fixed pressure of 350 kPa

Highest glycerol yield was obtained at 60°C, while at 42°C, the glycerol yield was comparable to that obtained at 60°C. The reason of this can be explained by the viscosity curve of glycerol with temperature which is presented in Fig. 8.

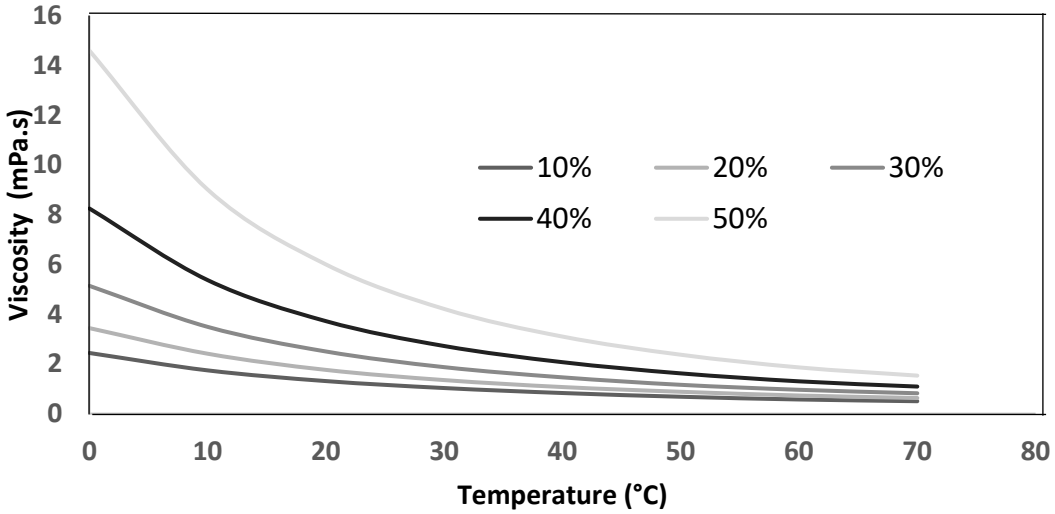

Fig. 8 Viscosity of aqueous glycerol solutions with increased temperature. (Drawn from the data. Source: Dow Chemicals, 2015)

At a temperature range of 40-60°C, the viscosity curve of glycerol reaches a plateau which suggests that the change in glycerol viscosity especially at 10wt% concentration is not significant in this temperature range. This may be the reason for similar membrane filtration performance i.e. similar glycerol yield at 42.5 and 60°C. Glycerol solution with lesser viscosity would be easily

passed through the membrane. This also explains inferior membrane performance at 25°C as the viscosity of glycerol is comparatively higher (~1.2 mPa.s) at 42.5°C, as compared to that at 25°C (~0.8 mPa.s) (DOW Chemicals, 2015). In experiments conducted at the same temperature, it can be seen in Fig. 8 that 1 kDa membrane produced greater glycerol yield than other membranes. With increased membrane pore size, decreased glycerol yield was obtained. This may be due to the incomplete filtration with increased pore size leading to impurities in filtrate and lesser relative glycerol content.

Pressure is the driving force in membrane separation processes such as MF and UF (Sdrula, 2010). The effect of pressure was studied at 100 and 350 kPa at a fixed temperature of 25°C. Due to the limitations of the membrane module (400 kPa maximum) pressure exceeding 350 kPa was not employed in the present work. Lower pressure of 50 kPa was not successful in purifying glycerol. Fig. 9 shows the data related to the effect of pressure on membrane filtration of treated feed.

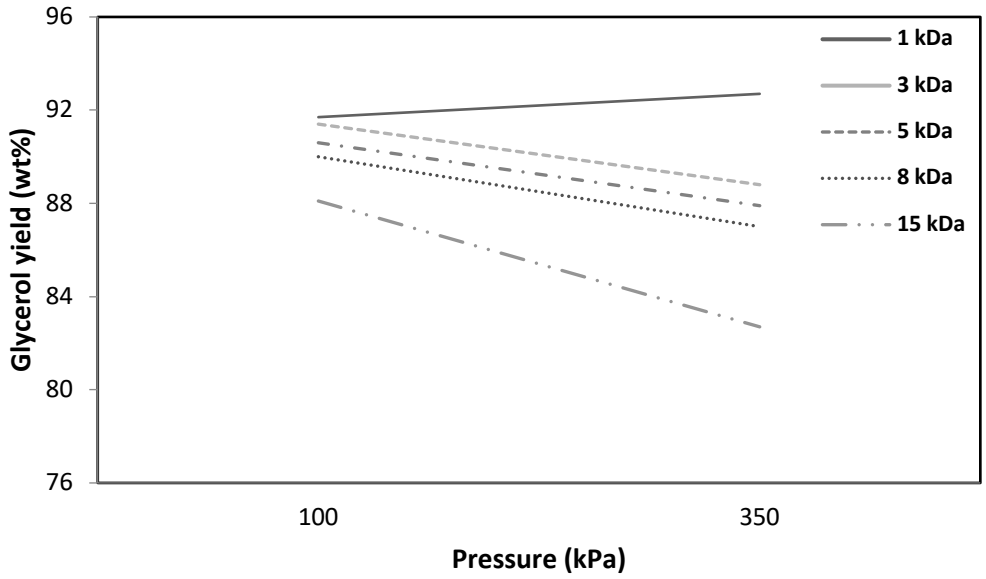

Fig. 9 Effect of pressure of membrane filtration on percent glycerol yield at fixed temperature of 25°C

At a lower pressure of 100 kPa, a higher yield of glycerol was obtained with the exception of 1 kDa membrane. Lower pressure also resulted in reduced flux through membrane as compared to that of 350 kPa. However, in the present study, flux was not determined and the focus of the study was to obtain higher yield of glycerol. With increased pore size of membrane at a fixed pressure, glycerol yield decreased, due to the increased concentration of impurities. As higher glycerol yield was obtained at the process conditions of 60°C, 350 kPa and 1 kDa MWCO membrane, these conditions can be considered most suitable for membrane filtration of treated feed.

2.2.4 Reduction in color and other impurities by activated charcoal treatment

In addition to color, adsorption on activated charcoal can also remove residual water, methanol and salt (Contreras-Andrade et al., 2015). The glycerol content is reported to remain unaffected by charcoal treatment, as the size of glycerol molecule (~0.3 nm) is higher than the pore size of activated carbon (AC) (0.1-0.3 nm) (Manosak et al., 2011). In the present study, the color of crude glycerol was dark brown which improved to light brown after the physico-chemical treatment and clear (colorless) solution similar to ACS grade glycerol was obtained after the treatment.

Improvement in relative glycerol content after membrane filtration and AC adsorption may have been achieved due to adsorption of impurities such as residual salt, methanol, and water on AC. It has been reported that with increased activated carbon dosage, color and impurity removal also increases. Manosak et al., (2011) reported that increasing the activated carbon dose from 65 to 100 g/L glycerol, led to the largest decrease in the ash content and at 200 g/L glycerol, almost all color was removed from the glycerol. In addition, they also obtained removal of some of the fatty acids such as lauric acid and myristic acid (Manosak et al., 2011). In the present work, a GAC concentration of 100 g/L was employed for AC treatment, which seemed appropriate for the treatment.

2.2.5 Characterization of crude and enriched (purified) glycerol to evaluate the effects of purification

The enriched (purified) glycerol samples after the treatment were characterized by FTIR which were compared with those of pure and crude glycerol (Fig. 10).

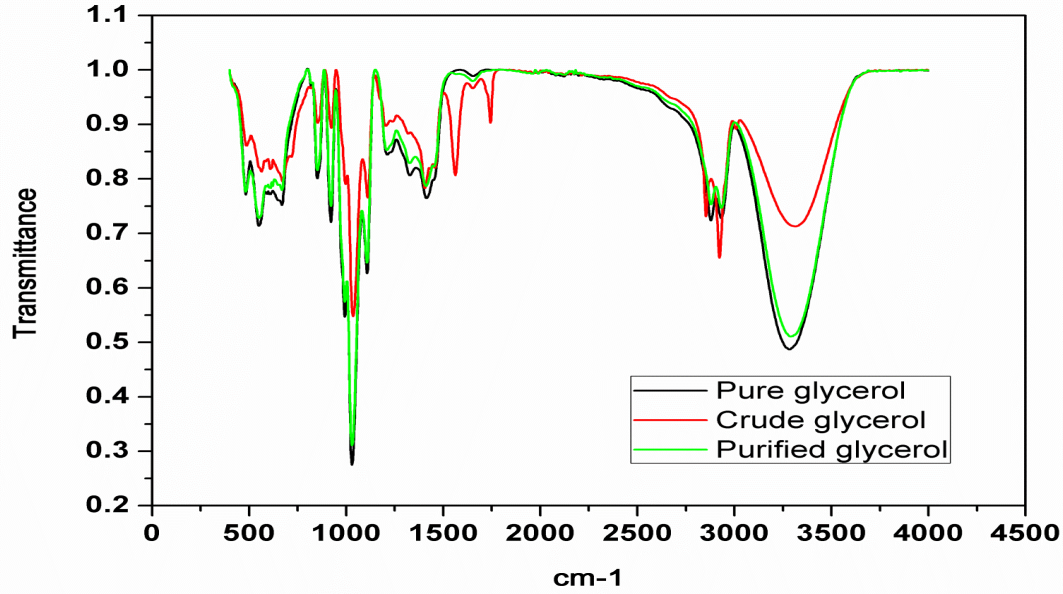

Fig. 10 Comparative FTIR spectra of crude, purified, and ACS grade glycerol samples

Similar FTIR spectra were obtained for ACS grade and enriched (purified) glycerol samples while there were clear distinction in spectra for crude glycerol owing to the impurities present in crude

glycerol. Broad peak at 3200-3400 cm^{-1} was obtained for all three glycerol samples, which is a characteristic of –OH stretching. For crude glycerol, relatively smaller peak was obtained. Two peaks at 2880 and 2930 cm^{-1} were due to –CH stretching, the later was more intense for crude glycerol. Some smaller peaks due to –COH bending were obtained at 1400-1460 cm^{-1}. Another peak was due to –CO stretching at 1450 cm^{-1} (primary alcohol) and intense peak at 1100 cm^{-1} (secondary alcohol) and –OH bond bending at 920 cm^{-1} (Tianfeng et al., 2013; Kongjao et al., 2010).

Small peaks for ACS grade and enriched (purified) glycerol at about 1550 and 1700 cm^{-1} are due to –C=O bond indicating very low ester of carboxylic acid or fatty acid in purified and ACS grade glycerol while a strong peak was obtained for crude glycerol (Tianfeng et al., 2013). Peaks at 2900, 1550, and, 1740 cm^{-1} indicate impurities in crude glycerol. The sharp band at 1550cm^{-1} represented the presence of soap COO^- (Isahak et al., 2013). The small band at about 2900 cm^{-1} indicated the presence of unsaturated C=C compound(s). The sharp peak at 1740cm^{-1} indicated the presence of C=O compound(s) of an ester or carboxylic acid of fatty acid (Kongjao et al., 2010). All these peaks were either not obtained or were very small for enriched (purified) and ACS grade glycerol samples.

Table 4 presents the comparison of physico-chemical properties between treated feed, ACS grade glycerol, and enriched (purified) glycerol. It shows the effects of physico-chemical treatment alone (treated feed) and in combination with membrane filtration and activated charcoal adsorption. Only representative samples are presented in Table 4.

Table 4 Glycerol compositional analysis after the treatment

Experimental conditions*	Glycerol concentration (wt%)	Water content (wt %)	Acid value	FFA (wt %)	Gross calorific value (kJ/kg)
ACS grade glycerol	99.7	<0.1	ND	ND	17678
3 kDa, 60°C, 350 kPa	84.7	3.6	1.1	0.6	16870
1 kDa, 25°C, 350 kPa	92.7	2.9	0.6	0.3	16865
1 kDa, 42.5°C, 350 kPa	96.6	2.2	0.6	0.3	16980
1 kDa, 60°C, 350 kPa	97.5	2.2	0.6	0.3	16949
5 kDa, 42.5°C, 350 kPa	91.1	2.7	0.6	0.3	16786
8 kDa, 42.5°C, 350 kPa	90.5	2.9	0.6	0.3	16876
15 kDa, 60°C, 350 kPa	88.3	2.9	1.1	0.3	16408
Treated feed	88.6	2.9	1.1	0.6	16808

*ND- Not determined

The water content of samples after the treatment was in the range of 2.2 to 3.6 wt%, which was found to be lower compared to that of crude glycerol (5.5 wt%). Acid value and free fatty acid content of all treated samples were in the range of 0.6-1.1% and 0.3-0.6%, respectively. The most important parameter, the glycerol content was found to be 88.6 wt%, after the physico-chemical treatment alone, and increased to a maximum value of 97 wt% after membrane filtration and activated charcoal adsorption. As glycerol is also a fuel, its calorific value stands out to be a very important characteristic for adjudging its purity. The calorific value of ACS grade glycerol was found to be 17,678 kJ/kg, while the calorific value of enriched (purified) glycerol was found to be as close as 95-96% of that of ACS grade glycerol (16,408-16,980 kJ/kg). These values are slightly lower than obtained by Thompson et al., (2006) for pure glycerol (~18,000 kJ/kg).

The physico-chemical treatment was successful in producing glycerol concentration of 88.6 wt% purity. The ash content in all the treated samples was found to be <1%. It has been reported that chemical treatment at a low pH is a better option as it can increase the glycerol yield and reduce the ash content in the recovered crude glycerin (Tianfeng et al., 2013). The results obtained in the present study suggest that this batch process is successful in producing technical grade glycerol (>95%). The enriched glycerol can be used as feedstock for the production of value-added chemicals such as glycerol carbonate and glycerol ethers.

3. Purification of crude glycerol by physico-chemical treatment and tubular membrane filtration in semi-continuous mode

(Manuscript in preparation)

Objective: Optimization of crude glycerol purification in semi-continuous mode.

Abstract

Crude glycerol was purified by a combination of physico-chemical purification processes and semi-continuous membrane filtration using a 5kDa ultrafiltration membrane. To study membrane filtration of treated glycerol feed, temperature, pressure, and flow rate were studied. A maximum glycerol purity of 85% was obtained from crude glycerol of 40% purity after the physico-chemical treatment and membrane filtration at a temperature range of 42.5-50^{o}C, low to moderate flow rate of 50-100 mL/min and low to moderate pressure of 50-150 psi.

3.1 Materials and methods

3.1.1 Materials

Crude glycerol samples were obtained from Milligan Biofuels, Foam Lake, SK, Canada, while ACS grade glycerol (99.5% wt. % purity) was purchased from Fisher scientific, Canada. All the chemicals used in the present study were analytical reagent grade and used without any purification.

Physico-chemical treatments was carried out as described in Section 31.

3.1.2 Membrane filtration of treated feed

Ultrafiltration membranes can filter out residual matter organic non-glycerol (glycerides, FFAs, etc) and some salts that are left in treated glycerol. In the first set of experiments in this phase, ultrafiltration membrane is used in batch mode while in the present work, tubular UF membrane in semi-continuous mode have been used. The variables are temperature, pressure, and flowrate and their effect on glycerol yield or purity during membrane filtration was observed. Temperature is varied from 25^{o}C to 60^{o}C, flow rate from 50 ml/min to 200 ml/min while, pressure is varied from 50 psi to 200 psi. The specific combinations of these three parameters are based on a central composite design (CCD). The schematic of the membrane filtration apparatus is presented in Fig. 11.

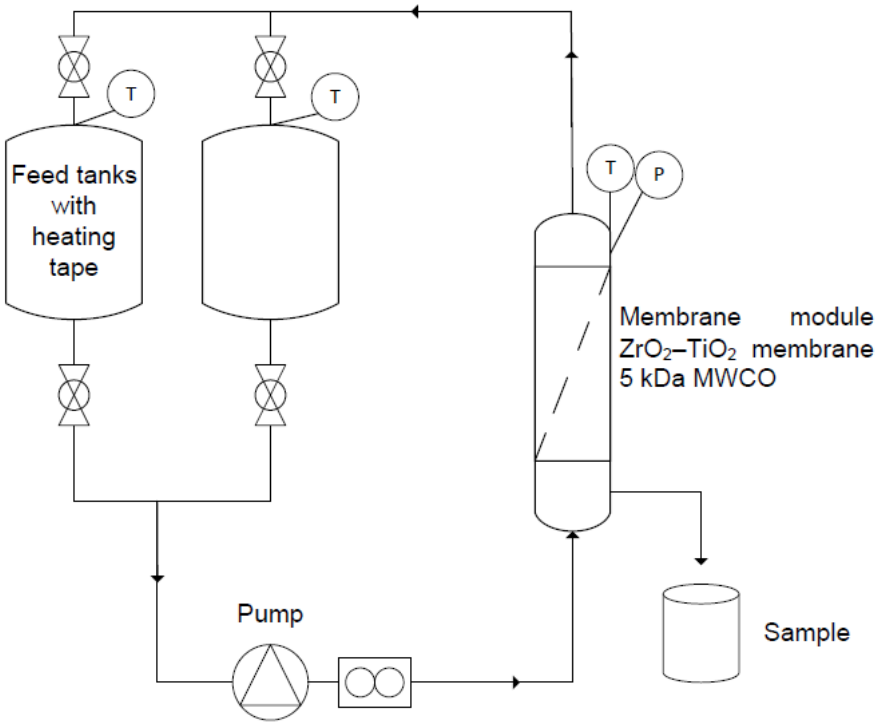

Fig. 11 Schematic of the tubular membrane filtration setup

The apparatus consisted of a two feed tanks connected with the membrane module (dead-end filtration) through a feed pump. Flow of treated feed in the stainless steel tubing was controlled by ball valves. Temperature control was achieved using a type K thermocouple (Omega) placed between the tubing and heating tape wrapped around the tubing. Temperature and pressure inside the feed tank and membrane module were monitored constantly and controlled by thermocouples (K type, Omega) and pressure transducers (Honeywell) connected to temperature and pressure monitors which were connected to PC using interface LabVIEW software via USB. The flow pattern in feed tanks was such that the purified liquid can either go to the same or different tank after membrane filtration. As both the tanks were independently connected to the pump. To study membrane filtration of treated feed, transmembrane temperature and pressure were varied in the range of 25-60ºC and 350-1400 kPa, respectively. The details of membrane filtration experiments are presented in Table 5. Preliminary membrane filtration is carried out using ultrafiltration membrane in batch mode to establish optimization trends (for temperature, pressure and flow rate) and then the trends will be used to choose appropriate conditions for optimization in semi-continuous mode.

Table 5 Experiment design for membrane filtration of treated feed

Exp. No.	Temperature	Pressure	Flow rate
1	25	50	50
2	60	50	50
3	25	200	50
4	60	200	50
5	25	50	200
6	60	50	200
7	25	200	200
8	60	200	200
9	25	125	125
10	60	125	125
11	42.5	50	125
12	42.5	200	125
13	42.5	125	50
14	42.5	125	200
15	42.5	125	125
16	42.5	125	125
17	42.5	125	125
18	42.5	125	125
19	42.5	125	125
20	42.5	125	125

3.1.3 Finishing steps

The third stage of the purification is adsorption with activated charcoal to improve glycerol color and purity by extracting color and free fatty acids. Adsorption using activated carbon is used as a finishing step in glycerol purification to reduce color and fatty acids. Increasing the dose of activated carbon has a significant effect on the color removal in refined glycerol. Up to 99.7% reduction in color is achieved using a high dose of activated carbon during glycerol purification (~200g/L activated carbon). Activated carbon removes from glycerol some of the fatty acids such as lauric and myristic acids while it may not remove oleic acid, palmitic acid and stearic acid. Some of the chemicals used to activate carbon are KOH, K_2CO_3 and H_3PO_4 (Ardi et al., 2015).

The final stage in the glycerol purification process after charcoal adsorption is water and methanol evaporation from glycerol to get the sample ready for characterization and analysis. This is done by heating the glycerol above the boiling points of water and methanol to vaporize them before glycerol is analyzed for purity using various characterization and analytical techniques. Care is taken not to burn glycerol samples.

3.1.4 Analytical methods

The analytical methodologies were same as described in Section 3.1.

3.2 Results and Discussions

In a previous study, we described that the combined physico-chemical treatment and dead-end membrane filtration is successful in purifying crude glycerol to a purity of >95%. As it was a dead-end filtration, the system was limited in its volume handling capability and the membrane needed to be replaced or requires frequent cleaning. Owing to these shortcoming of the system, in the present work, semi-continuous membrane filtration was coupled with the physico-chemical treatment to evaluate the efficiency of the process and to see the effect of the process. In addition, as glycerol purification involves multiple unit operations, a detailed techno-economic analysis of the process was carried out to determine economic feasibility and its profitability.

3.2.1 Effect of physico-chemical treatment on glycerol purity

As the crude glycerol contained FFA, soaps (in the form of saponified fatty acids), methanol, water and other colloidal impurities, physico-chemical treatment, which was based on the combined effect of temperature and chemical reaction, was employed. The enrichment of glycerol (%) after each stage of physico-chemical treatment is presented in Table 6. These are the average of glycerol percentage for >40 batches of treated glycerol after solvent removal.

Table 6 Enrichment of glycerol after each stage of physico-chemical treatment

Stage of physic-chemical treatment	Glycerol* % (v/v)	Methanol % (v/v)	Water % (v/v)
Crude glycerol	40.0	30.0	5.0
Saponification-acidification and Overnight separation	68.5	0	2.5-4.0
Petroleum ether extraction	75.0	0	2.5-4.0
Toluene extraction	78.5	0	2.5-4.0
Neutralization**	75.0	0	4.0-8.0

*Average of glycerol percentage for 38 batches of treated glycerol after solvent removal.

** Neutralization reduces the glycerol purity slightly due to water created in the reaction.

As it can be seen, after the treatment, glycerol increased from 40% initial to about 78%. Maximum impurities gets removed during this phase. Glycerol yield slightly decreased after neutralization because of formation of water during the reaction of HCl and KOH. It was also determined that after each stage how much of impurities are removed from crude glycerol by HPLC analysis of top layer of different batches and the results are presented in Table 7.

Table 7 Removal of impurities during physico-chemical treatment

Sample*	Triglycerides (vol. %)	Diglycerides (vol. %)	Mono glycerides (vol. %)	Free fatty acids (vol. %)	Esters (vol. %)
Petroleum ether extraction	0.58	0.99	0.41	3.16	4.43
Toluene extraction	0.31	1.27	2.11	2.91	0.00
Petroleum ether extraction (2X)	0.04	0.27	0.01	0.87	0.34
Toluene extraction (2X)	0.01	0.02	0.02	0.14	0.02
Total	0.93	2.55	2.55	7.08	4.79

*No glycerol was obtained in the top layer in any experiment

As it can be seen, >90% of impurities were removed in the first round of solvent extraction. However, to remove maximum impurities during the physico-chemical phase, second round of treatment was employed. About 90% of solvent was recovered after the process and was used in the further experiments.

3.2.2 Effects of operating parameters in membrane filtration process on glycerol purity

The physico-chemical treatment was only able to enhance the glycerol purity to about 75%, hence to obtain purified glycerol of up to 90% or more purity, membrane filtration studies were carried out. It was established in the previous study that the membrane filtration operating parameters have a strong and beneficial effect on glycerol purity. Effect of parameters on glycerol purity (yield) is presented in Fig. 12-14.

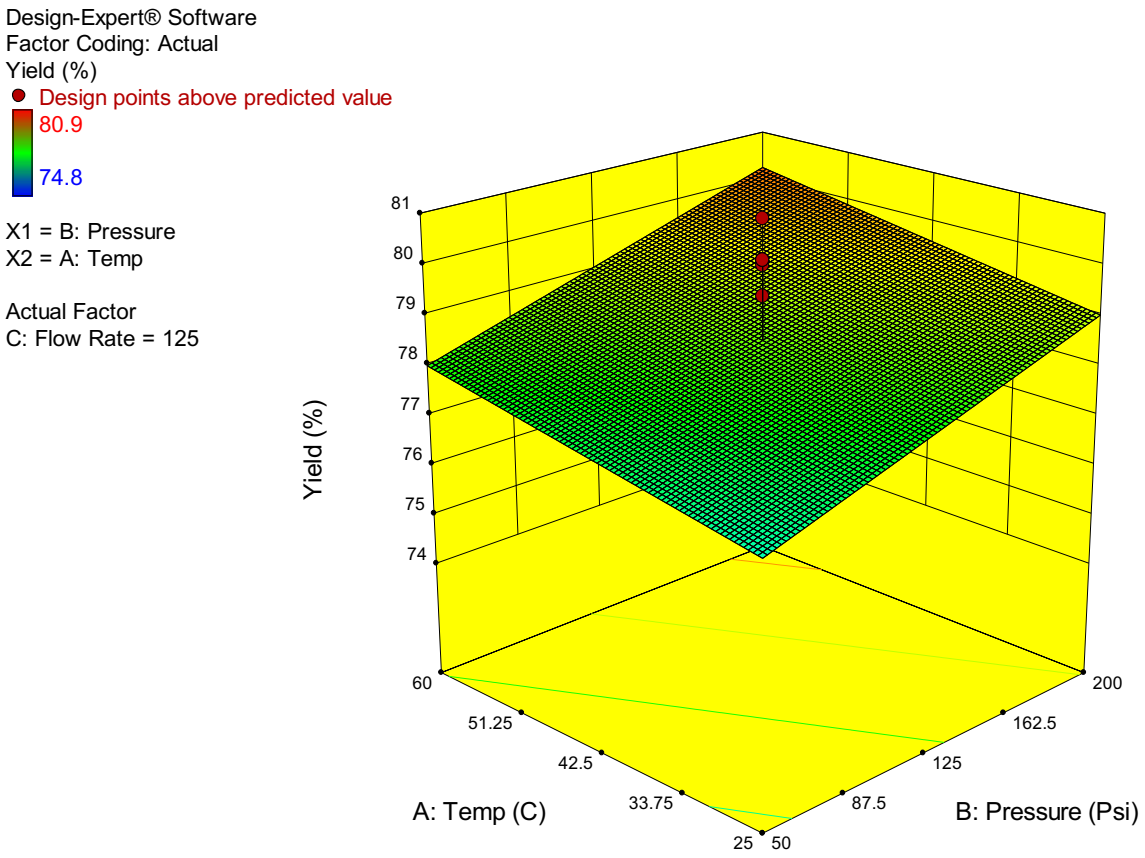

Fig. 12 Response surface plot of yield vs temperature and pressure

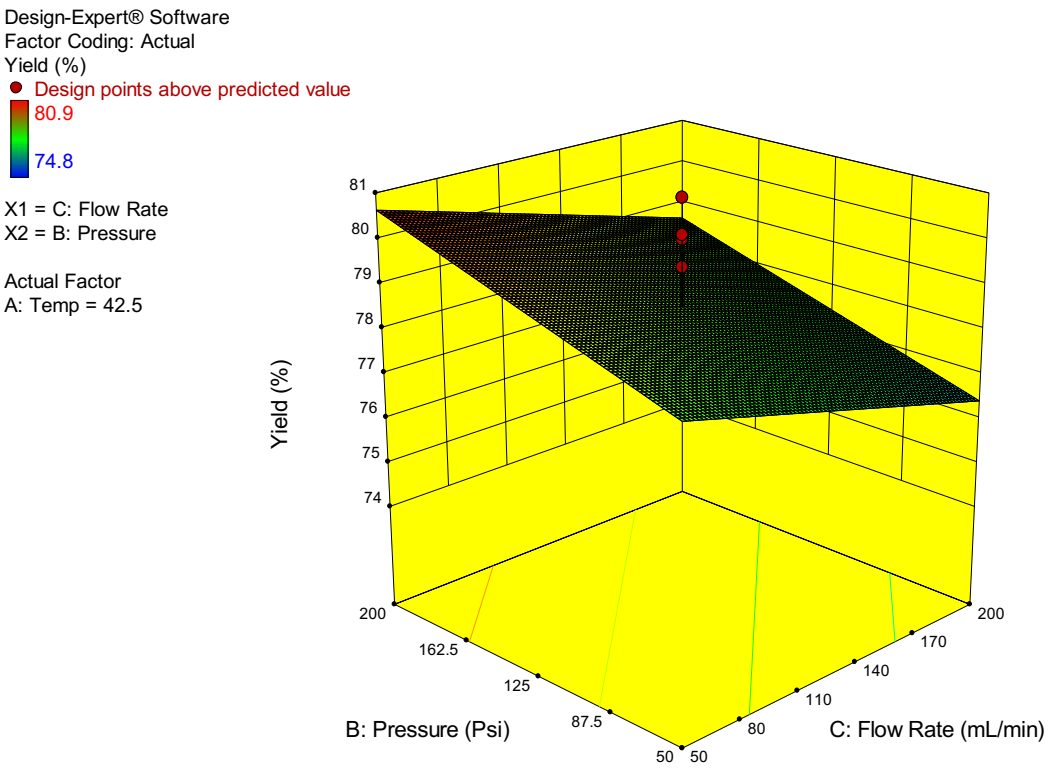

Fig. 13 Response surface plot of yield vs pressure and flow rate

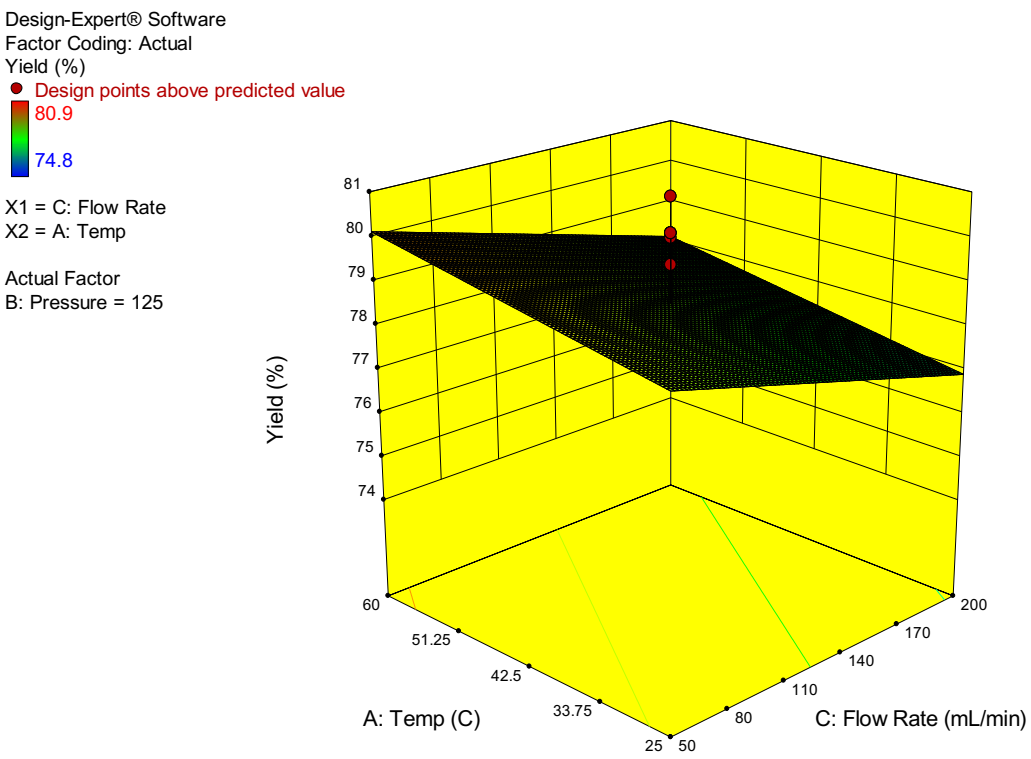

Fig. 14 Response surface plot of yield vs temperature and flow rate

The above response surfaces were prepared based on a central composite design (CCD) of experiment. From the response surface relating pressure, temperature and glycerol yield, it can be seen that moderate temperatures (42.5 – 50^{o}C) and moderate pressure (100-150Psi 700-900 kPa) give better glycerol yield results. In the response surface relating flow rate, pressure and yield, moderate flow rate (<=125mL/min) and moderate pressure (100-150Psi; 700-900 kPa) give best glycerol yield.

In terms of the model that best describes the effect of these three parameters (temperature, pressure and flow rate) on the response (glycerol yield), a linear model is the most appropriate. On the basis of sequential sum of squares from statistical analysis, a linear model or a mean model is suggested because its additional terms are significant. When choosing a model on the basis of lack of fit tests, a linear model is still suggested by the statistical analysis as this model has the most insignificant lack-of-fit (p-value = 0.0007). Linear model is also the one maximizing R-square and has a standard deviation of 1.94.

Activated carbon adsorption was employed as a finishing step to further improve glycerol purity as it adsorbs residual organic compounds like lauric acid and myristic acid in between its pores or on the pore surface. Organic compounds smaller than the pore sizes of activated carbon get

absorbed between its pores while those the same in size with the pores are adsorbed on the pore surface. Treatment with activated carbon further removes residual fatty acids and impurity colour in glycerol. Up to 99.7% reduction in colour is achieved using a high dose of activated carbon during glycerol purification (~200g/L activated carbon). Activated carbon removes from glycerol some of the fatty acids such as lauric and myristic acids while it may not remove oleic acid, palmitic acid and stearic acid. Some of the chemicals used to activate carbon are KOH, K_2CO_3 and H_3PO_4 (Ardi et al., 2015).

4. Catalytic conversion of glycerol to glycerol ethers

Objective: Utilization of purified glycerol to prepare value added chemicals such as glycerol carbonate, and glycerol ethers by using novel heterogeneous catalysts.

Abstract

The catalytic conversion of glycerol to value added chemicals and application of glycerol as biofuel are discussed. A solid acid (heterogeneous) catalysts for etherification of glycerol was developed. These zeolite based acid catalysts are highly active and the catalytic activity of these catalysts is tested in bench scale batch reactors. A 55% TPA (12-Tungstophosphoric acid)/H-β catalyst yielded 100% conversion, when 2.5 (w/v) % catalyst and 1:5 glycerol to tert-butanol (TBA) molar ratio were used at 120°C, reaction pressure of 1 MPa and reaction time of 5 h. Later the same catalyst was used for co-production of biodiesel and glycerol-ether, and the mixture of biodiesel and glycerol-ether is called biofuel. The fuel properties analysis indicates that biofuel has better fuel properties as compared to those for biodiesel. Our techno-economic analysis indicates that co-production of biodiesel and glycerol-ether is environment friendly.

4.1 Materials and methods

Unrefined green seed canola oil (4.25 wt% FFA) was obtained from Milligan Biotech Inc., Foam Lake, Saskatchewan, Canada. Commercial grade NH_4-β was purchased from ZEOLYST, PA, USA. A 12 - Tungstophosphoric acid (TPA) and *tert* –Butanol (TBA) were purchased from Alfa-Aesar, MA, USA. Glycerol was purchased from EMD Chemicals, Mississauga, Ontario, Canada.

Commercial grade NH_4-β was calcined at 550°C for 6 h to acquire H-β form. TPA impregnated H-β was prepared as follows: Calcined H-β zeolite was added into the solution of calculated amount of TPA. After stirring at room temperature, the samples were oven dried at 110°C for 12 h and calcined at 350°-850°C for 6 h. These catalysts were designated as X%TPA/S (T), where S represents the support, X represents wt% loading and T represents the calcination temperature in degree Celsius. However, throughout the work, symbol X%TPA/S was used for those catalysts, which were calcined at 450°C.

The synthesized catalysts BET surface area and pore size analysis were performed using Micrometrics adsorption equipment (Model ASAP 2000). The catalysts were heated at 200°C in a vacuum of 5×10^{-4} atm before the analysis. The surface area was calculated from the isotherms using Brunauer-Emmett-Teller (BET) method. The pore diameter and pore volume was calculated using BJH method from desorption branch of the isotherms. Raman spectra of the catalyst were recorded on powder samples at room temperature with a Renishaw system 2000 spectrometer (785 nm). The X-ray photoelectron spectroscopy (XPS) study was carried out at Canadian Light Source. The photon energy used for this study was 235 eV with the total energy resolution of 70 meV. All spectra were collected by Scienta SES100 spectrometer. X-Ray absorption spectra (XAS) were

recorded on HXMA beam-line at Canadian Light Source Inc., Canada, utilizing synchrotron radiation of 5-40keV and100 mA current. W L_{III} data were recorded both in transmission and fluorescence mode employing a Lytle detector typically over 45 min. For EXAFS analysis, the spectra were extracted by utilizing the cubic spline method and normalized to the edge height. The k^3-weighted EXAFS oscillation was Fourier transformed into r space using ATHENA software. Curve-fitting analysis was performed for the W=O and W-O_{ext}-W with the range between r = 1.0 and 2.0 Å using ARTHEMIS software. Temperature programmed desorption of ammonia (TPD) was conducted using Quantachrome (USA) instrument. In a typical experiment, at first 200 mg of each sample was pretreated in He (Helium) at 550° C for 1 h. The sample was later cooled to room temperature in flowing He and saturated with 1% NH_3/N_2 (v/v) mixture at a flow rate of 30 mL/min for 120 min. Then the spectra were recorded between 100°C to 750°C, with a temperature ramp of 10°C /min.

Etherification of pure glycerol reaction was also performed in the Parr reactor (Parr Instrument Co., ILL, USA) and the inert atmosphere was maintained with N_2 using optimized stirring speed of 800 rpm. The catalyst screening studies were performed with different loadings of TPA in H-β by maintaining the process conditions at 120^{0}C, 1 MPa, 1:5 molar ratios (glycerol/TBA), 2.5% (w/v) catalyst loading with respect to the reaction volume, and 800 rpm for 5 hours. The effects of various reaction parameters e.g. TPA loading in catalysts, catalyst loading in reaction mixture, temperature and molar ratio (glycerol: TBA) were studied to achieve one of the best conditions for glycerol ether production.

For etherification reaction, TBA was taken in excess in the reaction solution, and the conversion was based on the limiting reactant, glycerol. Samples were analyzed using a GC (Hewlett Packard 5890 series II) equipped with a stabil wax column (length 30 m, internal diameter 0.25mm and width 0.1μm) and a FID detector. The analysis was started at 40^{0}C, heated up to 240^{0}C with 20^{0}C/min ramp rate and kept at 240 for 5 minutes. The injector and detector temperatures were maintained at 280^{0}C.

$$\% \text{ Conversion of glycerol} = \{(\text{Initial Concentration} - \text{Final Concentration})/ \text{Initial Concentration}\} \times 100\% \quad \ldots(1)$$

$$\% \text{ Selectivity of Mono, Di or Tri Tert- Butyl Glycerol Ether} = \{(\text{Concentration of Mono, Di or Tri ether})/ \text{Concentration of (mono + di + tri) ether}\} \times 100 \quad \ldots(2)$$

$$\text{Ether Yield} = \text{Conversion} \times \text{Selectivity} \quad \ldots(3)$$

Later, this condition was used for etherification of crude glycerol produced from the transesterification of green seed canola oil in the same reactor vessel. In a typical sequential transesterification and etherification reaction, after finishing the transesterification reaction using the optimum reaction conditions, TBA was added for etherification of the glycerol derived from

the Green Seed Canola (GSC) oil as a byproduct of the methyl ester, and the experiments were performed at the best reaction conditions determined previously. Then the combined biofuel (GSC biodiesel + GSC glycerol-ether) properties were evaluated and compared against the pure biodiesel ASTM standard.

4.2 Results and Discussion

Table 8 depicts the textural properties of the different loadings of TPA in H-β zeolite. It depicts that with the increase in the loading, the micropore area, BET surface area, pore diameter, pore volume and surface density increase. It also depicts that the normalized BET surface area (per g of β zeolite) changes with the variation of TPA loading, which indicates that, the β zeolite structure changes with the TPA loading.

Table 8 Textural property of TPA/H-β catalysts

Sample	BET surface area (m^2/g)	Pore volume (cc/g)	Micropore area (m^2/g)	Normalized BET surface area (m^2/g - β)	Average Pore Diameter nm	Surface Density ($/nm^2$)[a]
25% TPA/ H-β	471	0.14	387	628	6.13	0.11
35% TPA/ H-β	233	0.05	168	359	3.82	0.31
45% TPA/ H-β	263	0.06	187	477	4.08	0.36
55% TPA/ H-β	297	0.24	196	661	9.84	0.39
65% TPA/ H-β	334	0.39	211	954	13.0	0.41

[a]Surface density = $[(WO_3\%/100) \times 6.023 \times 10^{23}]/[F.W. \times \text{BET surface area} \times 10^{18}]$ (Papai et al. 1994)

Fig. 15 and 16 show the Raman spectra of the β zeolite, and different loadings of TPA impregnated on H-β zeolite in the Raman shifting range of 100 – 600 cm^{-1} and 600-1100 cm^{-1}respectively. Raman scatterings at 464 cm^{-1}; 340 cm^{-1} (interlayer), 312 cm^{-1}(intralayer) and 396 cm^{-1}, 423 cm^{-1}, represent T-O_4 (T = Si or Al) tetrahedra of the four, five (intra layer and interlayer) and six membered ring of H-β respectively. Upon TPA impregnation the peak representing T-O_4 (T = Si or Al) tetrahedra of the four membered ring appears at higher wave number as compared to that for H-β, indicating the weakening the bonds of the 4 membered ring. On the other hand, peaks representing T-O_4 (T = Si or Al) tetrahedra of the five and six membered ring appear at lower wave

number as compared to that for H-β, indicating contraction of the bonds of the 5 and 6 membered ring (Fig. 12). Fig. 15 depicts that the Keggin structure of TPA is intact clearly up to 55% loading, when impregnated, by showing signature scattering pattern of TPA approximately at 1010 cm^{-1} (P-O in the central tetrahedron) and 989 cm^{-1} (terminal W=O). It also depicts that up to 55% TPA loading, peak approximately at 805 cm^{-1} (W=O stretching) and 711 cm^{-1} (W-O-W stretching) are observed, which arises probably due to the strong interaction of TPA Keggin structure with the zeolite structural alumina. Above 55% loading, very weak intensity of these peaks indicates the absence of strong interaction of TPA Keggin structure with the zeolite structural alumina. However, in all the cases, signature scattering pattern of TPA approximately at 1010 cm^{-1} (P-O in the central tetrahedron) and 989 cm^{-1} (terminal W=O) are observed.

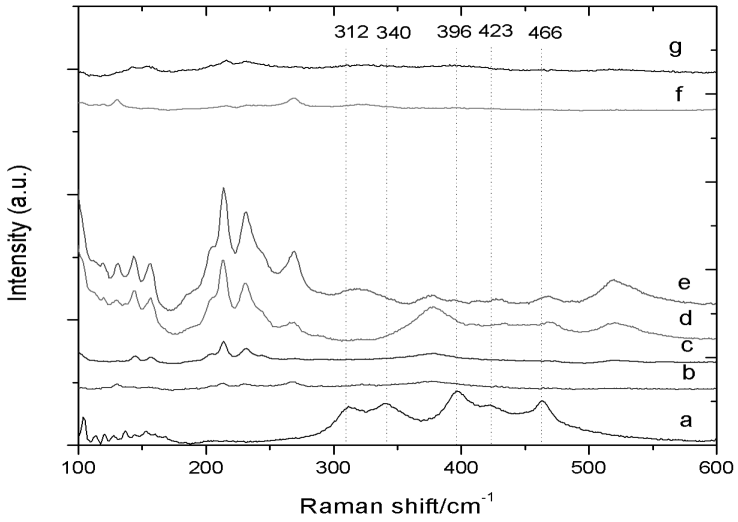

Fig. 15 Raman spectra of different amount of TPA loaded β: (a) H-β, (b) 25% TPA/H-β, (c) 35%TPA/H-β, (d) 45% TPA/H-β(e) 55%TPA/H-β, (f) 65% TPA/H-β and (g) 75% TPA/H-β

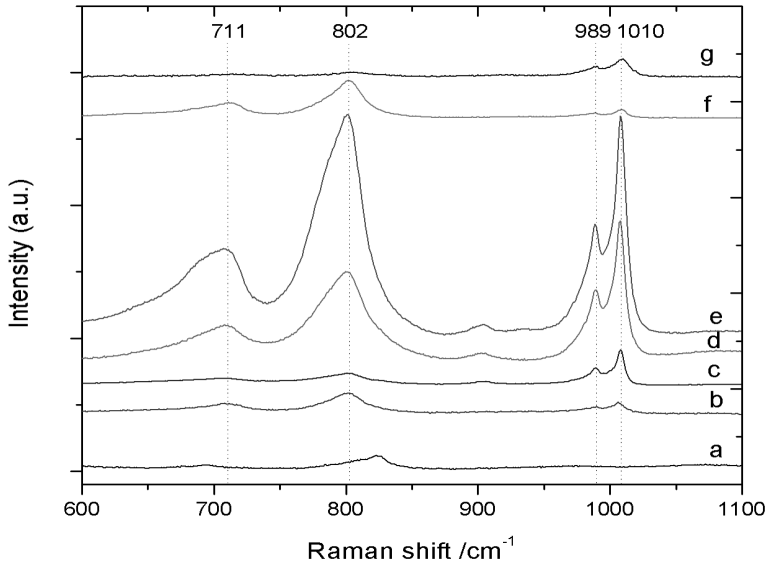

Fig. 16 Raman spectra of different amount of TPA loaded β: (a) H-β, (b) 25% TPA/H-β, (c) 35%TPA/H-β, (d) 45% TPA/H-β,(e) 55%TPA/H-β, (f) 65% TPA/H-β and (g) 75% TPA/H-β

Silica 2p depicts the peak to be formed approximately at 104 eV. The movement to higher binding energy refers to the shorter Si-O bonds whereas the lower binding energy refers to the elongated Si-O bonds and in the vicinity to the distorted [AlO_4^-] component of the zeolite framework. Upon TPA impregnation, Si (2p) peaks are to be found at around 101 eV and 108 eV (Table 4). The Full Width Half Maximum (FWHM) of the peak at 101 eV increases with the TPA loading indicating the creation of more elongated Si-O bonds and in vicinity to the distorted [AlO_4^-] component of the zeolite framework. Besides, the FWHM of the peak at 108 eV decreases with the TPA loading up to 55% TPA, beyond 55% loading, the FWHM of the peak at 108 eV increases (Table 4). The Al (2p) binding energy approximately at 74 eV corresponds to Al in IV-fold site β zeolite. Upon TPA impregnation, the FWHM of Al (2p) binding energy peak remains almost same up to 55% TPA loading, which increases for 65% TPA loading (Table 9). This increase in FWHM is an indication of the existence of the other co-ordination states of alumina when 65% TPA loading is used.

Table 9 The binding energy and FWHM of silica and alumina in the zeolite structure

Sample	Si (2P)		Al (2P)
	FWHM (at 101 eV) (eV)	FWHM (at 108 eV) (eV)	FWHM (at 74 eV) (eV)
H-β	-	6.9	4.1

45% TPA/H-β	1.8	3.3	4.7
55% TPA/H-β	1.9	3.3	4.4
65% TPA/H-β	2.1	4.3	8.6

The coordination number of W=O and W-O_{ext}-W bonds in TPA, 55%TPA/H-β, 65%TPA/H-β are found to be identical (Table 10). However, with an increase in TPA loading, the bond length of W=O decreases and the bond length of W-O_{ext}-W increases as compared to pure TPA (Table 5). The fitted W L_{III} EXAFS spectra of the 55%TPA/H-β sample are depicted in Fig. 17. The figure depicts the corresponding radial distribution functions for this material. The pattern of change in bond length is an indication of distortion in TPA kegging structure with an increase in TPA loading, especially for 65% TPA loading.

Table 10 Structural parameters derived from fitted EXAFS for supported and bulk TPA samples

Samples	Parameters	Coordination environment	
		W=[O]	W-[O_{ext}]-W
Pure TPA	C.N.	1	4
	r (^{0}A)	1.88	1.97
	R-factor	0.008	0.008
55% TPA/H-β	C.N.	1	4
	r (^{0}A)	1.62	1.98
	R-factor	0.01	0.01
65% TPA/H-β	C.N.	1	4
	r (^{0}A)	1.54	2.14
	R-factor	0.04	0.04

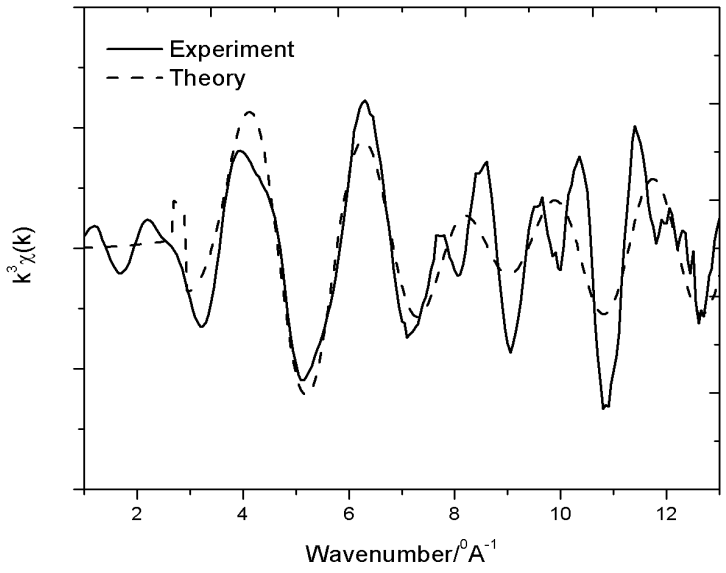

Fig. 17 (a) Fitted W L_{III} EXAFS of 55%TPA/H-β

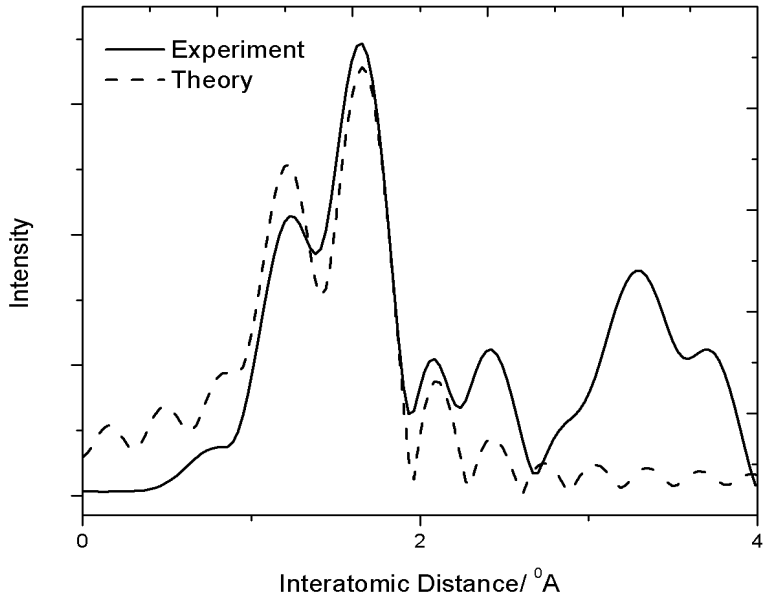

Fig. 17 (b) Fitted Redial distribution function (RDF) of 55%TPA/H-β

Fig. 18 depicts the NH_3-TPD results of different loadings of TPA on H-β zeolite. It depicts that the intensity of the low-temperature desorption peak (indicative of weak Brønsted acidity) increases with the increase in the loading. However, the high temperature peak indicating strong acidity diminishes beyond 55% loading, which is in agreement with the conclusion obtained from the Raman spectra, XPS binding energy pattern and distortion of TPA Keggin structure analyzed through EXAFS analysis.

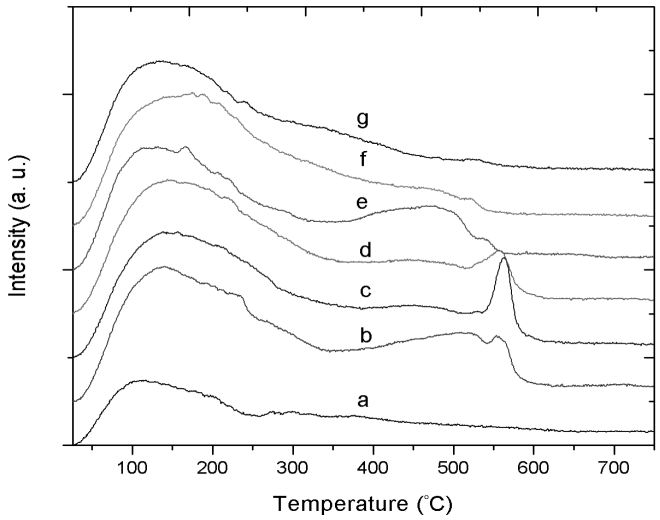

Fig. 18 NH_3-TPD of different amount of TPA loaded β: (a) H-β, (b) 25% TPA/H-β, (c) 35%TPA/H-β, (d) 45% TPA/H-β,(e) 55%TPA/H-β, (f) 65% TPA/H-β and (g) 75% TPA/H-β

Table 11 depicts the catalytic activity of different loading of TPA in H-β zeolite. It depicts that the conversion of glycerol reaches 100% for 45-65% TPA loading, when the etherification reaction is carried out at 120°C, 1 MPa, 1:5 molar ratio (glycerol: TBA) and 800 rpm for 5 hours. However, 55% TPA loading on H-β produces highest yields of (DTBG+TTBG) compared to those for 45% and 65% TPA loadings. Both the acid site strength and the porosity or pore volume limitation affect the catalytic activity. A 55% TPA loading on H-β has an optimum combination of acid site strength and porosity compared to those of 45% and 65% TPA loadings is responsible to obtain the highest combined yield of DTBG and TTBG.

Table 11 Effect of TPA loading on etherification reaction (2.5 (w/v)% catalyst, 120°C, 1 MPa, 1:5 molar ratio (glycerol: TBA) and 800 rpm for 5 h)

TPA loading on H-β zeolite (wt%)	Conversion of glycerol (%)	Yield of MTBG (wt%)	Yield of DTBG (wt%)	Yield of TTBG (wt%)	Yield of (DTBG+TTBG) (wt%)
45	100	31.1	40.6	28.3	68.9
55	100	7.9	13.5	78.6	92.1
65	100	23.1	4.6	72.3	76.9

Table 12 depicts the effects of catalyst loading on etherification reaction. It depicts that glycerol conversion and yield of (DTBG+TTBG) increase from 1.5 to 2.5 (w/v)% catalyst loading, and

above 2.5 (w/v)% both glycerol conversion and combined yield of DTBG and TTBG decrease. It implies that above 2.5 (w/v)% catalyst loading, secondary reactions becomes dominant, as excessive catalyst loading can catalyze dehydration of TBA to isobutylene, etherification of isobutylene to di-isobutylene (DIB) - precursors of gummy products and oligomerization reaction to produce gummy products instead of etherification of glycerol[107, 128].

Table 12 Effect of catalyst loading on etherification reaction (55% TPA/H- β, 120°C, 1 MPa, 1:5 molar ratio (glycerol: TBA) and 800 rpm for 5 h)

Catalyst Loading (w/v)%	Conversion of glycerol (%)	Yield of MTBG (wt%)	Yield of DTBG (wt%)	Yield of TTBG (wt%)	Yield of (DTBG+TTBG) (wt%)
1.5	98.1	45.4	52.6	0.1	52.7
2.5	100	7.9	13.5	78.6	92.1
3.5	86.7	27.5	26.1	43.1	69.2

Table 13 depicts the reaction temperature effects on the etherification reaction. It depicts that glycerol conversion increases with the increase in reaction temperature up to 120°C, above which the conversion remains the same. However, above 120°C reaction temperature, the combined yield of DTBG and TTBG drops, as the de-etherification reaction of the product ethers becomes important at high temperature.

Table 13 Effect of reaction temperature (2.5 (w/v)% catalyst, 55% TPA/H- β, 1 MPa, 1:5 molar ratio (glycerol: TBA) and 800 rpm for 5 h)

Reaction Temperature °C	Conversion of glycerol (%)	Yield of MTBG (wt%)	Yield of DTBG (wt%)	Yield of TTBG (wt%)	Yield of (DTBG+TTBG) (wt%)
90	84.5	64.6	3.6	16.3	19.9
120	100	7.9	13.5	78.6	92.1
180	100	26.3	39.9	33.8	73.7

Table 14 depicts the effect of glycerol to TBA molar ratio on the etherification reaction. It depicts that both the glycerol conversion and yield of (DTBG+TTBG) increase with the increase of the molar ratio up to 1:5, beyond which both the conversion and combined yield of DTBG and TTBG

decrease. Excess concentration of *tert*-butanol favors oligomerization reaction to form di-isobutylene, which might lessen the conversion and yield.

Table 14 Effect of Glycerol to TBA molar ratio (2.5 (w/v)% catalyst, 55% TPA/H- β, 1 MPa, 120°C and 800 rpm for 5 h)

Glycerol: TBA ratio	Conversion of glycerol (%)	Yield of MTBG (wt%)	Yield of DTBG (wt%)	Yield of TTBG (wt%)	Yield of (DTBG+TTBG) (wt%)
1:4	96.7	53.1	6.7	36.9	43.6
1:5	100	7.9	13.5	78.6	92.1
1:6	95.8	60.1	5.6	30.2	35.7

The catalyst reusability study was also carried out for etherification reaction. The best-performed catalyst was regenerated using a similar method as in for the transesterification reaction. After three consecutive runs, there was only 2% drop in the conversion of the glycerol.

The quality and properties, such as cloud point, cloud point and lubricity (wear and scare μm) of the produced combined biofueland biodiesel were measured according to ASTM D6751 standards. Table 14 depicts the comparison of the properties. It depicts that the properties of the produced biodiesel are close and the combined biofuelproperties are better than those reported by ASTM standards.

Table 15 Comparison of the properties of biodiesel and combined biofuelmeasured to those of ASTM standard

Properties	Biodiesel	Biofuel	Biodiesel ASTM standard
Cloud point (°C)	-2	-10	-2
Pour point (°C)	-15	-19	-15
Lubricity (HFRR, μm)	210	≈ 0	314

A techno-economic study is conducted based on the above experimental results. Figure 8 shows the flowsheet of the co-production of biodiesel and glycerol ether. In a typical co-production process, after biodiesel production, the glycerol is not separated from the biodiesel mixture (Fig. 19). Rather, optimized amount of TBA and catalysts ae added into the reactor. After etherification

of glycerol, biodiesel and glycerol-ether are extracted as a single fuel mixture (which is termed as Biofuel).

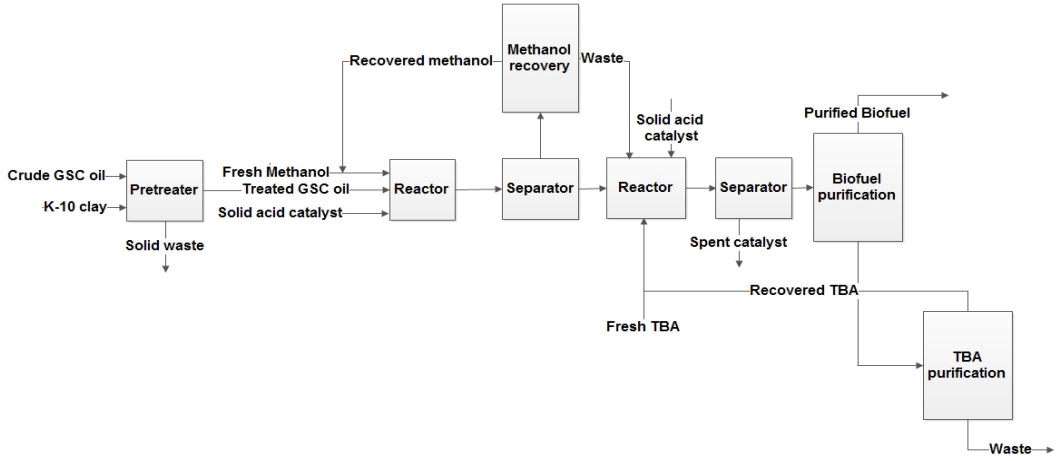

Fig. 19 Block flow diagram of biofuel production process

The process economics analysis indicated that biodiesel production process was more profitable process than biofuel production process (Table 15).

Table 16 Process economics comparison between biodiesel and biofuel process (USD in million)

	Biodiesel	Biofuel
Fixed Capital cost	1.89	2.38
Working Capital cost	0.28	0.36
Total Capital Investment	2.17	2.74
Total raw material cost	4.46	7.94
Total utility cost	0.29	0.41
Total Manufacturing costs	6.15	9.84
Revenue from sales	9.86	11.64
Net annual profit after tax	2.15	1.04
Project life (years)	20	20
Net Present Value (NPV)	9.2	3.04
Internal rate of return (IRR)%	68.26	27.97

The process efficiency obtained for biodiesel and biofuel production processes were 47.43% and 31.93% respectively. It indicated that the excess amount of energy in combined biofuel production

process was utilized in the reactor, but the heating value of the biofuel was not improved as compared to that for biodiesel.

The impact analysis indicated that biofuel production process is more environmentally friendly compared to that for biodiesel production process (Table 17).

Table 17 Toxicity Index comparison of the two processes

	Biodiesel	Biofuel
Human Toxicity Potential by Ingestion (HTPI)	2.47	2.12
Human Toxicity Potential by Exposure (HTPE)	0.86	3.04×10^{-2}
Terrestrial Toxicity Potential (TTP)	2.47	2.12
Aquatic Toxicity Potential (ATP)	0.93	1.49
Global Warming Potential (GWP)	0.67	1.09
Ozone Depletion Potential (ODP)	7.11×10^{-6}	1.14×10^{-5}
Photochemical oxidation potential (PCOP)	21.5	5.36
Acidification Potential (AP)	21	33.6
Total (PEI/h)	49.9	45.8

5. Catalytic conversion of glycerol to glycerol carbonate

(**Publication details:** Manuscript submitted to the journal Applied Catalysis B: Environmental Ti-SBA-15 as a highly active green catalyst for the production of glycerol carbonate, Parmila Devi, Umashankar Das, and Ajay. K. Dalai)

Objective: Utilization of purified glycerol to prepare value added chemicals such as glycerol carbonate, and glycerol ethers by using novel heterogeneous catalysts.

Abstract

The present work was focused on the development of a green process for the production of glycerol carbonate (GYC) from glycerol (GC) and dimethyl carbonate using a Ti-SBA-15 catalyst. Ti-SBA-15 catalysts with varying Si/Ti ratio were synthesized in situ using sol gel method and characterized using various chemical and spectroscopic techniques to study the effect of Ti incorporation on surface and catalytic properties of Ti-SBA-15 catalysts. The process parameters were optimized to obtain high glycerol conversion and glycerol carbonate selectivity. Ti-SBA-15 catalysts with lower Si/Ti ratio demonstrated higher glycerol conversion and GYC selectivity as compared to the catalysts with higher Si/Ti ratio. A regression model was developed to analyze the correlation between reaction parameters and reaction outcomes which suggest that the reaction temperature has the most significant effect on the glycerol conversion and GYC selectivity. A reaction mechanism portraying the role of Ti-SBA-15 in facilitating the formation of GYC was presented. GYC was formed via the formation of O-methoxy carbonyl intermediate and the reaction was catalyzed by the Lewis acidic nature of Ti-SBA-15 catalyst. A kinetic model was proposed based on the results obtained from this study. In addition, an economic feasibility study of the production of glycerol carbonate from glycerol using Ti-SBA-15 suggests that the process has the commercialization potential.

5.1 Materials and Methods

5.1 Materials

All the chemicals used in the present study were analytical reagent grade and used without any purification. Pluronic P123 (Aldrich, MW 5800) was used as a structure-directing agent, tetraethylorthosilicate (TEOS 98%, Aldrich) was used as a silicon source, and titanium isopropoxide (TIP 97%, Aldrich) was used as a titanium precursor. Hydrochloric acid (HCl) was used to maintain the solution pH. Glycerol, dimethyl carbonate, glycerol carbonate were purchased from Sigma Aldrich. TiO2 was obtained from commercial sources (source?). Hydrogen, helium, nitrogen and air with high purity grade (99.99%) were purchased from Praxair, Saskatoon, Canada.

5.1.2 Catalyst preparation for glycerol carbonate synthesis

SBA-15 and Ti-SBA-15 catalysts were synthesized by sol–gel method. In a typical sol-gel synthesis, pluronic P123 (9.28 g, 0.016 M) was dissolved in deionized water (228.6 g) and stirred at 40^{o}C for 2 h. After 2 h, HCl (4.54 g, 0.46 M) was added to the above mixture and stirred till a clear homogeneous solution was obtained (~2 h). Then, a premixed solution of TEOS (20.83 g,

0.979 M) and TIP (5.58 g, 0.19 M) was added dropwise to above homogeneous solution and the mixture was stirred for 24 h at 40°C. The resulting mixture was subjected to hydrothermal treatment at 100 °C for an additional 24 h to ensure further framework condensation. The solid products were recovered by filtration and dried in air at 100 °C for 24 h. Finally, the dried products were calcined at 550 °C for 6 h to obtain Ti-SBA-15 catalyst (Si/Ti ratio = 4). The calcined catalyst was designated as Ti-SBA-15(A).

Ti-SBA-15 (B-E) catalysts with varying Si/Ti ratio were prepared by changing molar quantities of TEOS and TIP following the above discussed synthesis procedure. The following gel compositions were used: 0.98 M TEOS/ 0.024-0.19 M TIP / 0.46 M HCl / 0.016 M P123/127 M H_2O. Ti-SBA-15 catalysts with Si/Ti ratios 8, 16, 24 and 32 were designated as Ti-SBA-15 (B), Ti-SBA-15 (C), Ti-SBA-15 (D), Ti-SBA-15 (E), respectively. SBA-15 was prepared following the above procedure except that titanium precursor TIP was not added in the reaction.

5.1.3 Catalyst characterization

The BET surface area, the pore volume and the pore diameter of the SBA-15 and Ti-SBA-15 catalysts (A-E) were determined using the N_2 adsorption–desorption isotherm at -196 °C using a Micromeritics ASAP apparatus (Model ASAP 2000). The catalysts were degassed under vacuum at 300 °C for 2 h before the adsorption measurements. The specific surface area was determined by the standard Brunauer-Emmett-Teller (BET) method at the relative pressure range of 0.05-0.2. The pore size was evaluated using the Barrett-Joyner-Halenda (BJH) method.

Crystal structure of the Ti-SBA-15 catalysts was analyzed by Bruker D8 Advance diffractometer (using Cu-Ka radiation (κ = 1.54 Å) at 40 kV/40 mA. Low-angle XRD patterns were recorded from 2θ = 0 to 10° at a scanning rate of 2θ = 3° per min. Wide-angle XRD patterns were recorded by scanning the samples from 2θ = 10 to 60 at a scanning rate of 2θ = 3° per min. The reference patterns of the different single metal oxides were obtained from the Powder Diffraction File 2 (PDF-2) database licensed by the International Center for Diffraction Data (ICDD).

Attenuated total reflectance infrared (ATR-IR) spectra were recorded using a Nicolet Magna 850 Fourier transform spectrometer equipped with a liquid nitrogen cooled narrow band MCT detector. Each spectrum was obtained from the acquisition of 32 scans at $4cm^{-1}$ resolution from 4000 to 400 cm^{-1}. Raman spectra of powdered catalyst samples (TiO_2, SBA-15 and Ti-SBA-15) was recorded using Renishaw system 2000 spectrometer equipped with argon laser. The 514 nm line from an argon ion laser operated at a power of 15 mW was used as the excitation source.

The surface morphology of the SBA-15 and Ti-SBA-15 catalysts (A-E) was determined by scanning electron micrograph (SEM) and transmission electron micrograph (TEM). Scanning electron microscopy (SEM) images were recorded on a Carl Zeiss Evo-40 SEM operating at 10 kV. Samples were mounted on aluminum stubs using adhesive carbon tape and gold splutter coated to reduce charging. TEM micrograph was recorded on FEI Tecnai F20 field emission gun TEM (Hitachi HT7700) operating at 200 kV. Samples were prepared by dispersing in methanol and drop casting onto a copper grid coated with a holey carbon support film (Agar Scientific Ltd.).

The composition of Si and Ti in Ti-SBA-15 (A and B) catalysts was determined using an inductively coupled plasma optical emission spectroscopy (Thermo Fisher Scientific iCAP 7000 series) in the fused catalysts samples. The whole rock analysis method was used for the fusion of fresh Ti-SBA-15 (A-E) and recycled Ti-SBA-15 (E). Briefly, 0.1 g of the catalyst was fused with lithium metaborate in Claisse Ox Automatic Fusion Machine at 1000^{o}C. After fusion and adequate cooling of residues, solutions were made up to 100 mL by adding 0.04N HNO_3 and the samples were analyzed using ICP-OES.

5.1.4 Experimental design

The experiments for glycerol carbonate synthesis were designed by a central composite design (CCD) defined under response surface methodology (RSM) using Design Expert software (version 9). Three independent variables (reaction temperature (A), glycerol to DMC molar ratio (B) and catalyst loading (C) were considered to design the experiments in order to investigate the effects of operational parameters on the conversion of glycerol to GYC. The range of the independent variables was selected based on preliminary studies and literature review. The variables were set at five-level and the number of experiments were set to 20 (Table S1). The individual and interaction effects of independent variables such as reaction temperature (65-110 ^{o}C), glycerol to DMC molar ratio (1:1 to 1:5) and catalyst loading (1 to 10 wt %) to the predicted response parameter (GC conversion and GYC selectivity) were determined. The mathematical relationship between independent variables and response parameters was analyzed by a second-order polynomial equation (Equation 1) and optimized.

$$Y = \beta_o + \sum_{i=1}^{3} \beta_i X_i + \sum_{i=1}^{3} \sum_{j=i+1}^{3} \beta_{ij} X_i X_j + \sum_{i=1}^{3} \beta_{ii} X_i^2 \quad (1)$$

where, Y is the predicted response (glycerol conversion or GYC selectivity); X_i and X_j are independent variables and β_o is the model constant. β_i and β_{ii} are the linear and quadratic effect of the independent variables, respectively. β_{ij} is the linear interaction effect between the independent variables. The significance level of model and interaction among variables were estimated by analysis of variance (ANOVA).

5.1.5 Experimental set-up and reaction procedure

The experiments for conversion of glycerol to GYC were performed according to the design of experiments (Table S1). The reactions were performed under nitrogen atmosphere in a 50 mL three-neck round bottle flask equipped with a reflux condenser and a thermometer. Uniform heating and stirring of the reaction mixture was maintained using temperature controlled oil bath equipped with a magnetic stirrer. In a typical procedure, a mixture of glycerol (5 g, 0.054 M, 1 mol equiv.), DMC (14.68 g, 0.163 M, 3 mol equiv.) and catalyst (500 g, 10 wt %) was heated at 65 ^{o}C and stirred at 600 rpm for 7 h. After 7 h, the sample was collected from the reaction mixture and the conversion of glycerol to GLY was monitored by gas chromatograph (GC). The round bottom flask was cooled to room temperature and catalyst was separated from reaction mixture by filtration. The catalyst was repeatedly washed with methanol (3 x 10 mL) and the filtrate was evaporated using a rotary evaporator to obtain crude GYC. High vacuum distillation of crude GYC

was carried out to obtain pure product. The purity of GYC sample was ensured by GC and ^{1}H NMR.

The conversion of GC to GYC, the selectivity of GYC formation and GYC yield were calculated using Equation 2-4, respectively.

$$Conversion\ (\%) = \frac{C_o - C_i}{C_o} \times 100 \quad (2)$$

$$Selectivity\ (\%) = \frac{C_{GYC}}{C_{TP}} \times 100 \quad (3)$$

$$Estimated\ yield\ (\%) = \frac{Conversion \times Selectivity}{100} \quad (4)$$

Where, C_o is the initial amount of glycerol in the reaction mixture, C_i is the final amount of the glycerol in the reaction mixture, C_{GYC} is the amount of GYC formed and C_{TP} is the amount of all the products formed.

5.1.6 Catalyst reusability study

The reusability of optimized catalyst Ti-SBA-15 (A) was studied by conducting three runs in duplets at the optimized reaction conditions obtained from the RSM optimization study. After each run, the catalyst was filtered and washed with methanol (3 x10 ml) and dried at 100 ºC for 12 h. In a batch reaction, there was around 5 % loss of catalyst during filtration, drying and handling. Therefore, the loss of catalyst was made up with reused catalyst from another batch.

5.1.7 Analytical methods

Glycerol, glycerol carbonate, and methanol content (in wt. %) were determined by gas chromatography (Agilent 7890A series) on a StabilWax column (30m× 250 µm× 0.5 µm; Restek Corp., USA) at 250°C, an FID detector at 300°C, nitrogen at 23 psi, and helium as the carrier. Water content was determined by an automated Karl-Fischer coulometric titrator (Mettler Toledo DL32) using methanol for dilution as the titrator is sensitive to water content of maximum 5 wt. %. Ash content was determined by burning 1 g of sample in muffle furnace at 750°C for 3-4 h. FFA (wt. %) and acid value were determined by acid base titration according to the Lubrizol test procedure (TP-TM-001C). Fourier transform infrared (FTIR) spectra were generated using a FTIR spectrometer (Bruker Vertex 70, MA, USA) with an ATR module. Each spectrum was the average of 16 co-addition scans with a total scan time of 15 s in the IR range of 400–4000 cm^{-1} at 4 cm^{-1} resolution. The formation of GYC was confirmed by GC, GC–MS, and ^{1}H NMR. Bruker AM500 ^{1}H NMR spectra of the samples was recorded in deuterated chloroform ($CDCl_3$) solvent using a 500 MHz NMR spectrometer with a BBO probe.

5.2 Results and discussions

5.2.1 Catalyst characterization

The effects of Ti loadings on surface properties and chemical nature of Ti species in Ti-SBA-15 catalysts were studied using different chemical and spectroscopic characterization techniques such as BET surface area, elemental analysis, XRD, FTIR, Raman spectroscopy, SEM, TEM and TGA.

The N_2 adsorption–desorption isotherms of SBA-15 and Ti-SBA-15 (A-E) catalysts with varying Si/Ti ratios are presented in Fig. 20. The catalysts A-E and SBA-15 showed a type IV isotherm with type H1 hysteresis loop at the relative pressure P/P_o ranging from 0.5 to 0.9. This indicates that all the catalysts are mesoporous in nature. In Ti-SBA-15 catalysts (A-E), the hysteresis loop is wide open beyond the P/P_o region of 0.8, indicating the presence of intra-aggregate voids of TiO_2 particles. The H1 hysteresis loop ends with horizontal plateau indicating narrow pore size distribution and the presence of ordered mesoporous structure.

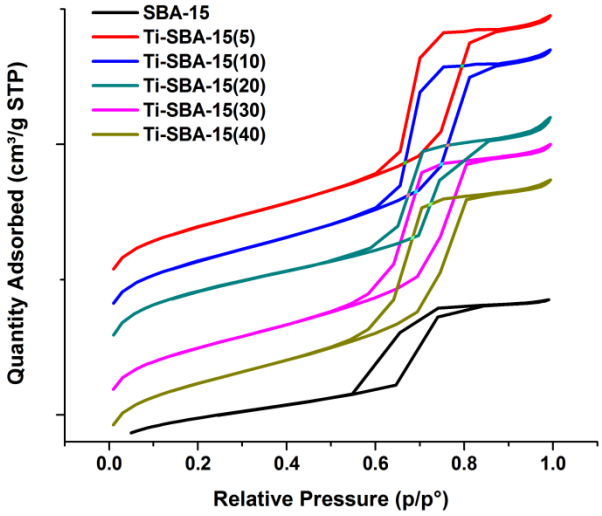

Fig. 20 N_2 adsorption-desorption isotherm of SBA-15 and Ti-SBA-15 catalysts A –E. The catalyst A-E vary in their Si/Ti ratio (Si/Ti ratio: A (4), B (8), C (16), D (24) and E (32).

The textural properties of the catalysts including BET surface area, total pore volume and pore diameter were calculated from desorption isotherms and are summarized in Table 18.

Table 18 Textural properties of SBA-15 and Ti-SBA-15 (A-E) catalysts

Catalyst	Si/Ti ratio	BET surface area (m^2/g)	Total pore volume (cm^3/g)	Micropore volume (cm^3/g)	Pore diameter (nm)
SBA-15	-	811.81	1.03	0.058	5.1
Ti-SBA-15 (A)	4	1000.37	1.24	0.016	4.96
Ti-SBA-15 (B)	8	1244.87	1.69	0.02	4.45
Ti-SBA-15 (C)	16	1319.04	1.49	0.07	4.52
Ti-SBA-15 (D)	24	1211.73	1.64	0.02	4.41
Ti-SBA-15 (E)	32	845.76	0.82	0.12	3.8

The surface area of SBA-15 was found to be 812 m^2/g which is within the range of 500-1300 m^2/g reported in the literature for good quality SBA-15 material. The data in Table 17 shows that the Ti-SBA-15 catalysts A-E have higher surface area than SBA-15 which suggests that titanium integration into the silica framework has contributed to an increase in the surface area of Ti-SBA-15 catalysts. There is a gradual increase in the BET surface area of the catalysts ($E_{BET(s)} < D_{BET(s)} < C_{BET(s)}$) with an increase in the wt % integration of Ti in silica framework in SBA-15 (decrease in Si/Ti ratio). However with further increase in Ti loading, the BET surface area was reduced gradually $C_{BET(s)} > B_{BET(s)} > A_{BET(s)}$ which could be due to the aggregation of Ti microcrystals on the catalyst surface. The results indicate that Ti incorporation in SBA-15 framework was well accomplished up to a Si/Ti ratio of 16. Further Ti loading beyond this Si/Ti ratio led to the formation of a layer in the catalyst surface. This phenomena was further evidenced from XRD analysis that is discussed later.

The total pore volume of the catalysts A-E was found in the range of 0.82-1.69 cm^3/g whereas SBA-15 had a total pore volume of 1.03 cm^3/g (Table 17). The results indicate that the integration of Ti into the silica frame-work in SBA-15 led to an increase in the pore volume when compared against SBA-15 except for the catalyst E. The lower total pore volume of catalyst E may be due to the aggregation of excess Ti microcrystals in the pores. The micropore volume of SBA-15 and the catalysts A-E was calculated using t-method. The results in Table 1 indicate that the integration of Ti into the silica frame-work reduced the micropore volume of the catalysts A, B and D (0.016 to 0.02 cm3/g) as compared to SBA-15 (0.058 cm^3/g) expect for the catalysts E (0.12 cm^3/g) and C (0.07 cm^3/g). The decrease in the micropore volume of a catalyst is attributed due to the incorporation of metal in micropores [22]. The pore diameter of the catalysts A-E was found lower than SBA-15. The above results suggest that Ti is present in Ti-SBA-15 catalysts in two phases. Initially Ti is incorporated into the silica frame to form a Si-O-Ti network and the excess Ti

aggregates as anatase microcrystals outside channels. This inference was also supported from the XRD data of the catalysts. The existence of a dual phase of Ti could be responsible for variation in the BET surface area, pore volume and pore diameter of the catalysts.

The composition of Si and Ti content in two catalysts Ti-SBA-15 (A) and Ti-SBA-15 (B) was determined by elemental analysis which is presented in Table 19. The Si/Ti ratio in Ti-SBA-15 (A) and Ti-SBA-15 (B) was found to be 3.81 and 7.89, respectively (Table S2) against expected values of 4 and 8, respectively.

Table 19 Elemental analysis of Ti-SBA-15 (A and B) catalysts

	Ti content	Si content	Si/Ti ratio
Ti-SBA-15 (A)	18.6	70.6	3.81
Ti-SBA-15 (B)	9.22	72.1	7.89

The low-angle XRD plot of SBA-15 and Ti-SBA-15 (A-E) catalysts are shown in Fig. 21. All the samples showed a diffraction peak of high intensity at 2θ = 1.1 corresponding to an ordered mesoporous structure and one broad diffraction peaks of low intensity 2θ = 1.9 - 2.3. These three peaks represent d_{100} (h), d_{110} (l) and d_{200}(k) planes, respectively and are characteristics of a hexagonal ordered mesoporous structure (*p*6mm symmetry).

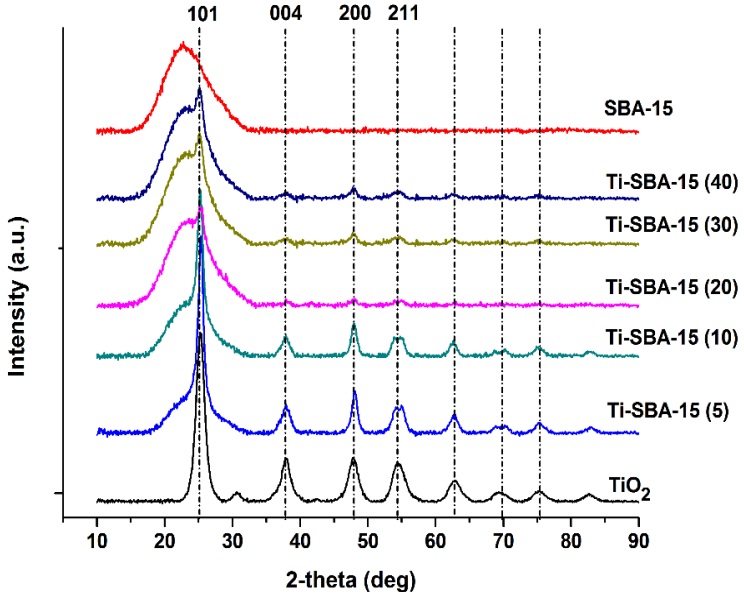

Fig. 21 XRD plot of SBA-15 and Ti-SBA-15 catalysts

These results suggest that incorporation of Ti into SBA-15 framework did not affect the standard structure of SBA-15 and the P6mm hexagonal symmetry structure was maintained in Ti-SBA-15 samples irrespective of variation in Ti loading. These results suggest that the incorporation of Ti in silica matrix lead to the formation of bulk anatase phase and resulted in the appearance of different lines associated to crystalline anatase TiO_2. The intensity of these peaks was found to decrease with an increase in Ti loadings ratio due to difference in the mass of Ti present in different samples. It was confirmed from the XRD plot that excess amount of Ti tends to form an extra-framework of anatase TiO_2 crystals that was further identified from Raman spectroscopy which is presented in Fig. 22.

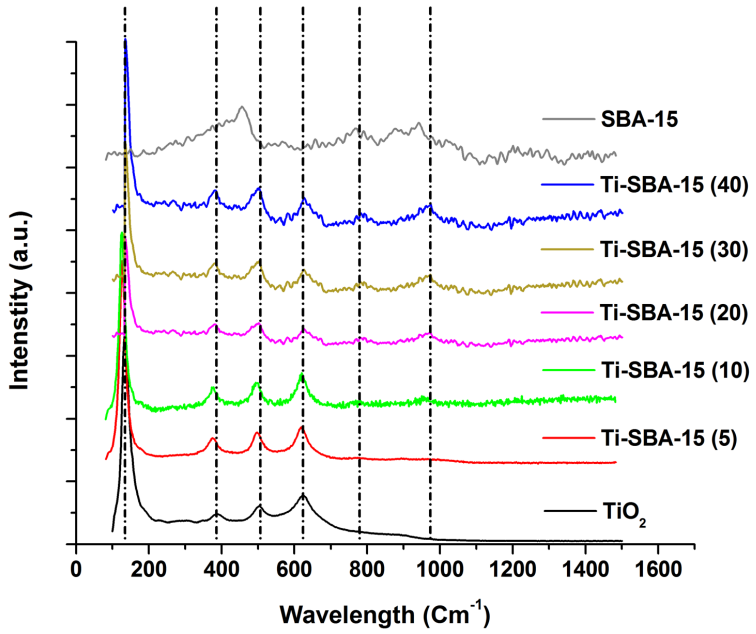

Fig. 22 Raman spectra of TiO_2, SBA-15 and Ti-SBA-15 (A-E) catalysts

Raman spectra of SBA-15 (Fig. 22) showed three peaks in the region of 480, 790 and 925 cm^{-1} which were due to asymmetric stretching (Si-O-Si) vibration, symmetric stretching (Si-O-Si) vibration and framework defects due to surface silanol groups, respectively. It was observed that the silanol peak in SBA-15 at 925 cm-1 shifted to 990 cm-1 in Ti-SBA-15 (A-E) catalysts due to resonance Raman effects of framework Ti species. This peak can be assigned to asymmetric stretching vibration of Si-O-Ti bond. Interestingly, the intensity of this peak decreased with an increase in Ti content in Ti-SBA-15 (A-E) catalysts due to change in amount of extra-framework of Ti species. These results can be explained based on the consideration that titanium ions should be located in the framework in isolated form in Ti-SBA-15 catalysts but at higher loadings some of titanium ions exist as extra-framework Ti species. These extra-framework Ti species absorb the Raman scattering and diminish the Raman signal intensity due to Ti framework as the formation of bulk anatase TiO_2 crystal phase was increased at higher Ti loadings [24]. In Ti-SBA-15 (A-E)

catalysts, a strong signal at 144 cm^{-1} and peaks at 395, 515, and 638 cm^{-1} confirm the presence of anatase phase TiO_2 crystal form.

FTIR spectra of SBA-15 and Ti-SBA-15 (A-E) catalysts are shown in Fig. 23.

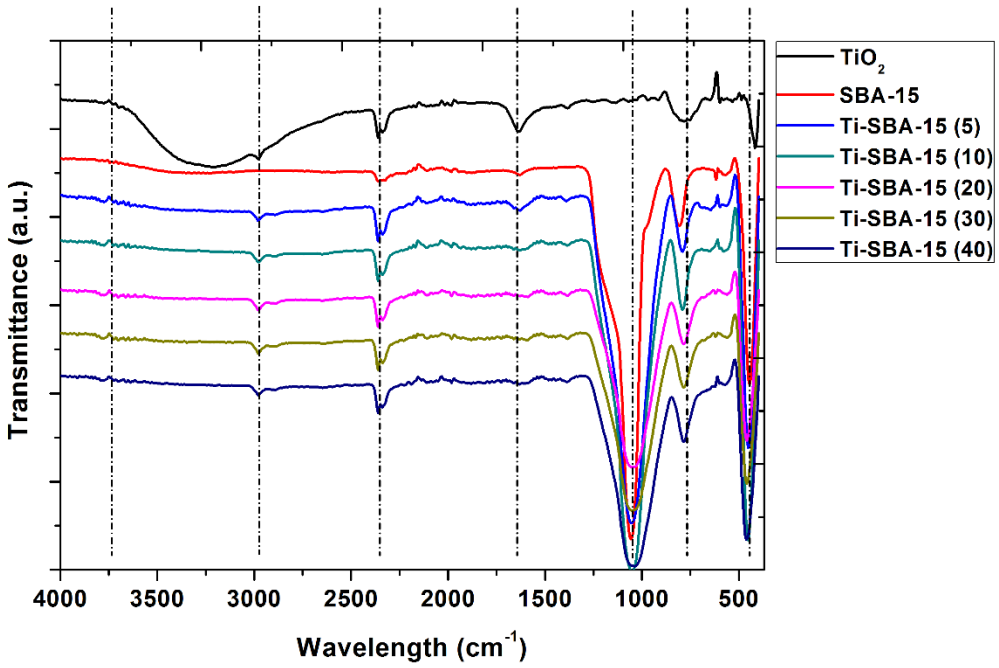

Fig. 23 FTIR spectra of TiO_2, SBA-15 and Ti-SBA-15 (A-E) catalysts

The broad band in the region of 800 to 1080 cm^{-1} attributed to Si-O bonding. The peak at 960 cm^{-1} belongs to symmetric Si-OH vibrations and peak at 1072 cm^{-1} belongs to symmetric Si-O-Ti vibrations. The overlapping of vibrations of Ti-O-Si and Si-OH bonds led to the appearance of a band centered at 1050 cm^{-1}. It was observed from Fig. 4 that intensity of the peak at 1050 cm^{-1} increased with decrease in Ti loadings in the catalysts Ti-SBA-15 (A) to Ti-SBA-15 (E). Increase in the intensity of peak indicates the formation of Ti-O-Si bond due to the interaction of Ti precursor with silanol group in silica matrix. Interestingly, an increase in the intensity of this band was pronounced at lower Ti loading (higher Si/Ti ratio) whereas a very slight change was observed at higher titanium loading. Pyridine adsorbed FTIR spectra of SBA-15 and Ti-SBA-15 (A-E) was recorded to characterize the nature of the acid sites of the catalysts (Fig. S1, supplementary information). It can be seen from Fig. 4 that very strong Brønsted (1545 and 1640 cm^{-1}) and strong Lewis (1620 and 1455 cm^{-1}) acid sites are absent in Ti-SBA-15 (A-E) catalysts. However, weak Lewis acid sites were observed around 1484 and 1580 cm^{-1}, which might be associated with the presence of Ti^{4+} ions. In addition, hydrogen-bonded pyridine peaks around 1595 and 1445 cm−1 were observed in SBA-15 and Ti-SBA-15 (A-E) catalysts.

The surface morphology of SBA-15 and Ti-SBA-15 catalysts was analyzed using SEM and TEM and the results are presented in Fig. 24 and Fig. 25, respectively.

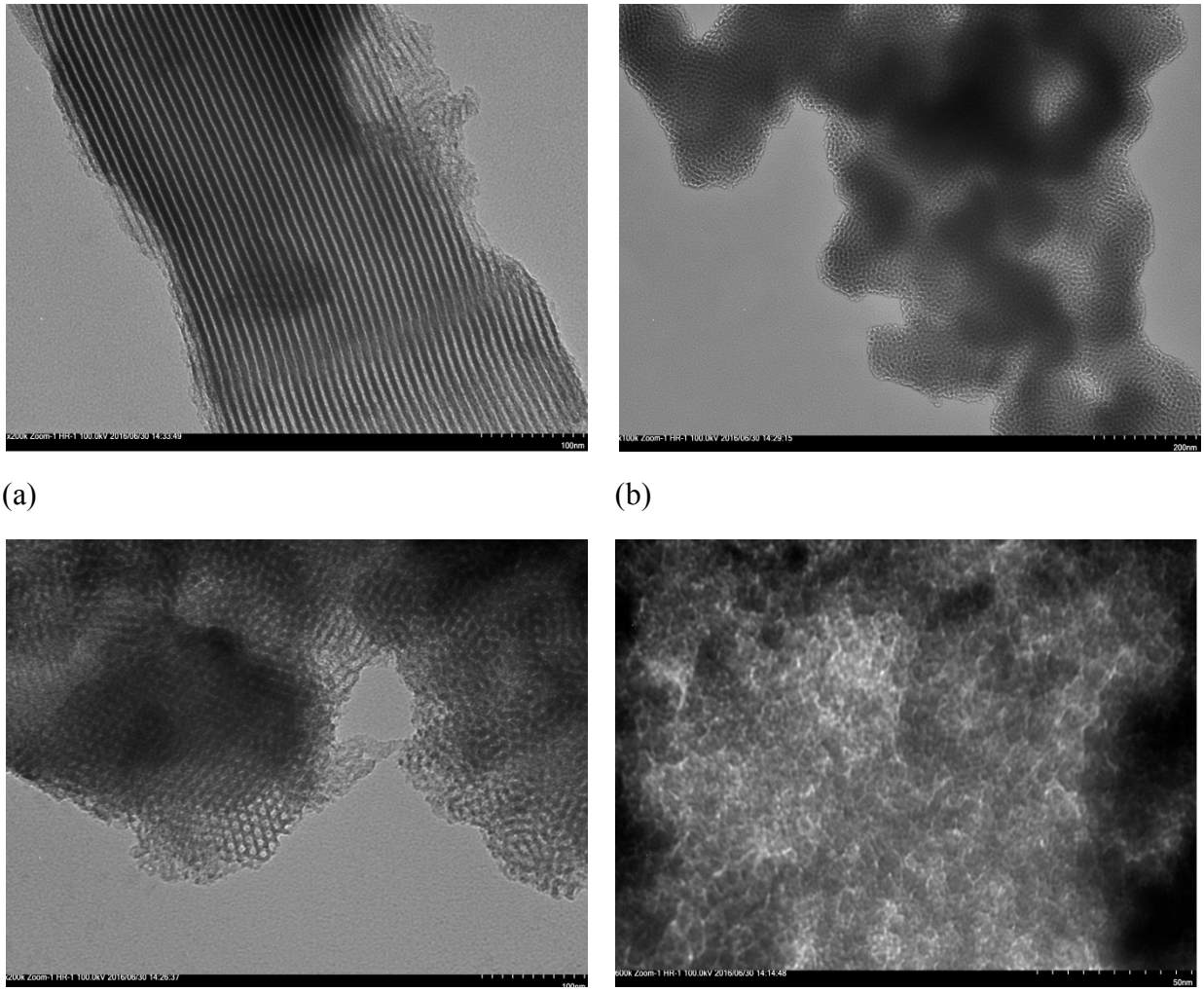

(a) (b)

(c) (d)

Fig. 24 TEM images of catalysts (a) horizontal view of SBA-15; (b) vertical view of SBA-15; (c & d) vertical view of Ti-SBA-15(A)

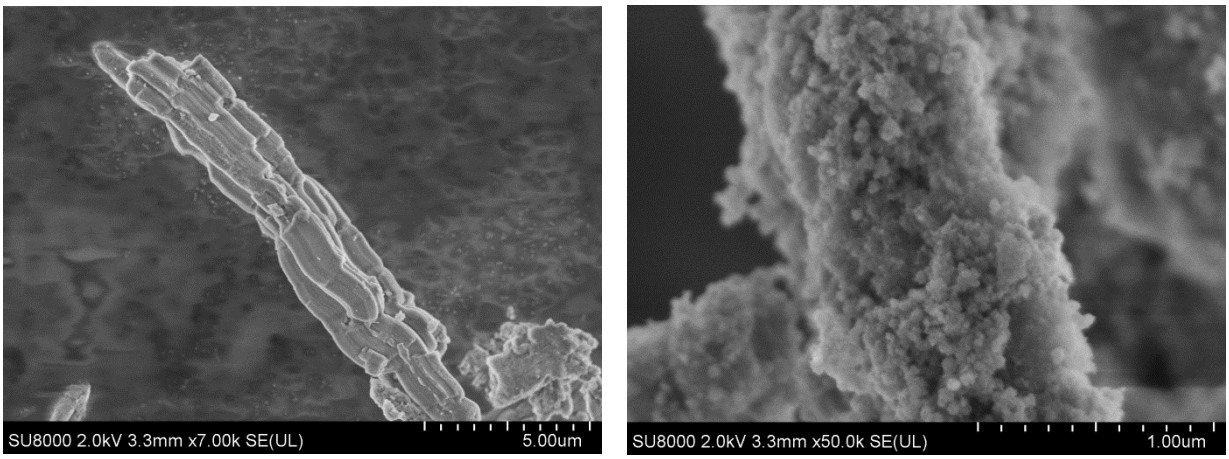

(a) **(b)**

Fig. 25 SEM images of catalysts (a) SBA-15; (b) Ti-SBA-15

Both SBA-15 and Ti-SBA-15 contain short rod-like morphologies, indicating that the original shape of pure SBA-15 is reserved in Ti-SBA-15. After incorporation of Ti, the formation of small bead of Ti species was observed on short rod-like structures while the formation of large aggregated particles was rarely observed indicating the uniform distribution of Ti species. TEM image of horizontal and vertical views of SBA-15. Horizontal view shows characteristic thin platelets of densely aligned straight mesoporous structures while the vertical view indicates the two- dimensional (2D) hexagonal pore structures. Further, TEM images of Ti-SBA-15 (A) in Fig. 6 c-d show a well-reserved mesoporous structure with highly dispersed Ti phase mesoporous silica frameworks. The black dotted particles in the mesoporous silica framework of Ti-SBA-15 are anatase TiO_2 microcrystals. This observation was in agreement with the results obtained from wide-angle XRD patterns and Raman spectra.

5.2.2 Catalyst activity study

Screening of Ti-SBA-15 catalysts

Ti-SBA-15 catalysts (A-E) with varying Si/Ti molar ratio (4 to 32) were screened for the conversion of glycerol to GYC and their catalytic activity was compared against TiO_2 and SBA-15 (Fig. 26).

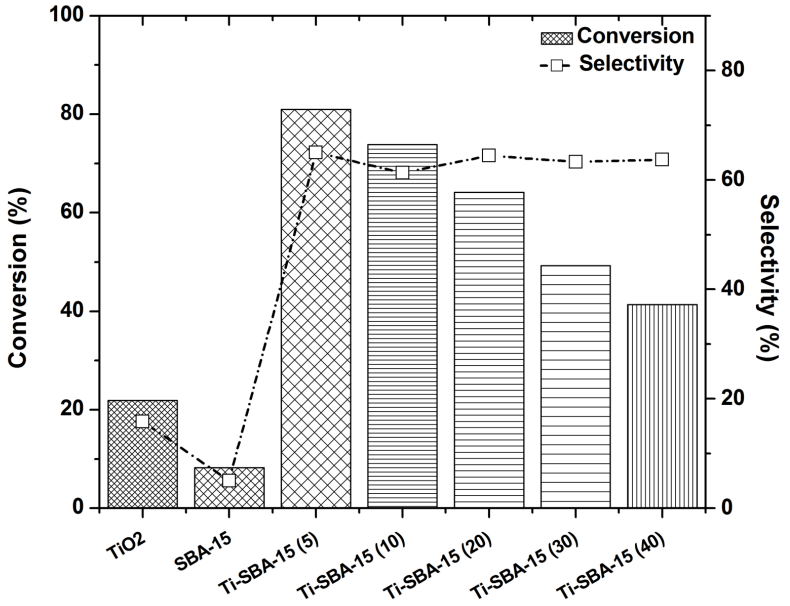

Fig. 26 Screening of catalysts for conversion of glycerol to glycerol carbonate. Reaction condition: glycerol: DMC molar ratio(1:3), catalyst loading, temperature (65 ^{o}C), stirring speed (600 rpm) and reaction time (7 h).

Ti-SBA-15 catalysts A-E showed much higher catalytic activity as compared to TiO_2 and SBA-15 which indicate that Ti plays an important role in facilitating the conversion of glycerol to GYC. The conversion of glycerol to GYC was increased with decrease in Si/Ti molar ratio of the Ti-SBA-15 catalysts. The conversion of glycerol to GYC was decreased from 81 % to 41 % with an increase in Si/Ti molar ratio from 4 to 32, while no significant change in selectivity of GYC was observed with an increase in Si/Ti molar ratio. Among the catalysts A-E, Ti-SBA-15 (A) demonstrated high glycerol conversion and high selectivity, therefore it was chosen for further experiments to optimize the reaction parameters.

Optimization of reaction parameters

A total of 20 experiments were designed using CCD in Design Expert software (version 9) and the detailed experimental plan is presented in Table S1. The effects of variables such as reaction temperature (65-110 ^{o}C), glycerol to DMC ratio (1:1 to 1:5) and catalyst loading (1 wt % to 10 wt %) on the glycerol conversion and GYC selectivity were studied and the results were fitted to a second-order polynomial model. The fitting of model was expressed by comparing the experimental and predicted responses.

This model predicts glycerol conversion (%) and GYC selectivity versus three main effects (linear terms), three two-factor effects (interaction terms) and two curvature effects (quadratic terms). The effects of the reaction parameters (reaction temperature, glycerol to DMC molar ratio and catalyst loading) on glycerol conversion (%) and GYC selectivity (%) are shown in Fig. 13. The results

indicate that glycerol conversion and GYC selectively increased with an increase in temperature up to 87.5 ^{o}C, however further increase in temperature had led to a reduction in GYC selectivity. The reaction was accelerated rapidly above 65◦C which could be due to co-produced methanol from the reaction system (above boiling point of methanol) and shifting the reaction toward the formation of GYC.

The effect of glycerol to DMC molar ratio varying from 1 to 5 was investigated (Fig. 27). The glycerol conversion and GYC selectivity increased with an increase in glycerol to DMC molar ratio from 1 to 3. Further increase in glycerol to DMC molar ratio > 3 does not have much effect on glycerol conversion, however a significant increase in GLY selectivity was increased.

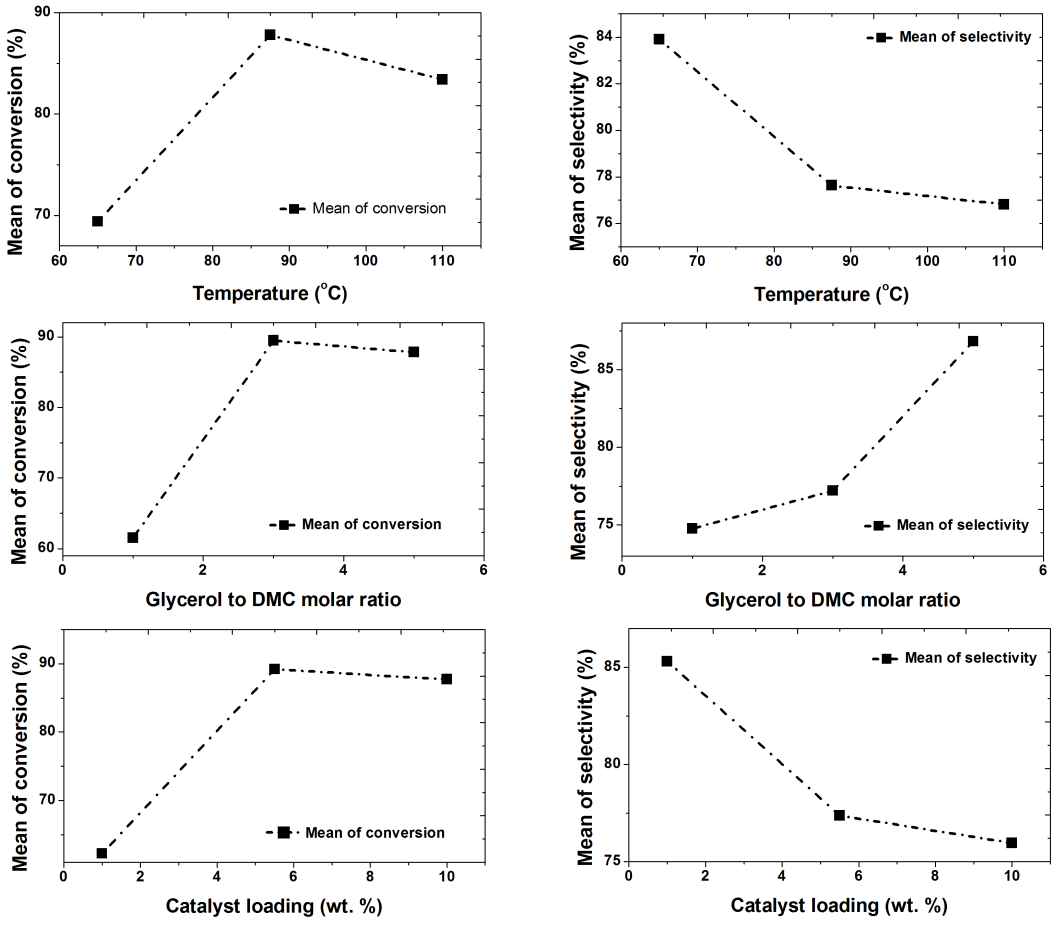

Fig. 27 Effect of different reaction parameters on glycerol conversion and glycerol carbonate selectivity. The reactions were conducted at a fixed reaction time of 7 hrs.

The effects of catalyst loading on glycerol conversion and GYC selectivity were investigated by varying Ti-SBA-15 (A) loading from 1 to 10 wt %. Glycerol conversion and selectivity were increased with an increase in the catalyst amount from 1 to 5.5 wt %. However further increase in

catalyst loading from 5.5 to 10% had led to a decrease in GYC selectivity due to the formation of side products.

The interaction plots of the effects of different operational parameters on glycerol conversion and selectivity are shown in Fig. 27 and Fig. 28. The glycerol conversion was found to be increased with an increase in catalyst loading and glycerol to DMC molar ratio at temperature 65 ^{o}C and 87.5 ^{o}C, respectively. However at 110 ^{o}C, glycerol conversion increased with an increase in catalyst loading (1 to 5 wt %) and glycerol to DMC molar ratio (1 to 3), while further increase in catalyst loading (> 5 wt%) and glycerol to DMC molar ratio (> 3) lead to a decrease in glycerol conversion. This behaviour indicates that an optimum combination of reaction variable (i.e. temperature, catalyst loading and glycerol to DMC molar) is required to achieve the desired response and an increase in variable value above optimum negatively affect the desired response.

The interaction plot of catalyst loading at different temperature and glycerol to DMC molar ratio is shown in Fig. 27 and 28. It was observed that glycerol conversion significantly increased with an increase in catalyst loading up to 5 wt% at different temperatures and glycerol to DMC molar ratio while further increase in catalyst loading does not have much effect on glycerol conversion. The interaction of glycerol to DMC molar ratio with reaction temperature and catalyst loading shows an enhancement in the glycerol conversion as the DMC to glycerol molar ratio increases. The conversion of glycerol increased with an increase in the reaction temperature at different catalyst loadings and approached to constant at higher catalyst loadings.

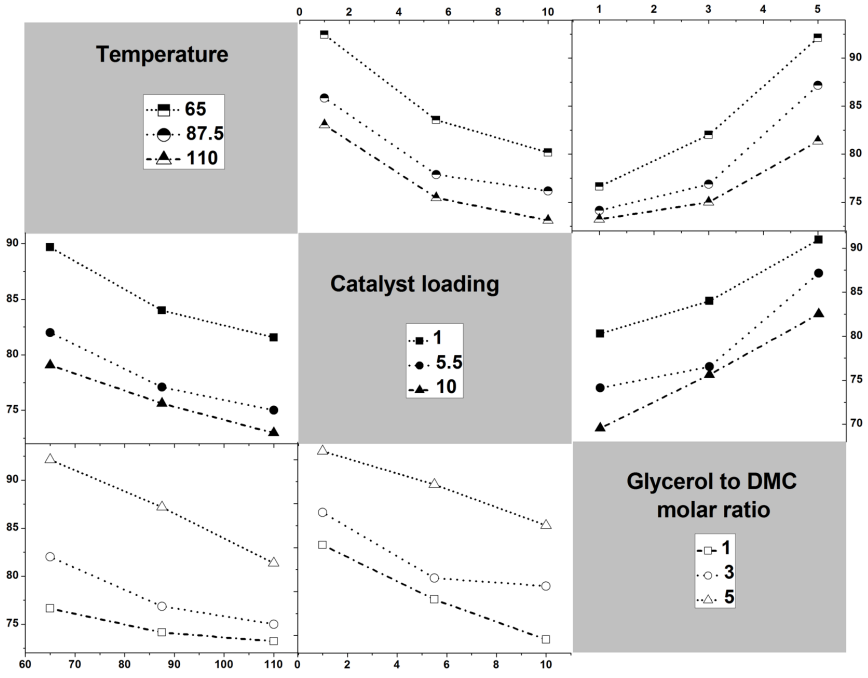

Fig. 28 Interaction plot of different reaction parameters and their effect on glycerol carbonate selectivity

Quadratic interaction reflects the cumulative effects of varying temperature, glycerol to DMC molar ratio and catalyst loading on response variables, i.e. glycerol conversion and GYC selectivity. According to this quadratic interactions the following conditions were found optimum: reaction temperature (87.5 ^{o}C), catalyst loading (5.5 wt%) and glycerol to DMC molar ratio (1:5). Therefore, these conditions were considered optimal for GYC production in high yield and selectivity. The effect of temperature was found to be most important parameter on glycerol conversion and GYC selectivity.

Statistical studies

The statistical significance of the model was analyzed by ANOVA which gives useful information about the interaction effect of reaction variables (reaction temperature, glycerol to DMC molar ratio and catalyst loading) with response variables (glycerol conversion and GYC selectivity) as well as their significance. An F-value (analysis factor) of 101.04 and very low p-values (0.00011 for glycerol conversion and <0.0001 for GYC selectivity) implies that the model was highly significant within 95% confidence level. The "Lack of Fit F-value" of the model of 8.79 and 197.77 were observed for glycerol conversion and GYC selectivity, respectively indicating that there is only 0.11 and 0.01% chances for occurrence of "Lack of Fit F-value" due to noise (Table S3 and Table S4). The values of the determination coefficient R^2 (0.98), the adjusted R^2 (0.97) and predicted R^2 (0.90) indicate that the quadratic response surface model is appropriate for predicting the performance of glycerol conversion.

Quadratic model was used to study the surface response for glycerol conversion and GYC selectivity using factors A,B, C, AB, BC, AC, A^2, B^2, C^2 and intercept, which were analysed as function of model where A, B and C represent reaction temperature, glycerol to DMC molar ratio and catalyst loading respectively. The quadratic model prediction for the response variables (glycerol conversion and GYC selectivity) were found statistically valid. Final quadratic equation for glycerol conversion and GYC selectivity was established, where positive sign before coefficient suggests synergistic effect of factor towards response and negative sign shows an antagonistic effect.

$$\text{Conversion} = +91.25 + 7.01 * \text{A} + 13.14 * \text{B} + 12.73 * \text{C} - 1.37 * \text{AB} - 0.20 * \text{AC} - 2.95 * \text{BC} - 0.94 * \text{A}^2 - 9.44 * \text{B}^2 - 7.94 * \text{C}^2 \quad (5)$$

$$Selectivity = +76.81 - 3.54 * A + 6.03 * B - 4.68 * C - 1.84 * AB + 0.50 * AC + 0.59 * BC + 0.30 * A^2 + 2.45 * B^2 + 1.62 * C^2 \quad (6)$$

The observed and predicted values of glycerol conversion and GYC selectivity are presented in Table S1. It was found that the experimental values for glycerol conversion and GYC selectivity were in good agreement with the predicted values obtained by the model. The significance of the model was also confirmed by linearity between normal probability graphs i.e. the predicted data is in good agreement with observed.

5.2.3 Reaction mechanism and model development

The reaction products formed at optimized reaction conditions using a Ti-SBA-15 (A) catalyst were quantified using GC and the structural identities of the products were confirmed by GC-MS and ^{1}H NMR spectroscopy. The reaction products were identified as GYC, methanol and 1-(o-methoxy-carbonyl) glycerol. It was observed that the conversion of glycerol to GYC progressed via 1-(o-methoxy-carbonyl) glycerol intermediate. Fig. 29 shows that GYC obtained from this process was similar to the GYC standard obtained from Sigma-Aldrich. A plausible reaction mechanism for the conversion of glycerol to GYC has been presented in Fig. 30.

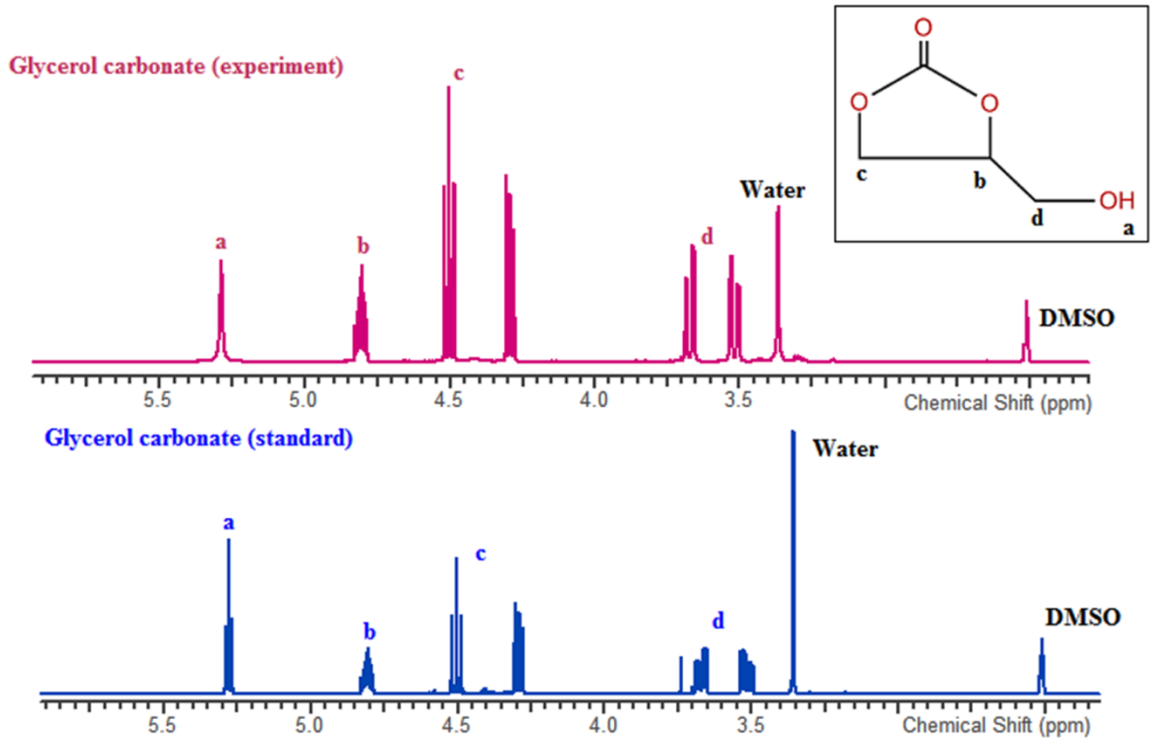

Fig. 29 Comparison of NMR plot of glycerol carbonate obtained from experiment with glycerol carbonate standard

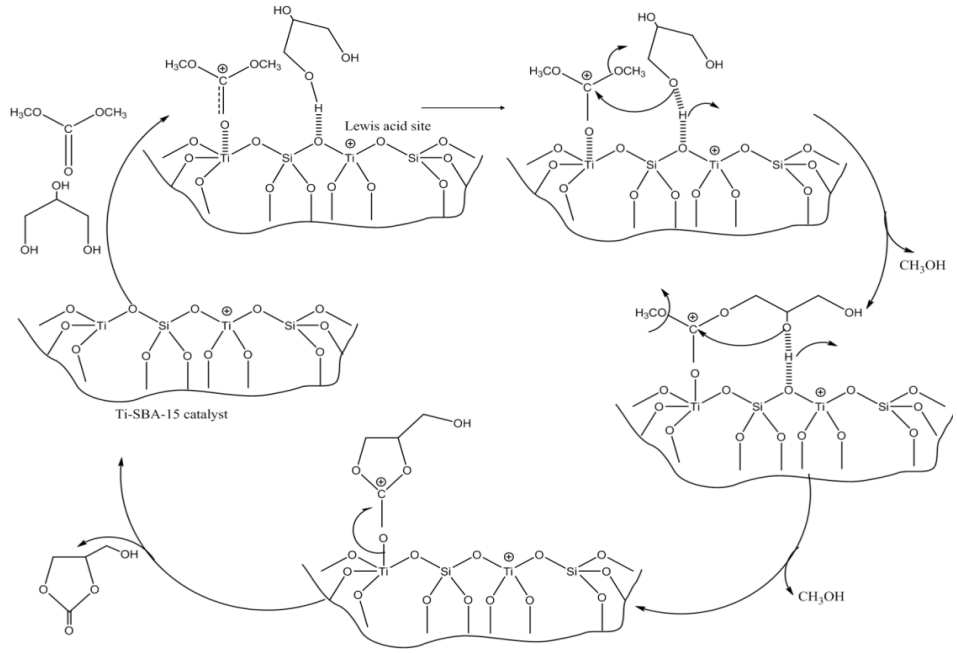

Fig. 30 A proposed reaction mechanism for the reaction of glycerol and DMC to produce glycerol carbonate using Ti-SBA-15 catalyst.

The catalytic reaction was progressed via adsorption, surface reaction and desorption mechanism on Ti-SBA-15 surface. The first step involves the adsorption of glycerol and DMC on catalyst surface through hydrogen bonding interactions. It is speculated that Lewis acid sites of Ti^{+4} activates the carbonyl group of DMC as evidenced from Py-FT-IR and oxygen framework of silica (Si-O-Ti) (weak conjugate base) activates the hydroxyl group of glycerol. The second step involves the surface reaction between glycerol and DMC in which hydroxyl group of glycerol reacts at the activated carbonyl carbon of DMC forming a 1-(o-methoxy-carbonyl)glycerol complex with a loss methanol molecule. The next step involves the cyclization and rearrangement reactions that lead to the formation of GYC and subsequently losing another molecule of methanol. Finally, GYC is desorbed from the catalyst surface and the regenerated catalyst further participates in the catalytic reaction. Various steps discussed above for the catalytic conversion of glycerol to GYC on Ti-SBA-15 surface can be explained by following equations:

Adsorption of glycerol on catalyst vacant sites can be given by Equation 7

$$G + S \overset{K_1}{\Longleftrightarrow} G.S \tag{7}$$

Adsorption of glycerol on catalyst vacant sites can be given by Equation 8

$$DMC + S \overset{K_2}{\Longleftrightarrow} DMC.S \tag{8}$$

The surface reaction of glycerol and DMC on catalyst surface leads to the formation of GYC and methanol.

$$G.S + DMC.S \overset{K_{SR}}{\Longleftrightarrow} M.S + GYC.S \quad (9)$$

The desorption reaction of methanol and glycerol and GYC from catalyst surface can be given by Equation 10 and Equation 11.

$$MS \overset{K_3}{\Longleftrightarrow} M + S \quad (10)$$

$$GYC.S \overset{K_4}{\Longleftrightarrow} GYC + S \quad (11)$$

The model was developed based on the following assumptions: (i) All the sites on the catalyst surface have similar physical and chemical properties; (ii) The rate of non-catalyzed reactions is slower in comparison to the catalyzed reactions, thus considered negligible; (iii) Surface reaction controls the rate of reaction; and (iv) The adsorption of reactants and desorption of products occur very fast.

As, it is assumed that the rate of reaction is controlled by surface reactions only, then the rate of reaction can be given by the following equation:

$$-r_G = -\frac{dC_G}{dt} = k_{SR}C_{G.S}.C_{DMS.S} - k'_{SR}C_{M.S}.C_{GYC.S} \quad (12)$$

$$-\frac{dC_G}{dt} = \frac{k_{SR}\{K_1K_2C_G.C_{DMS} - (K_3K_4C_M.C_{GYC}/K_{SR})\}C_t^2}{(1+K_1C_G + K_2C_{DMC} + K_3C_M + K_4C_{GYC})^2} \quad (13)$$

When reaction is away from equilibrium

$$= -\frac{dC_G}{dt} = \frac{k_r w C_G C_{DMS}}{(1+K_1C_G + K_2C_{DMC} + K_3C_M + K_4C_{GYC})^2} \quad (14)$$

where, $k_r w = k_{SR}K_1K_2C_t^2$; w is weight of catalyst

If the adsorption constants are very small, then Equation 7 reduces to

$$-\frac{dC_G}{dt} = k_r w C_G C_{DMC} \quad (15)$$

A large amount of DMC is used in the reaction, therefore $C_{DMC} \approx C_{DMC.O}$ can be assumed. The above equation can be written in terms of fractional conversion.

$$-\frac{dX_G}{dt} = k'(1 - X_G) \quad (16)$$

where, $k' = k_r w C_{DMC.O}$

By integrating the above equation and constant initial glycerol concentration, the final expression becomes.

$$-\ln(1 - X_G) = k't \quad (17)$$

The reaction kinetics of the conversion of glycerol to GYC was studied at different reaction temperatures (65 ^{o}C to 110 ^{o}C) and a reaction time ranging between 1 h to 7 h using Ti-SBA-15 (A) as a catalyst at optimized reaction conditions (catalyst loading (5.5 wt%) and glycerol to DMC molar ratio (1:5)) and results are shown in Fig. 31.

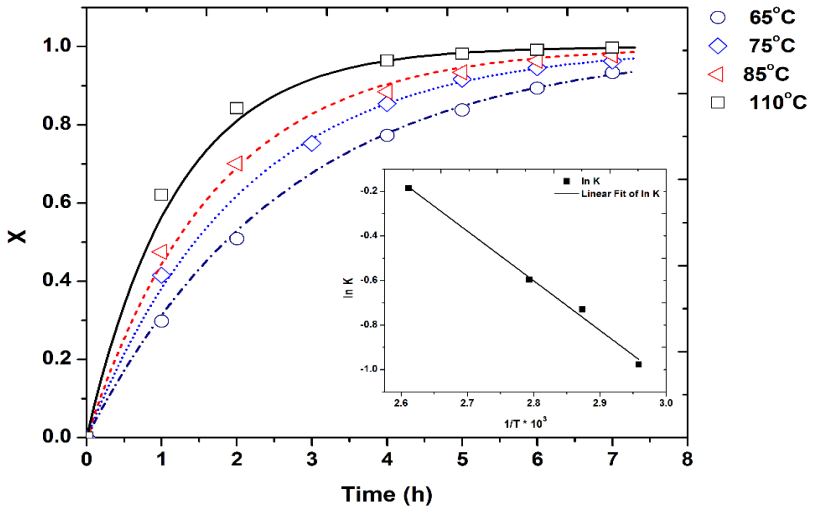

Fig. 31 Kinetic fit of experimental data obtained at different temperatures

Glycerol conversion increased rapidly up to 2h and then the conversion was sluggish with further increase in reaction time. While the selectivity of GYC was initially constant till 5 h and then decreased with an increase with reaction time due to the formation of side products. A plot of ln (1-X_A) versus time was made at different temperatures (Fig. 13). It is seen that the data fit well and hence validate the model. Arrhenius plot of ln k against 1/T (K) was plotted to obtain the apparent energy of activation. The apparent energy of activation of 39.2 kJ/mol shows that the reaction is intrinsically kinetically controlled.

5.2.4 Catalyst reusability study

The catalyst reusability study was performed to confirm its stability and the economic feasibility of the catalyst. The spent catalysts were used up to three cycles and the results are presented in Fig. 32. After each reaction, the catalyst was separated by filtration, washed with methanol and dried at 110 ^{o}C for using in next cycle. The results indicate that the activity of the catalyst was reduced only by 10% after three cycles, however GYC selectivity was significantly affected after 3rd cycle. To find out the reason behind the gradual loss of GYC selectivity, the catalyst sample obtained after third cycle was tested by ATR-FTIR and BET surface area analyzer. The N_2 physiosorption data indicated that the surface area of Ti-SBA-15 (5) catalyst decreased from 845 to 106 m^2/g for the regenerated catalyst. In addition, the micropore volume of the catalyst was also

dropped from 0.016 cm^3/g (fresh catalyst) to 0.009 cm^3/g (regenerated catalyst). These results suggest that after regeneration cycles, the catalytic active sites are probably closed by condensed silica frameworks and not fully accessible to the reactant molecules.

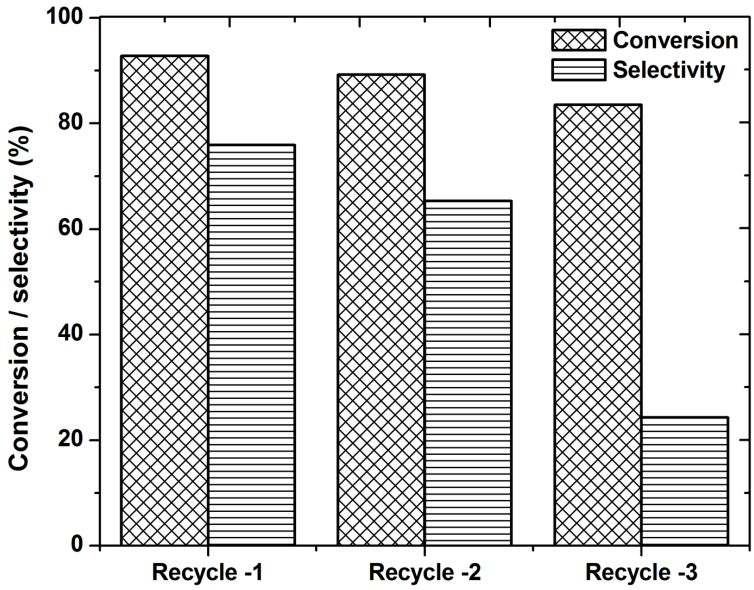

Fig. 32 Reusability study of Ti-SBA-15(5) catalyst

As BET and FTIR results suggest pore blocking in reused catalysts is either due to coke formation or amorphous silica species. To find out the exact reason, the catalyst (after 3rd cycle) was regenerated by calcination (500 ^oC for 4 h) and reused for further experiments. The selectivity of the calcined catalyst was found much improved compared to the previous reaction (non-calcined, 3rd cycle). The glycerol conversion of 91 % and selectivity of 73 % was achieved. Based on these results it can be concluded that the decrease in catalyst selectivity was due to the temporary pore blockage and activity of catalyst can be restored by calcination. It shows that this catalyst is promising for practical applications.

5.2.5 Comparison of Ti-SBA-15 (A) against reported solid catalysts

Various solid catalysts have been reported in the literature for the conversion of glycerol to GYC using DMC as the source of carbonylation. The catalytic activity of Ti-SBA-15 (A) was compared against some of these solid catalysts in relation to glycerol conversion, GYC yield and selectivity. Some of these catalysts showed very high catalytic conversion but low selectivity and some showed high selectivity but low glycerol conversion. The Ti-SBA-15 (A) catalyst demonstrated high glycerol conversion of 94%, GYC selectivity of 87% and yield 82%. The industrial application of this catalyst is warranted in view of the following reasons: (i) the performance of Ti-SBA-15 (A) is comparable to the reported catalysts and commercial catalysts as discussed in

Table 20, and (ii) Ti-SBA-15 is non-toxic having eco-friendly silica framework and easily recoverable from the reaction mixture.

Table 20 Comparison of Ti-SBA-15 (A) catalyst against reported solid catalysts

Catalyst	Reaction Temperature (^oC)	Reaction time (h)	Glycerol conversion (%)	Glycerol carbonate selectivity (%)	Glycerol carbonate yield (%)	References
Ni doped hydrotalcite	100	2	100	55	55	Liu et al., 2014
Mg–La oxide	85	1	81.3	90.0	75.71	Simanjuntak et al., 2013
SW21	140	4	52.1	95.3	49.7	Aresta et al, J. Catal. 2009, 268, 106
Au/Fe_2O_3	150	4	80	48	39	Aille et al., Catal. Lett. 1998,56,245
Au/Nb_2O_5	140	4	49.5	85.4	42.3	Aille et al., Catal. Lett. 1998,56,245
Zn/TPA	140	4	69.2	99.4	68.7	Kumar et al.ChemCatChem, 2012,4,1360
Zr-P	140	3	80	100	76	Aresta et al, J. Mol. Catal.A: Chem., 2006, 257, 188
Ti-SBA-15 (A)	88	7	94	87.17	82	Present study

6. Techno-economic analysis of glycerol purification process

(Publication details: Manuscript in preparation)

Objective: Industrial scale feasibility of the glycerol purification process.

Abstract

A techno-economic analysis based on a scenario where all the purified glycerol is converted to value added chemicals – solketal and glycerol carbonate was carried out and it showed that it is economically feasible to purify glycerol. In this scenario (Scenario 3), the required capital investment is $0.72 M and the net present value of the project is $26 M over 10 years of operation after start-up with capital investment in the initial three year period with no returns. The unit cost of purifying a kg of crude glycerol is $13.62 in this scenario and the unit revenue is $116.62, making it a promising undertaking. While this project will be an addition to a billion dollar biodiesel production plant meaning the $26 M in net present value is not substantial, it is still significant in offsetting the larger biodiesel plant costs and improving the overall company bottom-line.

6.1 Material and methods

The process in this work was modeled using Aspen Hysys software. Equipment are auto-sized by the software based on the material and energy balances and the operating conditions. Because the polar nature of most components in this process, non-random two liquid (NRTL) model was chosen as the fluid simulation package that can more accurately simulate the purification of crude glycerol. Universal quasi-chemical (UNIQUAC) model could do the job equally well as a fluid package of choice. NRTL was used together with the UNIFAC LLE (liquid-liquid equilibrium) to estimate the missing coefficients, particularly for hypothetical components that were created and added to the Hysys library (Zhang et al, 2003, Apostolakou et al, 2009).

Initial physico-chemical steps including saponification, acidification, neutralization as well as glycerol conversion into fuel additives were simulated in a Conversion Reactor model while phase separation was simulated in a Decanter model and solvent extraction in a liquid-liquid separator. Membrane separation was modeled in a Splitter model while a heat exchanger was used for cooling and pump for varying pressure at various points in the process. With all the above in place, the crude glycerol purification process was simulated.

Economic evaluation refers to the evaluation of capital and operating costs associated with the construction and operation of a chemical process (Ulrich et al, 2004, Turton et al, 1998). The criteria for economic evaluation in this work is based on capital cost, manufacturing cost and project profitability as measured by net present value or worth (NPV/W) of the project.

Basis and scope of Economic Analysis

Economic costs estimation was based on the assumptions that: the plant consumes 335.8 tons/year of crude glycerol to produce 134 tons/year of purified glycerol, 40% of which is converted to solketal, 35% to glycerol carbonate and 25% sold as pure glycerol. Glycerol recovery in this work is extremely high at 98wt%. Pure glycerol makes up 40% of the input crude glycerol (0.40 x 335.8tons/year). This is a small scale plant hence the low production but it will grow with better returns from this initial production. The plant operating hours are assumed to be 8059 (0.92 operating factor) per year. All prices for raw materials and solvents and catalysts are assumed to include the cost of transport.

6.2 Results and Discussion

The detailed techno-economic feasibility analysis of glycerol purification and value addition was carried out to see industrial feasibility and profitability of the process. In order to get the big picture of the process, three following scenarios were devised:

Scenario 1: 100% of the purified glycerol is sold as a product and there is no production of value-added products

Scenario 2: 50% of the purified glycerol is sold as a product and 25% of purified glycerol is converted to glycerol carbonate and 25% as solketal

Scenario 3: No purified glycerol is sold and all the purified glycerol is converted to value added products – 50% of purified glycerol is converted to glycerol carbonate and other 50% to solketal.

All the three scenarios have been presented in Table 21. Table 22 presents the detailed summary for scenario 3.

Table 21 Different scenario for economic analysis of crude glycerol purification (Basis 1000 kg of crude glycerol; all values are in USD)

Scenario 1: 100% of purified glycerol as product and no production of value-added products

Item	Annual Cost ($)	Per Unit Annual Cost or Revenue ($/Kg of crude glycerol)
Direct manufacturing costs	467643.85	3.48
Utilities	18767.41	0.140
Indirect manufacturing costs	18389.73	0.137
Maintenance & Repair (6% of fixed capital cost)	31525.26	0.235
Operating supplies (15% of maintenance & repair)	4728.79	0.035
Depreciation (10% of capital cost)	52542.09399	0.391
Total manufacturing expenses	**583597.13**	**4.34**
Total annual revenues	**349301.85**	**2.60**

Scenario 2: 50% of purified glycerol as product, 25% as glycerol carbonate and 25% as solketal

Item	Annual Cost ($US)	Per Unit Cost or Revenue ($/Kg of crude glycerol)
Direct manufacturing costs	1680308.42	12.51
Utilities	20396.57	0.152
Indirect manufacturing costs	22097.93	0.165
Maintenance & Repair (6% of fixed capital cost)	37882.16	0.28
Operating supplies (15% of maintenance & repair)	5682.32	0.04
Depreciation (10% of capital cost)	63136.93344	0.47
Total manufacturing expenses	**1829504.33**	**13.62**
Total annual revenues	**13933925.63**	**103.74**

Scenario 3: 0% is sold as purified glycerol, 50% as glycerol carbonate and 50% as solketal

Expenses			Daily Capacity (Kg, L, m3 (for wastes), persons)	Total Annual Cost ($/yr)	Cost/Unit product
Direct	Raw materials	Crude glycerol	1000	0.00	0.00
		Methanol	1026.48	982372.15	7.31
		CO2	67.008	9450.54	0.07
	By-product credits	Biodiesel	93.49	-18836.37	-0.14
		Methanol	1063.7	-1017992.81	-7.58
		Petroleum ether	216.63	-523759.35	-3.90
		KCl	2.2176	-131.81	0.00
	Catalysts & Solvents	KOH	3.408	748.44	0.01
		HCl	3.144	4434.17	0.03
		Petroleum ether	335.28	861290.73	6.41
		Toluene	0	0.00	0.00
		Acetone	315.84	1081802.53	8.05
		Amberlyst-15	1.60056	1289.92	0.01
		DMF	211.416	29817.27	0.22
		H-Beta Zeolite	1.40064	90304.30	0.67
	Operating labour	Workers	27	163198.80	1.22
	Supervisory & clerical labour (20% of operating labour)			16319.88	0.12
			Total Direct ME	1680308.42	12.51

Utilities	Electricity			17924.39	0.13
	Cooling water			114.55	0.00
	Heating oil			2499.55	0.02
	Conventional Waste disposal		0.35808	198.40139	0.00
			Total Utility Cost	20736.89	0.154
Maintenance & Repair (6% of Cfc)				37882.16	0.28
Operating supplies (15% of maintenance & repair)				5682.32	0.04
	Total			**1744609.79**	**12.99**
Indirect					
	Local taxes (2% Cfc)			12627.39	0.09
	Insurance (1.5% Cfc)			9470.54	0.07
	Total			**22097.93**	**0.16**
Total Manufacturing Expense = DME + IME				**1766707.72**	**13.15**
Depreciation (10% Cfc)				63136.93	0.47
	Total expenses			**1829844.65**	**13.62**
					0.00
Glycerol			0	0.00	0.00
Solketal			439.68	15502677.12	115.42
Glycerol carbonate			106.08	160297.49	1.19

Total Revenues				**15662974.61**	**116.61**

Table 22 Summary of different aspects of project Manufacturing Costs and Revenues

Item	**Annual Cost ($US)**	**Per Unit Cost or Revenue ($/Kg of crude glycerol)**
Direct manufacturing costs	1680308.42	12.51
Utilities	20736.89	0.154
Indirect manufacturing costs	22097.93	0.165
Maintenance & Repair (6% of fixed capital cost)	37882.16	0.28
Operating supplies (15% of maintenance & repair)	5682.32	0.04
Depreciation (10% of capital cost)	63136.93	0.47
Total manufacturing expenses	**1829844.65**	**13.62**
Total annual revenues	**15662974.61**	**116.61**

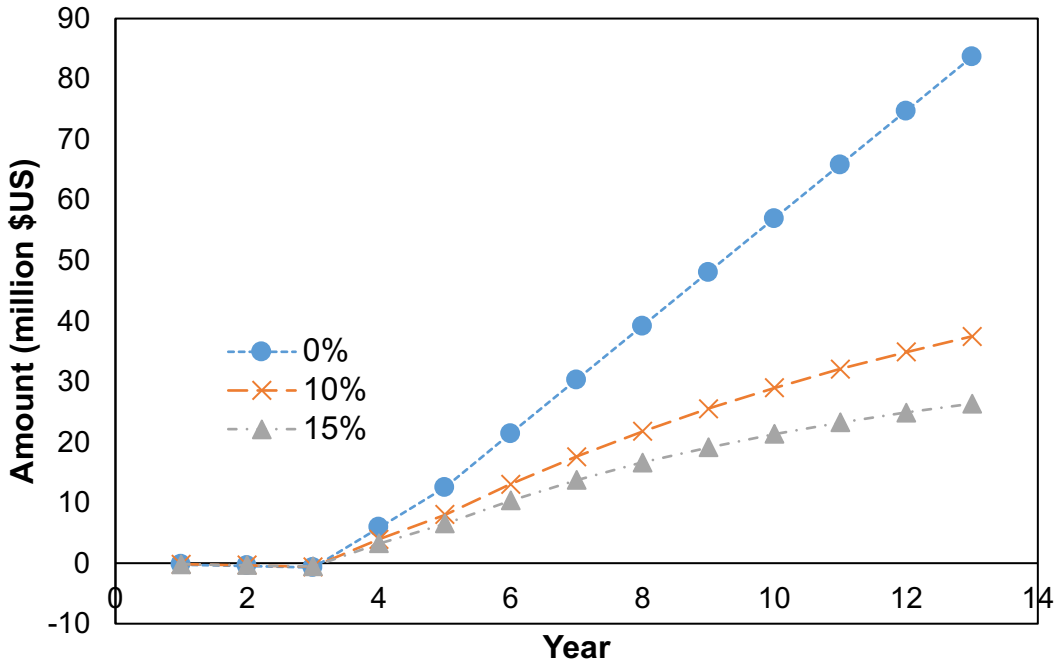

Fig. 34 Cash flow analysis at different discounting rates

Payback period is within the first year of project start-up (Year 4). This is the time period taken for the undiscounted project cash flow to repay the fixed capital invested ($0.64m). Discounted break-even period (DBEP) for the project is before the end of Year 4 as that is when the discounted cumulative project cash flow will become positive. It is between years 3 and 4 for both 10% and 15% discounting rates. So the net payout time is less than a year as it is the point from project start-up (Year 3) when cumulative cash flow becomes positive. Net present value (NPV) of the project is approximately $26 million at 15% discounting interest rate since that is the final discounted cumulative cash flow value at project conclusion.

Since this is an investment of just over half a million in total capital input ($0.72m) and expected discounted cumulative cash flow is $26 million in NPV, this is a highly lucrative project and it is worth undertaking. While capital investment will take three years with no returns, positive cash flows will start streaming in within the first year of project start-up (year 4) and will continue until the end of project life 10 years after start-up (Year 13).

It's also worth noting that, while a NPV of $26 million on a $0.72 million investment is such a great return, the glycerol purification plant is an addition to a billion dollar biodiesel plant and this is therefore an insignificant overall return but it helps in offsetting costs of the biodiesel plant and improving the company bottom-line.

7. Conclusions

Due to the increased production of biodiesel each year, the production of the main by-product of the process, glycerol, is also increasing steadily. As this glycerol contains a lot of impurities, it is called crude glycerol. In order to increase the value and spectrum of usage of glycerol, it must be purified. In this work, glycerol purification was carried out using a combined physico-chemical treatment and dead-end and tubular membrane filtration in batch and semi-continuous mode, respectively, using UF membranes. The process was studied to increase the yield of glycerol by combining physico-chemical treatment, membrane filtration and charcoal adsorption. Using the sequential treatment of saponification, acidification, neutralization, phase separation, solvent removal, membrane filtration (in batch mode) at conditions of 1 kDa membrane at 60°C temperature and 350 kPa pressure, and activated charcoal treatment, a maximum of 97.5% glycerol yield was obtained with very low residual FFA, water and ash content. In the case of tubular membrane filtration, at a moderate temperature of 42.5°C and pressure of 700 kPa, about 85% glycerol yield was obtained with very low residual FFA, water and ash content. This process showed the promise for purification of crude glycerol and its value addition.

An effective solid acid catalyst has been developed for etherification of glycerol. Later the same catalyst was used for co-production of biodiesel and glycerol-ether, and the mixture of biodiesel and glycerol-ether was deemed as biofuel. The fuel properties analysis indicates that biofuel has better fuel properties as compared to those for biodiesel.Ti-SBA-15 is disclosed as a highly active catalyst for the production of glycerol carbonate from glycerol in high yield (82%) and selectivity (85%). A sol gel method was employed for *in situ* incorporation of Ti into the silica framework of SBA-15. Ti-SBA-15 catalysts with varying Si/Ti ratio were synthesized and the influence of Ti on textural properties and surface morphology of Ti-SBA-15 catalysts and its catalytic activity were investigated. The activity of Ti-SBA-15 catalysts was found to increase with an increase in Ti loadings (lower Si/Ti ratio) and the catalyst with higher Ti loading (Ti-SBA-15 (A)) showed greater catalytic activity as compared to Ti-SBA-15 catalysts with higher Si/Ti ratio. Ti-SBA-15 (A) demonstrated more than 10-times greater activity than SBA-15 which indicates the important role of Ti in exhibiting higher catalytic properties. Investigation of XRD, FT-IR and Raman data suggests that higher Ti loadings led to the formation of an extra layer of anatase TiO_2 crystals on the catalyst surface. A reaction mechanism based on the products identified from the reaction mixture suggests that the reaction proceeded via the formation of an O-methoxy-carbonyl glycerol intermediate and the Lewis acidic nature of Ti was the main driving force in facilitating the reaction. A kinetic model was developed which suggests that temperature was a critical parameter for the conversion of glycerol to glycerol carbonate. Ti-SBA-15 displayed better performance compared to various solid catalysts reported in the literature.
The detailed techno-economic analysis suggested that the production of purified glycerol without the production of value added chemicals is not profitable and production of glycerol carbonate and solketal from purified glycerol can generate revenue of $116/kg of crude glycerol.

References

- A. Vlysidis, M. Binns, C. Webb, C. Theodoropoulos., "A Techno-economic Analysis of Biodiesel Biorefineries: Assessment of Integrated Designs for the Co-Production of Fuels and Chemicals," Energy, Vol. 36, 2011, pp 4671 - 4683.
- Acatrinei, A.I., Hartl, M.A., Eckert, J., Falcao, E.H.L., Chertkov, G., Daemen, L.L., 2009. Hydrogen adsorption in the Ti-doped mesoporous silicate SBA-15. J. Phys. Chem. C 113, 15634–15638.
- Álvarez, M.G., Frey, A.M., Bitter, J.H., Segarra, A.M., de Jong, K.P., Medina, F., 2013. On the role of the activation procedure of supported hydrotalcites for base catalyzed reactions: Glycerol to glycerol carbonate and self-condensation of acetone. Appl. Catal. B Environ. 134-135, 231–237.
- Álvarez, M.G., Plíšková, M., Segarra, A.M., Medina, F., Figueras, F., 2012. Synthesis of glycerol carbonates by transesterification of glycerol in a continuous system using supported hydrotalcites as catalysts. Appl. Catal. B Environ. 113-114, 212–220.
  Analysis of a Biodiesel Production Process from Vegetable Oils," Fuel Processing Technology, Vol. 90, 2009, pp 1023 - 1031.
  and Extraction of Crude Glycerol Obtained during Transesterification of Crotalaria
  and Polymers," Bioresource Technology, Vol. 215, 2016, pp 144 - 154
  and their applications in the separation of Cephalexin," Journal of Membrane Science,
- Araújo, M.M., Silva, L.K.R., Sczancoski, J.C., Orlandi, M.O., Longo, E., Santos, A.G.D., Sá, J.L.S., Santos, R.S., Luz, G.E., Cavalcante, L.S., 2016. Anatase TiO2 nanocrystals anchored at inside of SBA-15 mesopores and their optical behavior. Appl. Surf. Sci. 389, 1137–1147.
- Ardi, M. S., Aroua M. K., and Hashim N A, 2015. Progress, prospect and challenges in glycerol purification process: A review. Renewable and Sustainable Energy ReviewsRenew.wable and Sustainable. Energ. Rev., Vol. 42, pp. 1164–1173.
- Aresta, M., Dibenedetto, A., Nocito, F., Ferragina, C., 2009. Valorization of bio-glycerol: New catalytic materials for the synthesis of glycerol carbonate via glycerolysis of urea. J. Catal. 268, 106–114.
- Aresta, M., Dibenedetto, A., Nocito, F., Ferragina, C., 2009. Valorization of bio-glycerol : New catalytic materials for the synthesis of glycerol carbonate via glycerolysis of urea. J. Catal. 268, 106–114.
- Aresta, M., Dibenedetto, A., Nocito, F., Pastore, C., 2006. A study on the carboxylation of glycerol to glycerol carbonate with carbon dioxide: The role of the catalyst, solvent and reaction conditions. Atmos. Environ. 41, 407–416.
- Atadashi I .M., Aroua M .K., Abdul Aziz A .R., and Sulaiman N .M .N., 2011. Membrane biodiesel production and refining technology: A critical review, Renew. Sust. Energ. Rev.Renewable and Sustainable Energy Reviews, 15, (2011) 5051– 5062.
- Ayoub, MuhammadM, and Ahmad Z. Abdullah A Z, (2012a). "Critical Review on the Current Scenario and Significance of Crude Glycerol Resulting from Biodiesel Industry Towards More

Sustainable Renewable Energy Industry,." Renew. Sust. Energ. Rev. Renewable and Sustainable Energy Reviews 16, (5), (2012a): 2671-86.

- Bagheri, S., Julkapli, N.M., Yehye, W.A., 2015. Catalytic conversion of biodiesel derived raw glycerol to value added products. Renew. Sustain. Energy Rev. 41, 113–127.
- Bai, R., Wang, S., Mei, F., Li, T., Li, G., 2011. Synthesis of glycerol carbonate from glycerol and dimethyl carbonate catalyzed by KF modified hydroxyapatite. J. Ind. Eng. Chem. 17, 777–781.
- Bérubé, F., Khadhraoui, A., Janicke, M.T., Kleitz, F., Kaliaguine, S., 2010. Optimizing silica synthesis for the preparation of mesoporous Ti-SBA-15 epoxidation catalysts. Ind. Eng. Chem. Res. 49, 6977–6985.
- Bérubé, F., Kleitz, F., Kaliaguine, S., 2008. A comprehensive study of titanium-substituted SBA-15 mesoporous materials prepared by direct synthesis. J. Phys. Chem. C 112, 14403–14411.
- Bérubé, F., Noriair, B., Kleitz, F., Kaliaguine, S., 2010. Controlled postgrafting of titanium chelates for improved synthesis of Ti-SBA-15 epoxidation catalysts. Chem. Mater. 22, 1988–2000.

biodiesel production," Biotechnology for Biofuels (2012), 1-2.

Biorefineries," First Ed., John Wiley & Sons, Ltd. (2013), 205 -241.

- Busca, G. Chemical Reviews **2007** 107, 5366-5410.
- Calvino-Casilda, V., Mul, G., Fern??ndez, J.F., Rubio-Marcos, F., Ba??ares, M.A., 2011. Monitoring the catalytic synthesis of glycerol carbonate by real-time attenuated total reflection FTIR spectroscopy. Appl. Catal. A Gen. 409-410, 106–112.
- Chang, F., Wang, J., Luo, J., Sun, J., Deng, B., Hu, X., 2016. Enhanced visible-light-driven photocatalytic performance of mesoporous W-Ti-SBA-15 prepared through a facile hydrothermal route. Colloids Surfaces A Physicochem. Eng. Asp. 499, 69–78.
- Chang, J.S., Chen, D.H., 2011. Optimization on the etherification of glycerol with tert- butyl alcohol. J. Taiwan Inst. Chem. Eng. 42, 760–767.

charcoal adsorption," Separation and Purification Technology, Vol. 168 (2016) 101-106.

- Chen, S.Y., Mochizuki, T., Abe, Y., Toba, M., Yoshimura, Y., 2014. Ti-incorporated SBA-15 mesoporous silica as an efficient and robust Lewis solid acid catalyst for the production of high-quality biodiesel fuels. Appl. Catal. B Environ. 148-149, 344–356.
- Ciriminna R, Della Pina C., Rossi M, and Pagliaro M, (2014). Understanding the glycerol market, Eur. J. Lipid Sci. Technol. 2014, 116(10), 1432-1439.
- Contreras-Andrade I, Avella-Moreno E, Fabián Sierra-Cantor J, Guerrero-Fajardo CA, and Sodré JR, (2015). , Purification of glycerol from biodiesel production by sequential extraction monitored by 1H NMR, Fuel Processing Technology 132 (2015) 99–104, Fuel Processing Process. Technology Technol., 132, (2015) 99–104.
- Da Silva, C. R. B.; Gonclaves, V. L. C.; Lachter, E. R.; Mota, C. J. A. Journal of the Brazilian Chemical Society **2009** 20, 201-204
- Devassy, B. M.; Halligudi, S. B. Journal of Catalysis **2005** 236, 313-323

- Dow chemical company, (2015). Cited from: http://www.dow.com/optim/optim-advantage/physical-properties/viscosity.htm. Assessed on: 10 February 2016.
- Esteban, J., Domínguez, E., Ladero, M., Garcia-Ochoa, F., 2015. Kinetics of the production of glycerol carbonate by transesterification of glycerol with dimethyl and ethylene carbonate using potassium methoxide, a highly active catalyst. Fuel Process. Technol. 138, 243–251.
- F. Yang, M. A. Hanna, R. Sun, "Value-added uses for crude glycerol – a by-product of from Different Feedstocks in Biodiesel Production: Experimental and Simulation Study," from Glycerol," American Chemical Society, 2015, pp A - M.
- Gholami, Z., Abdullah, A.Z., Lee, K.T., 2014. Dealing with the surplus of glycerol production from biodiesel industry through catalytic upgrading to polyglycerols and other value-added products. Renew. Sustain. Energy Rev. 39, 327–341.
- Gu, Y.; Azzouzi, A.; Pouilloux, Y.; Jerome, F.; Barrault, J. Green chemistry **2008** 10, 183-190
- H.W. Tan, A.R. Abdul Aziz, M.K. Aroua, "Glycerol production and its applications as a
- Hájek M and Skopal F, (2010). Treatment of glycerol phase formed by biodiesel production, Bioresour. Technol., 101, 3242–3245.
- Hu, A. Apblett, "Nanotechnology for Water Treatment and Purification," New York: Industrial & Engineering Chemistry Research, Vol. 52, 2013, pp 14291 - 14296.
- Isahak W .N .R .W., Ismail M, Yarmo M .A, Jahim J .M,. and Salimon J, (2010). Purification of Crude Glycerol from Transesterification RBD Palm Oil over Homogeneous and Heterogeneous Catalysts for the Biolubricant Preparation, Journal J. of Appl.ied Sciences Sci. 10 (21), : 2590-2595, 2010.
- J. A. Posada, L. E. Rincon, C. A. Cardona, "Design and Analysis of Biorefineries based on Raw Glycerol: Addressing the Glycerol Problem," Bioresource Technology, Vol. 111, 2012, pp 282 - 293.
- J. V. Gerpen, B. Shanks, R. Pruszko, D. Clements, G. Knothe, "Biodiesel Production
- Jagadeeswaraiah, K., Kumar, C.R., Prasad, P.S.S., Loridant, S., Lingaiah, N., 2014. Synthesis of glycerol carbonate from glycerol and urea over tin-tungsten mixed oxide catalysts. Appl. Catal. A Gen. 469, 165–172.
- Jagadeeswaraiah, K., Kumar, C.R., Prasad, P.S.S., Loridant, S., Lingaiah, N., 2014. Synthesis of glycerol carbonate from glycerol and urea over tin-tungsten mixed oxide catalysts. Appl. Catal. A Gen. 469, 165–172.

Juncea Oil," Energy Conversion and Management, Vol. 118, 2016, pp 450 - 458.

- Jung, H., Lee, Y., Kim, D., Han, S.O., Kim, S.W., Lee, J., Kim, Y.H., Park, C., 2012. Enzymatic production of glycerol carbonate from by-product after biodiesel manufacturing process. Enzyme Microb. Technol. 51, 143–147.
- K. Y. Wang, T. Chung. "The characterization of flat composite nanofiltration membranes
- Kim, J.Y., Kim, J.Y., Kang, H.J., Kim, W.Y., Lee, Y.H., Lee, J.S., 2014. Isomorphic Ti substitution into SBA-15 without Ti loss and with lower TiO2 segregation. Inorg. Chem. 53, 5884–5886.

- Klepacova, K.; Mravec, D.; Hajekova, E.; Bajus, M. Petroleum and Coal **2003**, 45, 54–57
- Kongjao S, Damronglerd S, and Hunsom M, (2010). Purification of crude glycerol derived from waste used-oil methyl ester plant, Korean J. Chem. Eng., 27(3), 944-949 (2010).
- Kozhevnikov, I.V. Journal of Molecular Catalysis **2007** 262, 86 – 92.
- Kulkarni, M. G.; Gopinath, R.; Meher, L. C., Dalai, A. K. Green Chemistry **2006** 8, 1056 – 1062.
- L. K. Wang, J. P. Chen, Y. Hung, N. K. Shammas, "Membrane and Desalination
- Li, H., Jiao, X., Li, L., Zhao, N., Xiao, F., Wei, W., Sun, Y., Zhang, B., 2014. Synthesis of glycerol carbonate by direct carbonylation of glycerol with CO_2 over solid catalysts derived from Zn/Al/La and Zn/Al/La/M (M = Li, Mg and Zr) hydrotalcites. Catal. Sci. Technol. 5, 989–1005.
- Li, H., Jiao, X., Li, L., Zhao, N., Xiao, F., Wei, W., Sun, Y., Zhang, B., 2014. Synthesis of glycerol carbonate by direct carbonylation of glycerol with CO 2 over solid catalysts derived from Zn/Al/La and Zn/Al/La/M (M = Li, Mg and Zr) hydrotalcites. Catal. Sci. Technol. 5, 989–1005.
- Li, Y., Zaera, F., 2015. Sensitivity of the glycerol oxidation reaction to the size and shape of the platinum nanoparticles in Pt/SiO2 catalysts. J. Catal. 326, 116–126.
- Liu, J., Li, Y., Zhang, J., He, D., 2016. Glycerol carbonylation with CO2 to glycerol carbonate over CeO2 catalyst and the influence of CeO2 preparation methods and reaction parameters. Appl. Catal. A Gen. 513, 9–18.
- Liu, P., Derchi, M., Hensen, E.J.M., 2013. Synthesis of glycerol carbonate by transesterification of glycerol with dimethyl carbonate over MgAl mixed oxide catalysts. Appl Catal A – Gen. 467, 124-131.
- Liu, P., Derchi, M., Hensen, E.J.M., 2013. Synthesis of glycerol carbonate by transesterification of glycerol with dimethyl carbonate over MgAl mixed oxide catalysts. Appl. Catal. A Gen. 467, 124–131.
- Liu, P., Derchi, M., Hensen, E.J.M., 2014. Promotional effect of transition metal doping on the basicity and activity of calcined hydrotalcite catalysts for glycerol carbonate synthesis. Appl. Catal. B Environ. 144, 135–143.
- Lu, P., Wang, H., Hu, K., 2013. Synthesis of glycerol carbonate from glycerol and dimethyl carbonate over the extruded CaO-based catalyst. Chem. Eng. J. 228, 147-154.
- M. S. Ardi, M. K. Aroua, N. A. Hashim, "Progress, Prospects and Challenges in Glycerol
- Manosak R, Limpattayanate R, and Hunsom M, (2011). Sequential-refining of crude glycerol derived from waste used-oil methyl ester plant via a combined process of chemical and adsorption, Fuel Processing Process. Technology Technol. 92 (2011) ,92–99.
- Mario P, and Rossi M, 2010. The future of glycerol, Royal Society of Chemistry, PDF eISBN: 978-1-84973-108-9, DOI:10.1039/9781849731089, 1-28.2010
- Mei, B., Becerikli, A., Pougin, A., Heeskens, D., Sinev, I., Grünert, W., Muhler, M., Strunk, J., 2012. Tuning the acid/base and structural properties of titanate-loaded mesoporous silica by grafting of zinc oxide. J. Phys. Chem. C 116, 14318–14327.

  membranes to non-electrolytes," Biochim. Biophys. Acta 27 (1958) 229.

- O. Kedem, A. Katchalsky. “Thermodynamic analysis of the permeability of biological
- Ochoa-Gómez, J.R., Gómez-Jiménez-Aberasturi, O., Maestro-Madurga, B., Pesquera-Rodríguez, A., Ramírez-López, C., Lorenzo-Ibarreta, L., Torrecilla-Soria, J., Villarán-Velasco, M.C., 2009. Synthesis of glycerol carbonate from glycerol and dimethyl carbonate by transesterification: Catalyst screening and reaction optimization. Appl. Catal. A Gen. 366, 315–324.
- Okuhara, T.; Watanabe, H.; Nishimura, T.; Inumaru, K.; Misono, M. Chemistry of Masterials **2000** 12, 2230 – 2238.
- Pott R W M, Howe C J, and Dennis J S, (2014). The purification of crude glycerol derived from biodiesel manufacture and its use as a substrate by Rhodopseudomonas palustris to produce hydrogen, Bioresource Bioresour.Technology Technol. 152 (2014) , 464–470.
  Purification Process: A Review,” Renewable and Sustainable Energy Reviews, Vol. 42,
- Qian, X.F., Kamegawa, T., Mori, K., Li, H.X., Yamashita, H., 2013. Calcium phosphate coatings incorporated in mesoporous TiO2 /SBA- 15 by a facile inner-pore sol−gel process toward enhanced adsorption-photocatalysis performances. J. Phys. Chem. C 117, 19544−19551.
- Quispe C A G, Coronado C J R, and Carvalho Jr J A, (2013). Glycerol: Production, consumption, prices, characterization and new trends in combustion, Renew. Sust. Energ. Rev. Renewable and Sustainable Energy Reviews 27, (2013) 475–493.
- R. Dhabhai, E. Ahmadifeijani, A. K. Dalai, M. Reaney. “Purification of crude glycerol
- R. Singh, “Membrane Technology and Engineering for Water Purification: Application,
  raw material: A reviw,” Renewable and Sustainable Energy Reviews, Vol. 27 (2013),
- S. Rawaswamy, H. Huang, B. V. Ramarao, “Separation and Purification Technologies in
- S. Sadhukhan, U. Sarkar, “Production of Purified Glycerol using Sequential Desalination
- Saifuddin N, Refal H, and Kumaran P, (2014). Rapid Purification of Glycerol by-product from Biodiesel Production through Combined Process of Microwave Assisted Acidification and Adsorption via Chitosan Immobilized with Yeast, Research Res. Journal J. of Applied . SciencesSci. , Engineering. and Technology. 7(3),: 593-602, 2014.
- Saleh J., Tremblay A Y, Dubé M A, (2010). Glycerol removal from biodiesel using membrane separation technology, Fuel, Volume 89(, Issue 9), September 2010, Pages 2260–2266.
- Sharma, R.V., Baroi, C., Dalai, A.K. 2014. Production of biodiesel from unrefined canola oil using mesoporous sulfated Ti-SBA-15 catalyst. Catal. Today 237, 3-12.
- Simanjuntak, F.S.H., Choi, J.S., Lee, G., Lee, H.J., Lee, S.D., Cheong, M., Kim, H.S., Lee, H., 2015. Synthesis of glycerol carbonate from the transesterification of dimethyl carbonate with glycerol using DABCO and DABCO-anchored Merrifield resin. Appl. Catal. B Environ. 165, 642–650.
- Simanjuntak, F.S.H., Kim, T.K., Lee, S.D., Ahn, B.S., Kim, H.S., Lee, H., 2011. CaO-catalyzed synthesis of glycerol carbonate from glycerol and dimethyl carbonate: Isolation and characterization of an active Ca species. Appl. Catal. A Gen. 401, 220–225.

- Simanjuntak, F.S.H., Kim, T.K., Lee, S.D., Ahn, B.S., Kim, H.S., Lee, H., 2011. CaO-catalyzed synthesis of glycerol carbonate from glycerol and dimethyl carbonate: Isolation and characterization of an active Ca species. Appl. Catal. A Gen. 401, 220–225.
- Simanjuntak, F.S.H., Widyaya, V.T., Kim, C.S., Ahn, B.S., Kim, Y.J., Lee, H., 2013. Synthesis of glycerol carbonate from glycerol and dimethyl carbonate using magnesium-lanthanum mixed oxide catalyst. Chem. Eng. Sci. 94, 265–270.

Springer (2014), 1-20.
Systems Design and Operation," 2 nd Edition, Colorado Springs (2015), 1-200.

- T. Peters. "Membrane Technology for Water Treatment," Chemical Engineering &
- Tan H W, Aziz A R, and Aroua M K, , (2013). Glycerol production and its applications as a raw material: A review, Renew. Sust. Energ. Rev. Renewable and Sustainable Energy Reviews 27, (2013)118–127.

Technologies," New York Handbook of Environmental Engineering, 13 (2011), 1-27.
Technology, Vol. 33, No.8 (2010) 1233-1240.
Technology," National Renewable Energy Laboratory, Colorado, (2004), 1-105.

- Teng, W.K., Ngoh, G.C., Yusoff, R., Aroua, M.K., 2016. Microwave-assisted transesterification of industrial grade crude glycerol for the production of glycerol carbonate. Chem. Eng. J. 284, 469–477.
- Thompson J C and He B B, (2006). Characterization of crude glycerol from biodiesel production from multiple feedstocks, Appl. Eng. Agricult. 22(2), 261-265.
- Tianfeng C, Huipeng L, Hua Z, Kejian L, (2013). Purification of Crude Glycerol from Waste Cooking Oil Based Biodiesel Production by Orthogonal Test Method, , China Petroleum Processing and Petrochemical Technology, , 2013, Vol. 15(, No. 1), pp 48-53.

using a sequential physico-chemical treatment, membrane filtration, and activated
Vol. 247 (2005) 37-50.

- Wang, L., Ma, Y., Wang, Y., Liu, S., Deng, Y., 2011. Efficient synthesis of glycerol carbonate from glycerol and urea with lanthanum oxide as a solid base catalyst. Catal. Commun. 12, 1459–1462.
- Wessendorf, R.; Erdol, Erdgas, K. Petrochemie **1995** 48, 138-142
- X. Luo, X. Ge, S. Cui, Y. Li, "Value-added Processing of Crude Glycerol into Chemicals
- Xiao Y, Guomin Xiao G, and Varma A, (2013). A Universal Procedure for Crude Glycerol Purification from Different Feedstocks in Biodiesel Production: Experimental and Simulation Study, Ind. Eng. Chem. Res. 2013, 52, 14291−14296.
- Xiao, L.; Mao, J.; Zhou, J.; Guo, X.; Zhang, S. Applied catalysis. A: General **2011** 393, 88–95.
- Y. Xiao, G. Xiao, A. Varma, "A Universal Procedure for Crude Glycerol Purification
- Yang F, Hanna M A and Sun R, (2012). Value-added uses for crude glycerol–a byproduct of biodiesel production, Biotechnology for Biofuels 2012, 5:13.

- Zhan, W., Yao, J., Xiao, Z., Guo, Y., Wang, Y., Guo, Y., Lu, G., 2014. Catalytic performance of Ti-SBA-15 prepared by chemical vapor deposition for propylene epoxidation: The effects of SBA-15 support and silylation. Microporous Mesoporous Mater. 183, 150–155.
- Zhang, J., He, D., 2014. Journal of Colloid and Interface Science Surface properties of Cu / La 2 O 3 and its catalytic performance in the synthesis of glycerol carbonate and monoacetin from glycerol and carbon dioxide. J. Colloid Interface Sci. 419, 31–38.
- Zhang, W.H., Lu, J.Q., Han, B., Li, M.J., Xiu, J.H., Ying, P.L., Li, C., 2002. Direct synthesis and characterization of titanium-substituted mesoporous molecular sieve SBA-15. Chem. Mater. 14, 3413–3421.
- Zhao, W.; Yi, C.; Hu, B. Y. J.; Huang, X. Fuel Processing Technology **2013** 112, 70–75